

Elevated Pressure Electrochemical CO₂ Reduction

Girichandran, N.

DOI

[10.4233/uuid:09d12b6a-def0-44c2-b6cf-d6f50f11a656](https://doi.org/10.4233/uuid:09d12b6a-def0-44c2-b6cf-d6f50f11a656)

Publication date

2024

Document Version

Final published version

Citation (APA)

Girichandran, N. (2024). *Elevated Pressure Electrochemical CO₂ Reduction*. [Dissertation (TU Delft), Delft University of Technology]. <https://doi.org/10.4233/uuid:09d12b6a-def0-44c2-b6cf-d6f50f11a656>

Important note

To cite this publication, please use the final published version (if applicable).
Please check the document version above.

Copyright

Other than for strictly personal use, it is not permitted to download, forward or distribute the text or part of it, without the consent of the author(s) and/or copyright holder(s), unless the work is under an open content license such as Creative Commons.

Takedown policy

Please contact us and provide details if you believe this document breaches copyrights.
We will remove access to the work immediately and investigate your claim.

Elevated Pressure Electrochemical CO₂ Reduction

Dissertation

for the purpose of obtaining the degree of doctor
at Delft University of Technology,
by the authority of the Rector Magnificus prof. dr. ir. T.H.J.J. van der Hagen,
chair of the Board for Doctorates,
to be defended publicly on 25th of September 2024 at 17:30 hours

by

Nandalal GIRICHANDRAN

Master of Science in Chemical Engineering,
Technical University of Delft, The Netherlands
born in Chennai, India

This dissertation has been approved by the promotor.

Prof.dr.ir. W. de Jong	Delft University of Technology, promotor
Prof.dr.ir. J.R.van Ommen	Delft University of Technology, promotor
Dr. R. Kortlever	Delft University of Technology, promotor

Composition of the doctoral committee:

Rector Magnificus	Chairperson
Prof.dr.ir. W. de Jong	Delft University of Technology, promotor
Prof.dr.ir. J.R.van Ommen	Delft University of Technology, promotor
Dr. R. Kortlever	Delft University of Technology, promotor

Independent members:

Prof. dr.ir. J.T. Padding	Delft University of Technology
Prof.dr. G. Mul	Twente University
Prof.dr.ir. P.P. Pescarmona	Groningen University
Dr. W. van der Stem	Utrecht University

Reserve member:

Prof. Dr. Ir. R. Pecnik	Delft University of Technology
-------------------------	--------------------------------

The research presented in this thesis has been carried out in the Large-Scale Energy Storage (LSES) group, part of the Process and Energy Department, Faculty of Mechanical Engineering, Delft University of Technology.



This work received financial support from the Electrons to Chemical Bonds programme (E2CB) on behalf of the Dutch Research Council (NWO).

Copyright © 2024 Nandalal Girichandran

Front & Back Cover design by Nandalal Girichandran

Printed by Ridderprint

An electronic version of this thesis is freely available at:

To Amma, Appa, and Radha

To Vaishu

Contents

Summary	ix
Samenvatting	xiv
Chapter 1 : A Brief Overview of the Electrochemical CO₂ Reduction	1
1.1 Climate Change Chronicles: The CO ₂ Connection	2
1.2 Background.....	5
1.3 Performance Metrics.....	6
1.3.1 Current Density.....	6
1.3.2 Faradaic Efficiency.....	7
1.3.3 Overpotential.....	7
1.3.4 Energy Efficiency.....	8
1.3.5 Tafel Equation and its Parameters	8
1.4 Fundamental Challenges with CO ₂ RR	9
1.5 Catalysts.....	10
1.6 Electrolyser Design.....	14
1.7 Electrolyte.....	16
1.8 Pressure Effects.....	17
1.9 Thesis Objective and Outline.....	19
1.10 References	21
Chapter 2 : Design of an Elevated Pressure Electrochemical Flow Cell for CO₂ Reduction	28
2.1 Introduction	30
2.2 Experimental Section.....	33
2.2.1 Materials	33
2.2.2 Electrochemical Measurements	34
2.2.3 Product analysis.....	35
2.3 Results and Discussion.....	36
2.3.1 Apparatus Design	36

2.3.2 Reactor Assembly Design.....	38
2.3.3 Reference Electrode.....	38
2.3.4 Pressure Regulation.....	39
2.3.5 Reservoir Sizing.....	40
2.3.6 Pump Sizing.....	40
2.3.7 General Operation.....	41
2.3.8 Effect of Pressure on Reference Electrode Potential.....	41
2.3.9 Electrochemical Measurements.....	42
2.3.10 GC Response Time.....	45
2.3.11 Extended Operation.....	48
2.3.12 Conclusions.....	48
2.4 Supporting Information.....	50
2.4.1 Exploded View of the Flow Cell.....	50
2.4.2 PEIS at Different Applied Gas Pressures.....	51
2.4.3 Reservoir Design.....	52
2.4.4 GC Response Time Calculations – Switching Flow Rate Strategy.....	53
2.4.5 Comparison of High-Pressure CO ₂ Reduction Studies.....	57
2.4.6 Standard Curve of a HPLC Measurement.....	58
2.4.7 GC Analysis and Faradaic Efficiency Calculations.....	59
2.5 References.....	60
Chapter 3 : Electrochemical CO₂ Reduction on a Copper Foam Electrode at Elevated Pressures	66
3.1 Introduction.....	68
3.2 Experimental Section.....	70
3.2.1 Materials.....	70
3.2.2 Electrochemical Measurements.....	71
3.2.3 Electrode preparation.....	72
3.2.4 Characterization.....	72

3.3 Results and Discussion.....	73
3.3.1 Effect of Pressure and Current Density on CO ₂ Electroreduction.....	73
3.3.2 Effect of Cation at Elevated Pressure	79
3.3.3 Effect of Electrolyte Concentration at Elevated Pressure.....	80
3.3.4 Conclusions.....	82
3.4 Supplementary Information.....	83
3.4.1 Schematics of the High-Pressure Setup	83
3.4.2 Product Analysis	84
3.4.3 Faradaic Efficiency Calculation	86
3.4.4 Electrochemical Surface Area Measurements	87
3.4.5 SEM images of Copper Foam Pre and Post Experiment.....	88
3.4.6 XPS Spectra Carbon Species.....	89
3.4.7 XPS Spectra Copper Species.....	90
3.4.8 X-Ray Diffraction Spectra.....	91
3.4.9 Faradaic Efficiency of Products – 0.5M KHCO ₃	92
3.4.10 Faradaic Efficiency of Products – Cation Effect and Electrolyte Concentration	96
3.4.11 Reference Plot for HPLC.....	99
3.4.12 NMR Calibrated Component Peaks with a Sample Experimental Peak for 2- Propanol	100
3.4.13 Comparison of High-Pressure CO ₂ Reduction Studies on Copper based Electrodes....	101
3.4.14 Partial Current Densities of H ₂ , CO, and HCOOH in 0.5M KHCO ₃	102
3.5 References.....	103
Chapter 4 : Elevated Pressure Cascade Electrocatalytic Conversion of CO₂ to C₃ Products.....	110
4.1 Introduction	112
4.2 Experimental.....	114
4.2.1 Materials	114
4.2.2 Electrochemical Apparatus and Measurement.....	115
4.2.3 Electrode Preparation	116

4.2.4 Electrode Characterization	117
4.3 Results and Discussion.....	117
4.3.1 Custom Electrochemical Cell Design	117
4.3.2 Electrochemical CO ₂ Reduction at High Pressures	119
4.4 Conclusions.....	126
4.5 Supplementary Information.....	127
4.5.1 Schematics of the High-Pressure Cascade Setup.....	127
4.5.2 Gas and Liquid Product Analysis.....	128
4.5.3 Faradaic Efficiency Calculation	130
4.5.4 Reactor Assembly Drawing	131
4.5.5 SEM Images of Silver and Copper Oxide Foils.....	132
4.5.6 XRD Spectra of Freshly Prepared Silver and Annealed Copper Oxide Foils.....	133
4.5.7 Faradaic Efficiencies of Products	134
4.6 References	135
Chapter 5 : Conclusions and Recommendations.....	139
5.1 Conclusions.....	141
5.2 Recommendations	143
Acknowledgements.....	146
Curriculum Vitae.....	149
Publications.....	151

Summary

Confronted with escalating environmental issues such as global warming due to rising CO₂ emissions mainly caused by human activities, the need for innovative technologies and strategies to address these challenges is more pressing than ever. It is crucial to find sustainable methods to transition away from our current fossil fuel-based carbon-intensive energy systems, while simultaneously ensuring the continued technological advancement of our society. One key approach is the capture of CO₂ from the atmosphere and its transformation into valuable commodities and fuels. The electrochemical reduction of CO₂ can play a pivotal role in this context, as it can bridge the gap between intermittent renewable energy sources and the availability of bulk chemicals and fuels. This process enables the conversion of renewable electrical energy into chemical energy, effectively storing the energy within the chemical bonds of bulk (base) chemicals and fuels. Moreover, this approach aids in mitigating the adverse effects of climate change and provides a pathway towards a circular carbon economy.

By recycling carbon emissions, we can reduce our dependency on fossil fuels and move towards a more sustainable and resilient energy infrastructure. Furthermore, the development and optimization of catalysts and operating conditions for the electrochemical reduction of CO₂ can lead to a more efficient and selective conversion processes. This can open new avenues to produce a wide range of chemicals and fuels, thereby diversifying our energy portfolio. Ultimately, the integration of renewable energy sources with CO₂ conversion technologies could play a significant role in shaping a sustainable and carbon-neutral future.

This thesis focuses on the use of elevated pressures for the electrochemical conversion of CO₂ towards higher reduction products like alcohols. A focus on reactor design, catalyst configuration (cascade) and operating conditions is presented.

In **Chapter 1**, a brief introduction into the status quo of climate change is provided and its relation to increasing global CO₂ emissions is discussed. The importance of carbon capture and utilisation to curb these emissions is highlighted with a specific focus on the relevance of electrochemical CO₂ conversion as an important technique in this process. Further, this chapter outlines the electrochemical reduction of CO₂ into useful chemicals and fuels. It explains the different reactions, their potentials and introduces metrics for assessing new components. The chapter highlights challenges and discusses the role of catalysts, particularly copper, which can yield higher reduced carbon products like alcohols, aldehydes, and hydrocarbons from CO₂. It also covers the impact of electrolytes, including the effects of cations, anions, and pH. Lastly, it addresses how increased pressure can help overcome solubility issues in aqueous media and influence product selectivity.

In **Chapter 2**, the design and successful validation of a novel modular elevated pressure electrochemical CO₂ reduction reaction (CO₂RR) flow cell setup is presented. Key design features included minimizing pressure differentials across the ion exchange membrane separating the cathode from the anode and optimizing reservoir and pump sizing. The cell assembly/disassembly was quick due to a unique clamp design. The cell performed well electrochemically, with a stable reference potential across various pressures. Standard electrochemical experiments were successfully conducted, and product characterization was achieved through in-line GC. The Faradaic efficiency for CO₂RR products increased

significantly from 26% at 2 bar to about 60% at 30 bar, with H₂ being suppressed. The system explained here in detail is successful in its aims and configurable enough to be useful in studying a range of CO₂RR related research questions concerning elevated-pressure reactors.

The effect of elevated pressure on the electrochemical CO₂ reduction using a copper foam electrode revealed key findings as detailed in **Chapter 3**. A systematic investigation was carried out by varying the applied current density, CO₂ pressure, electrolyte cation and electrolyte concentration. At 25 bar pressure, the electrode showed 70% selectivity for formate in a 0.5 M CsHCO₃ solution, with a current density of -12.7 mA/cm², indicating potential for formate production. Isopropanol, an unusual product for CO₂ electrolysis, was produced with 11% Faradaic efficiency in a 0.5 M KHCO₃ solution at the same pressure. This is the highest selectivity for isopropanol under moderate pressures from a polished copper foam electrode. Our experiments highlight the potential of electrolyte engineering coupled with optimal operating conditions to enhance selectivity towards desired products on a simple copper electrode. We discovered that pressurized CO₂ feed could potentially unlock new C-C coupling pathways on copper, leading to the production of elusive higher CO₂ reduction products. These findings suggest that elevated pressure conditions could be crucial in assessing the performance of newly developed catalysts.

Chapter 4 introduces a novel high-pressure sequential cascade reactor for CO₂RR using two electrodes (silver and copper) working in a bi-potentiostatic mode. The reactor uses convective flow to transfer CO from silver to copper. Pressurized conditions helped unlock new products from copper electrode. Under a pressure of 25 bar, adjusting the potentials (-1.0V for silver and -0.7V for copper, vs RHE) and electrolyte flow rate (15 ml/min) resulted in the formation of

2-propanol with an FE of 40%, which is the highest selectivity compared to literature for this uncommon product from a copper electrode. Moreover, the C₃:C₂ oxygenate ratio which is the ratio of liquid products generated from the Cu electrode (mainly considered products – for C₃: 2-propanol, and for C₂: ethanol, acetaldehyde, and ethylene glycol) rose to about 7 in the cascade mode, compared to about 0.6 in non-cascade mode with only copper as the active catalyst. The combined effect of high pressure and cascade operation increases the intermediate CO (produced from upstream silver electrode) concentration on copper, enhancing its surface coverage and promoting the formation of higher alcohols from CO₂. Further optimizations and operando studies could improve this reaction and clarify the mechanism.

In **Chapter 5**, the conclusions of this dissertation and recommendations for future work are provided.

Samenvatting

Geconfronteerd met toenemende milieuproblemen zoals de opwarming van de aarde als gevolg van de stijgende CO₂-uitstoot, voornamelijk als gevolg van menselijke activiteiten, is de behoefte aan innovatieve technologieën en strategieën om deze uitdagingen aan te pakken urgenter dan ooit. Het is van cruciaal belang om duurzame methoden te vinden om af te stappen van onze huidige, op fossiele brandstoffen gebaseerde, koolstofintensieve energiesystemen, en tegelijkertijd de voortdurende technologische vooruitgang van onze samenleving te garanderen. Eén belangrijke aanpak is het opvangen van CO₂ uit de atmosfeer en de transformatie ervan in waardevolle grondstoffen en brandstoffen. De elektrochemische reductie van CO₂ kan hierin een cruciale rol spelen, omdat het de kloof kan overbruggen tussen intermitterende hernieuwbare energiebronnen en de beschikbaarheid van bulkchemicaliën en brandstoffen. Dit proces maakt de omzetting van hernieuwbare elektrische energie in chemische energie mogelijk, waarbij de energie effectief wordt opgeslagen in de chemische bindingen van bulkchemicaliën en brandstoffen. Bovendien helpt deze aanpak bij het verzachten van de negatieve effecten van klimaatverandering en biedt het een weg naar een circulaire koolstofeconomie.

Door de CO₂-uitstoot te recyclen kunnen we onze afhankelijkheid van fossiele brandstoffen verminderen en evolueren naar een duurzamere en veerkrachtigere energie-infrastructuur. Bovendien kan de ontwikkeling en optimalisatie van katalysatoren en bedrijfsomstandigheden voor de elektrochemische reductie van CO₂ leiden tot efficiëntere en selectievere conversieprocessen. Dit kan nieuwe wegen openen voor de productie van een breed scala aan chemicaliën en brandstoffen, waardoor onze energieportfolio wordt gediversifieerd.

Uiteindelijk zou de integratie van hernieuwbare energiebronnen met CO₂-conversietechnologieën een belangrijke rol kunnen spelen bij het vormgeven van een duurzame en koolstofneutrale toekomst.

Dit proefschrift richt zich op het gebruik van verhoogde druk voor de elektrochemische omzetting van CO₂ naar hogere reductieproducten zoals alcoholen. Er wordt aandacht besteed aan reactorontwerp, katalysatorconfiguratie (cascade) en bedrijfsomstandigheden.

In **hoofdstuk 1** wordt een korte introductie gegeven over de status quo van de klimaatverandering en wordt de relatie ervan met de toenemende mondiale CO₂-uitstoot besproken. Het belang van koolstofafvang en -gebruik om deze emissies terug te dringen wordt benadrukt met een specifieke focus op de relevantie van elektrochemische CO₂-conversie als belangrijke techniek in dit proces. Verder schetst dit hoofdstuk de elektrochemische reductie van CO₂ tot bruikbare chemicaliën en brandstoffen. Het legt de reacties en hun mogelijkheden uit en introduceert maatstaven voor het beoordelen van nieuwe componenten. Het hoofdstuk belicht uitdagingen en bespreekt de rol van katalysatoren, met name koper, die producten met een lager koolstofgehalte kunnen opleveren, zoals alcoholen, aldehyden en koolwaterstoffen uit CO₂. Het behandelt ook de impact van elektrolyten, inclusief de effecten van kationen, anionen en pH. Ten slotte wordt ingegaan op de manier waarop verhoogde druk oplosbaarheidsproblemen in waterige media kan helpen overwinnen en de productselectiviteit kan beïnvloeden.

In **Hoofdstuk 2** wordt het ontwerp en de succesvolle validatie van een nieuwe modulaire verhoogde druk elektrochemische CO₂-reductiereactie (CO₂RR) stroomcelopstelling gepresenteerd. Belangrijke ontwerpkenmerken waren onder meer het minimaliseren van

drukverschillen over het ionenuitwisselingsmembraan, dat de kathode van de anode scheidt, en het optimaliseren van de afmetingen van het reservoir en de pomp. De celmontage/demontage verliep snel dankzij een uniek klemontwerp. De cel presteerde elektrochemisch goed, met een stabiel referentiepotentieel bij verschillende drukken. Standaard elektrochemische experimenten werden met succes uitgevoerd en productkarakterisering werd bereikt via in-line GC. De Faradaic-efficiëntie voor CO₂RR-producten nam toe aanzienlijk van 26% bij 2 bar tot ongeveer 60% bij 30 bar, waarbij de vorming van H₂ wordt onderdrukt. Het hier in detail uitgelegd systeem is succesvol in zijn doelstellingen en configureerbaar genoeg om bruikbaar te zijn bij het bestuderen van een reeks CO₂RR-gerelateerde onderzoeksvragen met betrekking tot hogedrukreactoren.

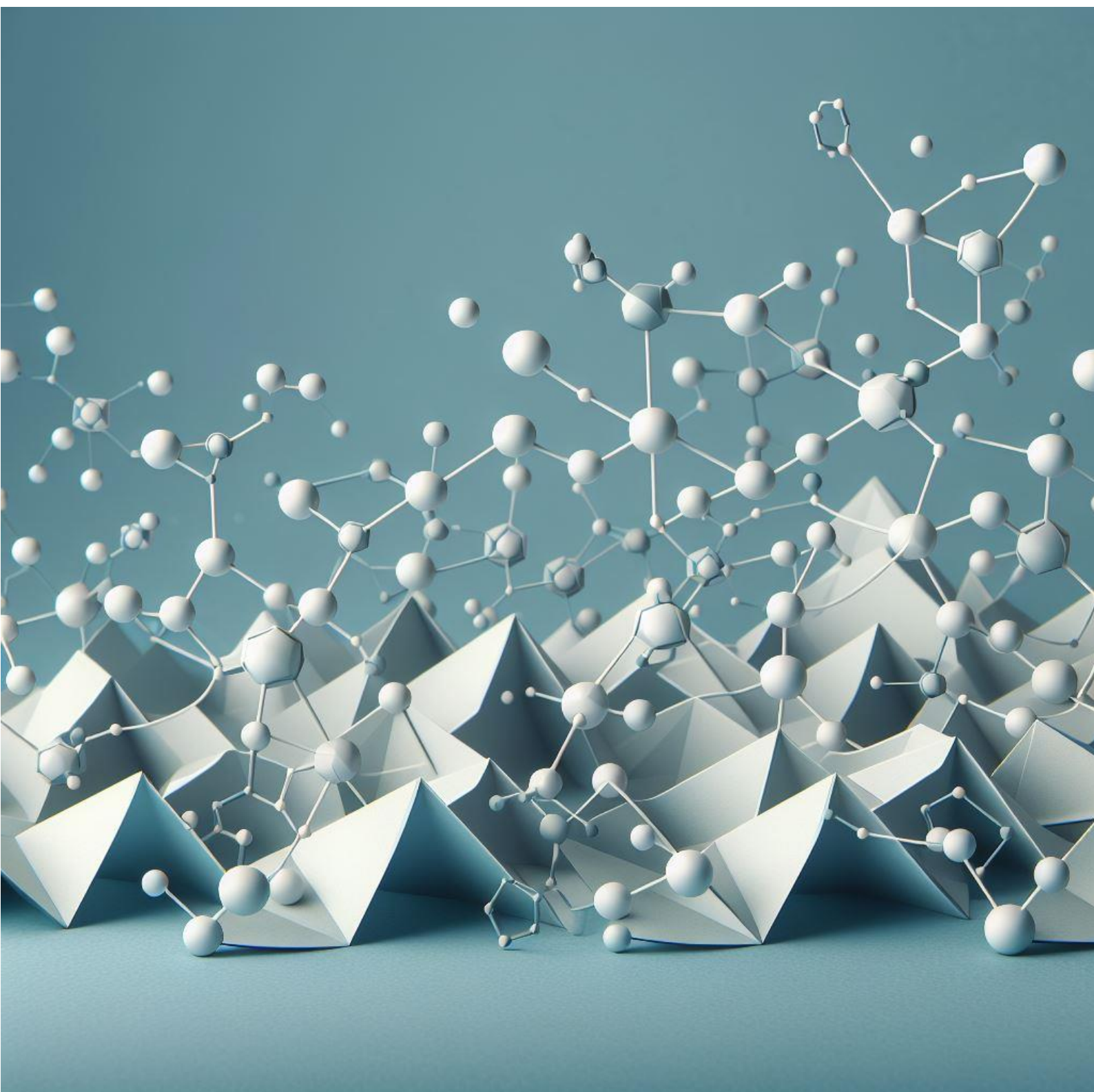
Het effect van verhoogde druk op de elektrochemische CO₂-reductie met behulp van een koperschuimelektrode onthulde de belangrijkste bevindingen, zoals beschreven in **Hoofdstuk 3**. Een systematisch onderzoek werd uitgevoerd door de toegepaste stroomdichtheid, CO₂-druk, elektrolytkationen en elektrolytconcentratie te variëren. Bij een druk van 25 bar vertoonde de elektrode een selectiviteit van 70% voor formiaat in een 0,5 M CsHCO₃-oplossing, met een stroomdichtheid van -12,7 mA/cm², wat wijst op potentieel voor formiaatproductie. Isopropanol, een ongebruikelijk product voor CO₂-elektrolyse, werd geproduceerd met een Faradaic-efficiëntie van 11% in een 0,5 M KHCO₃-oplossing bij dezelfde druk. Dit is de hoogste selectiviteit voor isopropanol onder gematigde druk op een gepolijste koperen schuimelektrode. Onze experimenten benadrukken het potentieel van elektrolyttechniek en optimale bedrijfsomstandigheden om de selectiviteit naar gewenste producten op een eenvoudige koperelektrode te verbeteren. We ontdekten dat CO₂-toevoer onder druk mogelijk

nieuwe C-C-koppelingsroutes op koper zou kunnen ontsluiten, wat zou leiden tot de productie van ongrijpbare producten met een hogere CO₂-reductie. Deze bevindingen suggereren dat verhoogde drukomstandigheden cruciaal kunnen zijn bij het beoordelen van de prestaties van nieuw ontwikkelde katalysatoren.

Hoofdstuk 4 introduceert een nieuwe hogedruk sequentiële cascaderactor voor CO₂RR met behulp van twee elektroden (zilver en koper) die in een bi-potentiostatische modus werken. De reactor gebruikt convectieve stroming om CO van zilver naar koper over te brengen. Onder druk staande omstandigheden hielpen nieuwe producten uit de koperelektrode te ontsluiten. Onder een druk van 25 bar resulteerde het aanpassen van de potentiaal (-1,0 V voor zilver en -0,7 V voor koper, versus RHE) en de elektrolytstroomsnelheid (15 ml/min) in de vorming van 2-propanol met een FE van 40%, wat de hoogste selectiviteit is in vergelijking met de literatuur voor dit ongebruikelijke product uit een koperelektrode. Bovendien steeg de C₃:C₂-oxygenaatverhouding, de verhouding van vloeibare producten gegenereerd door de Cu-elektrode (voornamelijk beschouwd als producten – voor C₃: 2-propanol en voor C₂: ethanol, acetaldehyde en ethyleenglycol) in de cascade naar ongeveer 7. in de niet-cascademodus, vergeleken met slechts ongeveer 0,6 in de niet-cascademodus met alleen koper als actieve katalysator. Het gecombineerde effect van hoge druk en cascaderwerking verhoogt de tussenliggende CO-concentratie (geproduceerd door de stroomopwaartse zilverelektrode) op koper, waardoor de oppervlaktebedekking wordt vergroot en de vorming van hogere alcoholen uit CO₂ wordt bevorderd. Verdere optimalisaties en operandostudies zouden deze reactie kunnen verbeteren en het mechanisme kunnen verduidelijken.

In **Hoofdstuk 5** worden de conclusies van dit proefschrift en aanbevelingen voor toekomstig werk gegeven.

Chapter 1 : A Brief Overview of the Electrochemical CO₂ Reduction



1.1 Climate Change Chronicles: The CO₂ Connection

As the human population continues to grow, the global energy demand is expected to rise by 20% in the next couple of decades. Most of the current energy requirements are met by traditional fossil fuels which has led to a detrimental impact on the climate. Climate change, a pressing global issue, is largely driven by the increase in greenhouse gases, particularly carbon dioxide (CO₂) emissions^{1,2}. These emissions are influenced by various human activity related factors including economic growth, industry structure, and urbanization, alongside energy consumption². The Intergovernmental Panel on Climate Change (IPCC) provides comprehensive assessments on climate change and its potential environmental and socioeconomic impacts¹. Understanding the relationship between CO₂ emissions and these driving factors is crucial for developing effective strategies to mitigate climate change².

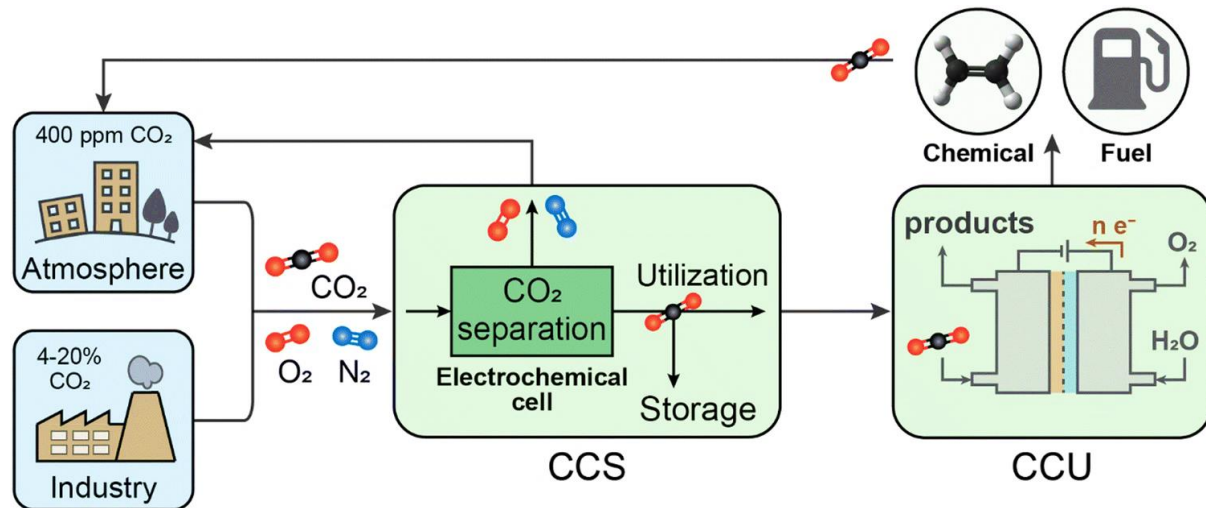


Figure 1.1: Carbon capture storage (CCS) and carbon capture utilisation (CCU) via the direct electrochemical conversion route (reused with permission from ref 6).

The compelling need to counteract the escalating levels of atmospheric CO₂ has spurred the efforts of researchers across the globe to create carbon capture methods that can curb the emissions³. While low-cost methods like reforestation show potential for carbon capture, their

land (including soil type and nutrient composition) and water need limit high-throughput CO₂ fixation.

Complementary approaches such as biochemical, thermochemical, and electrochemical processes involve converting CO₂ into economically viable compounds, such as algae-based biofuels, carbonates⁴, and bulk chemicals and fuels⁵. CCU is indispensable in realizing a sustainable future while curbing these emissions (**Figure 1.1**). It relies on a suite of

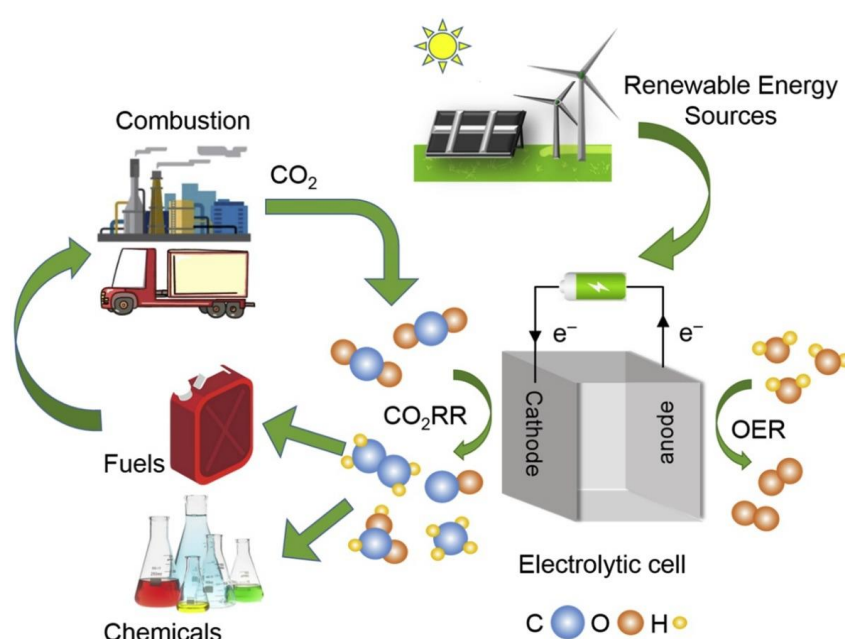


Figure 1.2: Depiction of electrochemical CO₂ reduction to chemical feedstocks and fuels using renewable energy sources (reused with permission from ref 8).

technologies, that extract CO₂ from industrial exhausts, bio-based conversion processes or ambient air and transform it into various products such as fuels, chemicals, and materials potentially powered by renewable electricity. Among these, the electrochemical conversion of CO₂ is a vital technique (**Figure 1.2**). Electrochemical methods offer a direct, efficient way to convert captured CO₂, eliminating the need for less efficient steam heating. It also opens new

opportunities for understanding and designing capture and separation processes at the atomic scale⁶.

Electrochemical CO₂ reduction is a proton-electron mediated process wherein the charge balance is provided by the protons and electrons in the system. There is a proton gradient between the anode (where they are produced) and cathode (where they get consumed)⁷. In neutral/alkaline pH this will be an OH⁻ gradient (production at cathode/consumption at anode). The reaction is driven by an externally supplied voltage that helps overcome the energy barrier and subsequently in the conversion of CO₂ to useful products like CO, formic acid, ethylene, ethanol, propanol etc. The process can be coupled to renewable energy sources, thereby, offering a sustainable solution to tackle the climate change while transitioning to a greener future⁸.

1.2 Background

The electrochemical CO₂ reduction reaction (CO₂RR) is a chemical conversion process that takes place on a catalyst/cathode that is supplied with electric energy in the form of electrons.

Table 1.1: Commonly observed CO₂RR and HER products with the number electrons involved in their formation and at standard potentials vs RHE (1 atm, 25°C, pH 14)⁹⁻¹¹

Product (phase)	Cathode Reaction	E° [V vs. RHE]	Z (electrons)
CO (g)	$\text{CO}_2 (\text{g}) + 2\text{H}_2\text{O} (\text{l}) + 2\text{e}^- \leftrightarrow \text{CO} (\text{g}) + 2\text{OH}^-$	-0.934	2
HCOO ⁻ (aq)	$\text{CO}_2 (\text{g}) + 2\text{H}_2\text{O} (\text{l}) + 2\text{e}^- \leftrightarrow \text{CHOO}^- (\text{aq}) + \text{OH}^-$	-1.078	2
CH ₃ OH (l)	$\text{CO}_2 (\text{g}) + 5\text{H}_2\text{O} (\text{l}) + 6\text{e}^- \leftrightarrow \text{CH}_3\text{OH} (\text{l}) + 6\text{OH}^-$	-0.812	6
CH ₄ (g)	$\text{CO}_2 (\text{g}) + 6\text{H}_2\text{O} (\text{l}) + 8\text{e}^- \leftrightarrow \text{CH}_4 (\text{g}) + 8\text{OH}^-$	-0.659	8
C ₂ O ₄ ⁻ (aq)	$2\text{CO}_2 (\text{g}) + 2\text{e}^- \leftrightarrow \text{C}_2\text{O}_4^{2-} (\text{aq})$	-0.590	2
CH ₃ COO ⁻ (aq)	$2\text{CO}_2 (\text{g}) + 5\text{H}_2\text{O} (\text{l}) + 8\text{e}^- \leftrightarrow \text{CH}_3\text{COO}^- (\text{aq}) + 7\text{OH}^-$	-0.703	8
C ₂ H ₅ OH (l)	$2\text{CO}_2 (\text{g}) + 9\text{H}_2\text{O} (\text{l}) + 12\text{e}^- \leftrightarrow \text{CH}_3\text{CH}_2\text{OH} (\text{l}) + 12\text{OH}^-$	-0.744	12
C ₂ H ₄ (g)	$2\text{CO}_2 (\text{g}) + 8\text{H}_2\text{O} (\text{l}) + 12\text{e}^- \leftrightarrow \text{C}_2\text{H}_4 (\text{g}) + 12\text{OH}^-$	-0.764	12
C ₃ H ₇ OH (l)	$3\text{CO}_2 (\text{g}) + 13\text{H}_2\text{O} (\text{l}) + 18\text{e}^- \leftrightarrow \text{CH}_3\text{CH}_2\text{CH}_2\text{OH} (\text{l}) + 18\text{OH}^-$	-0.733	18
H ₂ (g)	$2\text{H}_2\text{O} (\text{l}) + 2\text{e}^- \leftrightarrow \text{H}_2 (\text{g}) + 2\text{OH}^-$	-0.828	2

A potentiostat supplies the electrons to the working electrode (cathode) for this reaction to occur whereas the counter electrode (anode) loses electrons as species get oxidized (e.g. by the

oxygen evolution reaction). The reaction is proton-electron mediated wherein the charge balance is provided by the protons and electrons in the system (Figure 1.3a)⁷. At a neutral/alkaline pH this will be an OH⁻ gradient (production at cathode/consumption at anode). An ion exchange membrane (either cation exchange membrane (eg : Nafion), anion exchange membrane (eg: selemion) or bipolar membrane (eg: Fumasep)) separates the anode from the cathode, allowing charge transfer and preventing cross contamination between the two chambers¹².

The mechanisms underlying CO₂RR have been extensively studied and the following pathways have been widely considered¹³: (a) CO₂* molecule undergoes hydrogenation and desorbs as a formate ion; (b) CO₂* reduces to CO* which then either desorbs readily to give CO or further reacts with other adsorbed species to produce alcohols, and hydrocarbons. The most common CO₂RR products are carbon monoxide (CO), formate (HCOOH), methane (CH₄), methanol (CH₃OH), ethylene (C₂H₄), acetate (CH₃COOH), ethanol (CH₃CH₂OH), and propanol/isopropanol (CH₃CH₂CH₂OH/ CH(CH₃)₂OH). Irrespective of the configuration of a CO₂RR electrolyser, a certain performance standards/metrics can be used to characterize the nature of the electrolyser. A few of the most important ones are current density, faradaic efficiency, over potential, energy efficiency, catalyst activity and electrode stability¹². A brief description of these metrics is given below.

1.3 Performance Metrics

1.3.1 Current Density

Current density (j) is a quantification of the reaction rate leading to the formation of all products under specific conditions. The reaction rate is directly linked to the number of electrons engaged or exchanged during the reaction. By multiplying j with the fraction of

electrons involved in a particular reaction, we obtain the partial current density (j_i) towards that reaction, and consequently, the specific product. This metric holds significant importance in large-scale industrial production since a higher partial current density towards a specific product results in greater production per given electrode area, thereby, enhancing system efficiency.

1.3.2 Faradaic Efficiency

The Faradaic efficiency (FE) is the percentage of electric charge that is utilised in the formation of the desired product with respect to the total charge transferred between the two electrodes.

$$FE = \frac{nZF}{Q} \times 100 \% \quad (1.1)$$

where n is the number of moles of the desired product, Z is the number of electrons required per mole of product, F is Faraday's constant (96485 C/mol electrons), and Q is the total charge exchanged between the electrodes. FE is the selectivity of the reaction to a particular product, and thus improving it will increase in the amount of CO_2 converted to a desired product, reduce downstream separation costs, and reduce the energy requirements of the process.

1.3.3 Overpotential

The overpotential (η) is the surplus voltage applied beyond the thermodynamically required voltage for a reaction to take place. It comprises of the following three main categories: the activation overpotential ($\eta_{\text{activation}}$), necessary to surpass the activation energy barriers of the reactions to occur on the electrocatalyst, the concentration overpotential ($\eta_{\text{concentration}}$), resulting from limitations in CO_2 mass transport within the electrolyte and the Ohmic drop (IR)/ohmic overpotential (η_{ohmic}) arising due to movement of ions through the electrolyte, membrane and

the flow of electrons through the electrodes involved^{14,15}. A special case of $\eta_{\text{concentration}}$ is the bubble overpotential caused by the evolution of bubbles during the reaction. This can block the surface of electrodes and also affect the movement of species/ions in the electrolyte.

1.3.4 Energy Efficiency

Energy Efficiency is calculated as the product of FE and voltage efficiency, the latter being the ratio of standard electrode potential (E°) to the sum of E° , η , and IR across the cell,

$$EE = \frac{E^\circ}{E^\circ + \eta + IR} \times FE, \% \quad (1.2)$$

The energy efficiency is an important metric for evaluating the costs of operating the system.

1.3.5 Tafel Equation and its Parameters

The Tafel equation indicates a relationship between the η and j given by,

$$\eta = a + b \log(i) = -2.303 \times \frac{RT}{\alpha F} \times \log(i_o) + 2.303 \times \frac{RT}{\alpha F} \times \log(i) \quad (1.3)$$

The charge transfer coefficient α and exchange current density (i_o) are essential factors related to the activity and kinetics of a reaction, representing the current density at equilibrium. By examining the Tafel slope, we can determine the value of α , which indicates the catalyst's level of activity. A smaller slope corresponds to a higher α , signifying a more active catalyst. Changes in the catalyst's surface and reactant concentration can be deduced from shifts in the Tafel slope. For analysing individual products, it is necessary to utilize the partial current density instead of the total, particularly in the complex multi-step process of CO₂RR, where various

products are generated via different reaction mechanisms. This presents a challenge in the determination of Tafel parameters.

1.4 Fundamental Challenges with CO₂RR

One of the inevitable requirements to reduce CO₂ to products at appreciable rates is the amount of energy required. This is because the energy input to conduct CO₂RR is usually higher than the thermodynamic value, known as the thermodynamic overpotential as mentioned in the

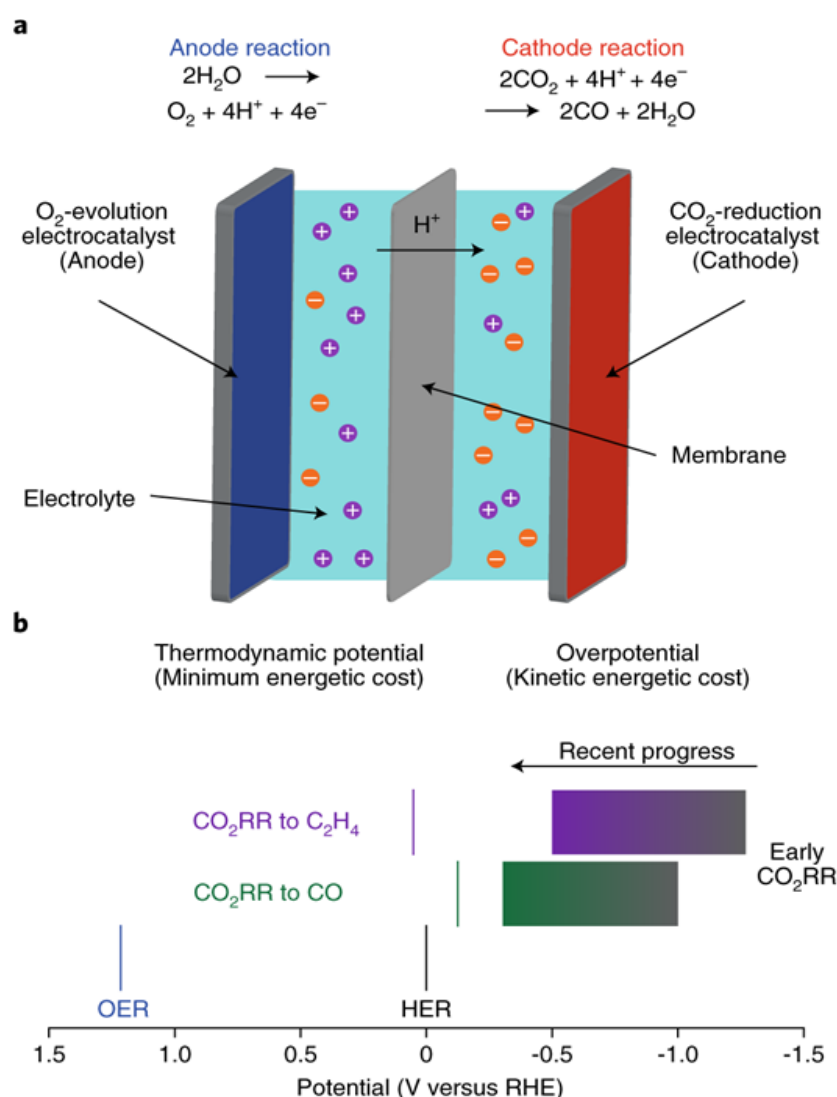


Figure 1.3: (a) An electrochemical system with the cathode and anode catalyst separated by the membrane, (b) The thermodynamic (ideal) potentials on the RHE scale are indicated for OER (+1.23V), HER (0V), CO₂ to CO (-0.11V), and CO₂ to C₂H₄ (+0.07V). Additionally, the overpotentials required for CO₂RR and the advancements made in reducing them (colour bars) are depicted (reused with permission from ref 30).

previous section (1.3.3)¹⁶. Moreover, CO₂RR involves complicated reaction pathways having multiple steps leading to slow kinetics that contribute to even higher overpotentials. Overlapping adsorption strengths of different reaction intermediates during CO₂RR results in scaling relations making it extremely difficult to optimize their binding strengths¹⁷⁻¹⁹. These relations are compounded when targeting multi-carbon products. Additionally, protons, which are integral to the reduction reactions, can reduce to H₂ alongside CO₂RR further complicating the process²⁰. This coupled to the fact that CO₂ can reduce to a multitude of different products, leads to a poor product selectivity.

To overcome these challenges and accelerate the viability of electrochemical CO₂ reduction, ample work has been conducted in the development of new catalysts, designing optimal reactor configurations, and engineering the electrolytes. A brief discussion on these topics is provided in the following sections.

1.5 Catalysts

There is no denying that catalysts form the heart of chemical conversions and electrochemical CO₂RR is no exception. Pure metal-based catalysts (copper(Cu), gold(Au), silver(Ag), tin(Sn)), single atom catalysts^{21,22}, non-metals like carbon nanotubes and other metallic complexes²³ have established themselves as the go-to materials due to their excellent ability to reduce CO₂. The choice of the catalyst dictates intermediates formed and therefore the reaction mechanism. Techniques like spray-coating, drop casting, electrodeposition, and electroless depositions are commonly used to synthesize catalysts, or they can simply be purchased commercially.

Preparation of an electrocatalyst with optimal intrinsic properties is crucial to achieve an efficient electrochemical conversion. The focus is on creating more active sites to achieve a high turnover frequency (TOF). While increased catalyst loading can improve performance, it may introduce additional mass transport limitations and leads to higher costs, especially for precious metals. Given the low solubility of CO₂ in aqueous media, modifying the electrochemically active surface area (ECSA) through intrinsic property tuning, including morphology, size, defects, interface, electronic state, and alloying, is vital for rational design of a catalyst²⁴.

Conversion of CO₂ to CO at high efficiencies has been well studied and reported²⁵, but production of higher hydrocarbons and oxygenates with high partial current densities still suffers from poor selectivity, availability of fewer catalyst materials, and slow reaction rates coupled with low energy conversion efficiencies²⁶. Hitherto, only Cu has shown appreciable yields for CO₂RR to multicarbon products like ethylene, ethanol, 1-propanol etc. For example, Dinh et al., synthesised ethylene at a FE of 70% on Cu in KOH at -0.55V vs a reversible hydrogen electrode (RHE)²⁷. The overall energy efficiency of the CO₂RR process is also lowered by the high energy demanding ($E^{\circ} = 1.23\text{V}$ vs. RHE) oxygen evolution reaction (OER) at the anode which produces the less valuable O₂ as the product²⁸. This results in a required cell voltage that is way higher than the thermodynamic value.

Most of the current efforts to tackle the problems mentioned above focus on finding new catalysts, altering their facets, structure or designing membrane electrode assemblies^{29,30}. But

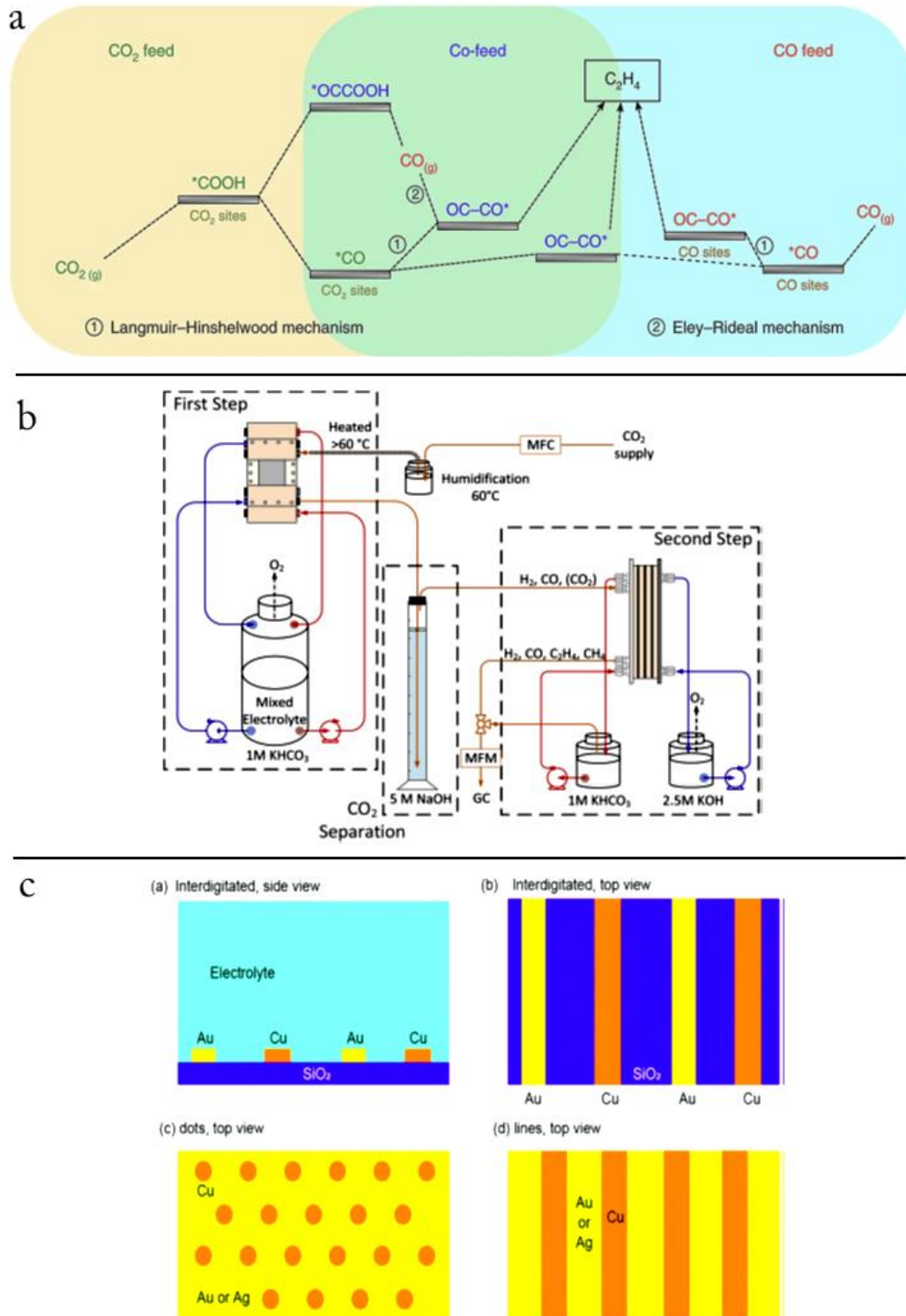


Figure 1.4: a) Pure CO₂ feed, and pure CO feed compared to the co-feeding case (reused with permission from ref 31). b) Two step CO₂ to ethanol cascade (reused with permission from ref 32). c) Interdigitated bimetallic electrodes (reused with permission from ref 34).

there have also been some innovative methods (**Figure 1.4**) employed to address some of these issues like (a) Co-fed CO₂/CO electrocatalytic reduction towards high value products³¹, (b) Tandem/cascade/interdigitated CO₂RR for in-situ consumption of intermediates to produce more valuable chemicals³²⁻³⁶, (c) Integrated hybrid CO₂RR wherein the OER at the anode is replaced by a more energy efficient process³⁷.

A key underlying principle behind these concepts is the poorly understood spillover effect of reaction intermediates, which is simply the transfer or movement of one or more species formed on one catalyst on to another where its further consumed. To understand this spillover effect, we can consider a good synergistic catalyst couple such as Ag (a good catalyst that facilitates the formation of CO) and Cu (a good catalyst that enhances the conversion of CO) with the key intermediate being CO. There are two proposed pathways for CO spillover: (1) CO produced on Ag first desorbs into the electrolyte, followed by readsorbing on Cu nearby; (2) *CO that is adsorbed on Ag can directly diffuse through the grain boundaries of Ag and Cu, and transfer to Cu³⁸. In the physically separated configuration such as the cascade mode, convection also plays a role in controlling this transfer of intermediates³⁵.

With improved selectivity, conversion, activity, and reduced potentials, these new routes show promise but are still in their infancy. Parameters like operating conditions, catalyst configurations, flow behaviour etc. still need to be studied and improved to understand the primary phenomena. These techniques lay down a foundation for further integration possibilities to address problems related to poor solubility of CO₂, mass transfer limitations, higher overpotentials etc. especially in aqueous CO₂ reactor systems. One such interesting case could be combining a sequential cascade catalytic system with a pressurized CO₂ feed to

increase the concentration of CO_2 available and the surface coverage of the reactants to boost the formation of higher reduction products^{35,39,40}. In this manner we can leverage the benefits of these two different concepts in a single integrated reactor.

1.6 Electrolyser Design

As already mentioned in the previous chapter, the reactor/electrolyser configuration plays an important role among other factors in the electrochemical CO_2RR process. Electrolysers come in batch and continuous flow-cell configurations⁴¹. An example of one of the most used

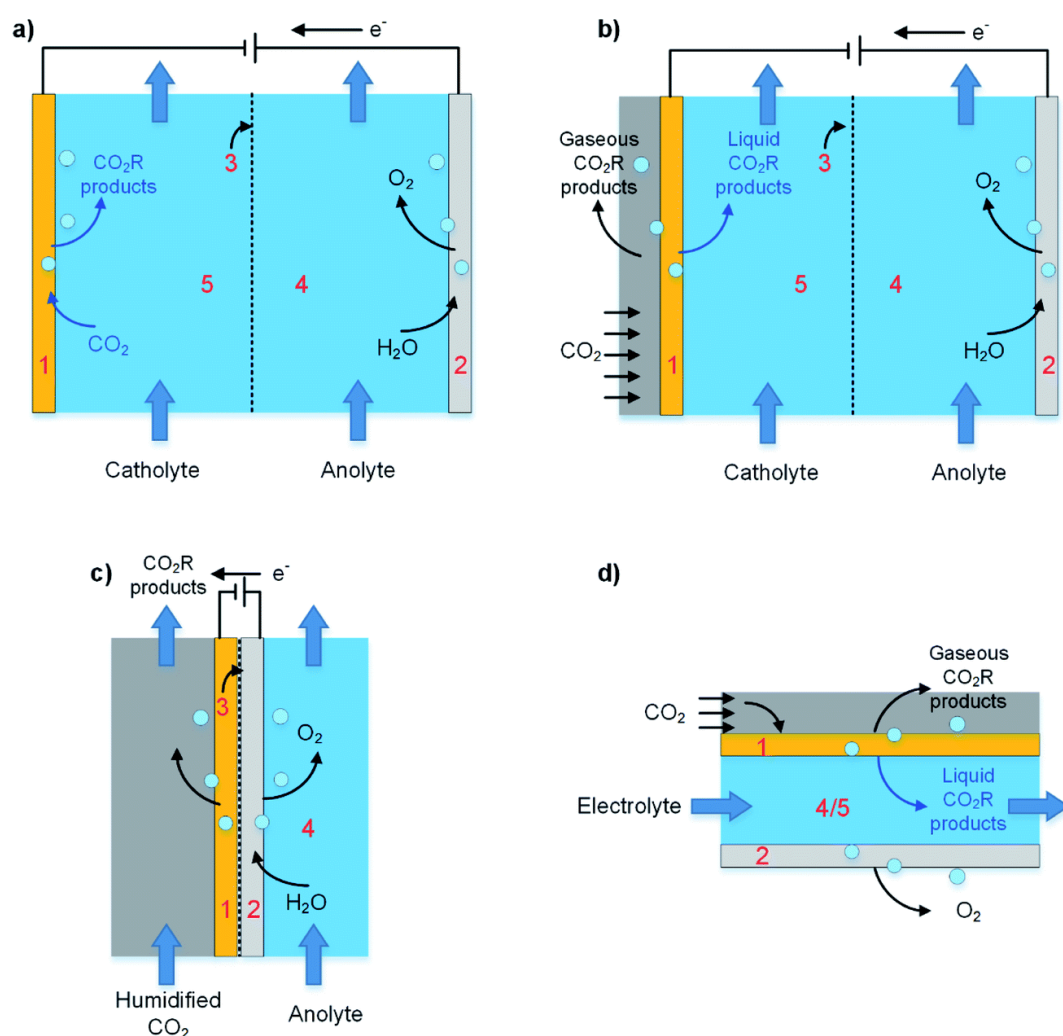


Figure 1.5: Schematic of electrolyser configurations. (a and b) Liquid-fed electrolyser, (c) vapor-fed electrolyser, (d) microfluidic electrolyser. Components are (1) cathode, (2) anode, (3) membrane, (4) anolyte, and (5) catholyte (reused with permission from ref 41).

laboratory scale semi-batch electrolysers is the H-cell. In an H-cell, the electrodes are brought in contact with the liquid electrolyte and the CO₂ gas is bubbled through the catholyte to saturate it. It is a simple and economical setup that allows for quick screening of catalysts and electrolytes. However, there are problems like low CO₂ mass transfer rates, accumulation of cations in the cathode chamber which hamper the reaction kinetics and poor selectivity of products making this configuration less practical for scaling up.

In a flow cell configuration, there are three common types of electrolysers namely: continuous liquid-fed, vapor-fed, and microfluidic electrolyser as shown in **Figure 1.5**. A brief description of the three types is given below.

- **Continuous liquid-fed electrolyser:** In this setup, the catholyte is usually saturated with a CO₂ feed before entering the reactor or a gas diffusion electrode (GDE) is used, wherein a gaseous CO₂ feed on one side of the GDE is made to meet the catholyte flowing through the reactor on the other side of the GDE. In the latter case, solubility limitations of CO₂ are reduced thereby enhancing the current densities of products. The flow rate of the catholyte in such electrolysers gives a control over the mass transfer rate as it affects the superficial liquid and/or gas velocities⁴². Another advantage of these configurations is the possibility for large active electrode area to electrolyte volume ratios compared to batch type which increases the overall reaction rates, reduces ohmic losses and improves detection of low concentration products like acetone, glycolaldehyde, glyoxal etc⁴³.
- **Vapor-fed electrolyser:** Here, the CO₂ gas is sent in a humidified form directly over the membrane (zero gap) assembly which helps in keeping it hydrated and at the same time reducing ohmic losses with lower chances of catalyst poisoning. One main problem in such

vapor fed systems is the flooding of the pores of GDE because of liquid reaction products, thereby blocking some of the reaction active sites for CO₂.

- Microfluidic electrolyser: Kenis et al. developed a reactor in which a 1mm channel separates the cathode from the anode without any membrane in the reactor⁴⁴. The gaseous CO₂ feed contacts the electrode-electrolyte interface by passing through a gas diffusion layer (GDL). Since the channel dimensions are in the micro to milli meter scale, the flow remains in the laminar regime. Key advantages of using a small-scale reactor like this are a high surface to volume ratio, higher mass transfer rates thereby leading to higher current densities of products. They also offer flexibility in operation and could be scaled up (in numbers, in series or parallel configurations).

1.7 Electrolyte

The electrolyte plays a key role in the process of CO₂RR as it has a direct impact on the reaction environment in the vicinity of the electrode surface. The composition (cations and anions), and concentration of the electrolyte can directly influence the electronic interactions between different species and the electrode surface, local pH, reaction intermediates, and surface bound water species (proton donor)⁴⁵⁻⁴⁷. Solvated metal cations accumulate near the vicinity of the electrode under reduction conditions. A recent study by Monteiro et al. confirmed the absence of any CO₂RR without cations⁴⁸. They can stabilize intermediates like *COO, *CO and *OCCO through coordination. Meanwhile, the concentration of cations at the outer Helmholtz plane contributes to an increased interfacial electric field, supporting the stability of intermediates with larger dipole moments. Additionally, the fluctuating pKa values, linked to cation sizes, impact local pH and CO₂ concentration, affecting product selectivity⁴⁹⁻⁵³. pH of

the electrolyte especially in the vicinity of the catalyst surface has long intrigued researchers and has been the subject of various studies⁵⁴⁻⁵⁶. During CO₂RR, the pH becomes alkaline near the catalyst surface due to the depletion of H⁺ and formation of OH⁻. The product selectivity and current density depend on the local pH change which is impacted by the nature of the electrolyte⁵⁷. When the local pH rises, the concentration of CO₂ decreases because it is converted into bicarbonate or carbonate, thereby reducing the amount of the active reactant, CO₂, in the system⁵⁷⁻⁶⁰. Additionally, the pH may be influenced by the catalyst surface morphology. A rough surface can produce more OH⁻ ions during reduction, potentially raising the pH near the surface compared to a smoother surface.⁶¹

1.8 Pressure Effects

It is well understood from Henry's law that increasing the pressure of a gaseous species increases its concentration in the dissolved state. Several studies have been conducted to understand the impact of pressure on CO₂R/COR^{53,62-65}. Under 1 atm, HER becomes dominant as the partial pressure of CO₂ and CO drops^{53,65}. However, with increased pressures, the current density of CO₂RR has been shown to increase. Pressure also has been shown to increase C₂H₄ selectivity due to increased CO concentration on the catalyst surface⁶⁴. Increased pressures can also aid in bubble detachment from the surface of the electrode, thus helping to lower the potential. This is because pressure affects the bubble detachment diameter thereby facilitating its quicker release.

Ramdin et al. experimentally obtained a high formic acid FE of 80 % at 50 bar with a current density of 30 mA/cm² and η of 3.5 V at low pH⁶⁶. Simulations on formic acid or formate

formation at elevated pressures (up to 50 bar) showed an incremental trend in partial current density with FE capping off at 95% above 10-20 bars. It was determined that the economic profit follows a similar trend as the CO₂ solubility and maximum partial current density, thus showing the importance of current density as a performance metric. This is quite favourable on an industrial scale as high specific product synthesis (due to high pressure) is always profitable. Elevated pressures, exemplified by CO₂RR studies such as those by Shen et al.⁶⁷, Hashiba et al.⁶², and Welch et al.⁶⁸, have demonstrated the ability to not only overcome mass transfer limitations but also stabilize targeted reaction pathways. The inhibition of undesired reactions, notably hydrogen evolution, coupled with an amplified yield of sought-after products like formic acid, highlights the profound impact of increased CO₂ pressure. Certain studies have underscored the importance of operating pressure in modulating the catalytic performance through an intricate interplay of factors such as reaction thermodynamics, the delicate balance of acid/base buffers (CO₂/HCO₃⁻/CO₃²⁻), and the extent of surface coverage of CO₂ and its intermediates such as *CO on the catalyst surface^{40,69}. Using increased pressures of more than 45 atm for CO₂RR on copper-based electrodes have been proven to inhibit undesirable reactions, such as hydrogen evolution, and improve the yield of desired products like formic acid reaching close to 100% selectivity⁷⁰. A recent study by Hou et al., revealed the influence of high pressure on the electrochemical CO reduction reaction (CORR) on a copper catalyst. It was determined that the increase in the surface coverage of the reactant species with pressure results in a switch in the reaction mechanism towards oxygenates, generating elusive products like ethylene glycol, glycolaldehyde, allyl alcohols etc., highlighting the importance of pressure

in understanding and optimizing CO₂RR⁴⁰. Overall, high-pressure environments prove beneficial, enhancing CO₂ concentration and catalytic performance in CO₂RR studies.

Yet, the number of experimental and operando studies done on high pressure systems is still limited. This paves the way for further research to conduct systematic investigations to understand the influence of pressure on the electrochemical CO₂ reduction process and also improve the mechanistic understanding of the different electrochemical/chemical steps involved and optimizing the productivity and selectivity of existing CO₂RR systems especially towards liquid products by identifying the best operating conditions²⁶.

1.9 Thesis Objective and Outline

The main goal of this dissertation is to optimize a two-catalyst system for electrochemical CO₂RR by tuning the operating conditions. The study places particular emphasis on the use of pressurized CO₂ feed, the design of the pressurized flow reactor, and the arrangement of the catalysts. To accomplish these objectives, the dissertation delves into the following distinct but interconnected subtopics. The findings in each of these subtopics are presented as individual chapters in this thesis.

☞ In **Chapter 2**, a modular lab-scale CO₂RR flow reactor setup is presented, highlighting its performance under high pressure. Initially, we delve into the intricacies of the design of the whole setup, particularly addressing areas where high pressure presents an interesting design challenge. Subsequently, we validate the electrochemical behaviour of the reactor. Lastly, we showcase the reactor's adeptness in product characterization.

- ∞ In **Chapter 3**, the designed reactor is used to study the effect of pressure, current density, cation effects and electrolyte concentration on the electrochemical CO₂ reduction on a copper foam electrode.
- ∞ In **Chapter 4**, design of a novel elevated pressure sequential cascade reactor is described and used to investigate the synergistic role of high pressure on a silver – copper electrode pair in boosting the synthesis of higher alcohols during electrochemical CO₂ reduction.
- ∞ In **Chapter 5**, the main conclusions are drawn and a few recommendations for future research are presented.

1.10 References

- 1 Ju, J. & Kocaoglu, D. in Proceedings of PICMET '14 Conference: Portland International Center for Management of Engineering and Technology; Infrastructure and Service Integration.
- 2 Jana, A., Snyder, S. W., Crumlin, E. J. & Qian, J. Integrated carbon capture and conversion: A review on C₂+ product mechanisms and mechanism-guided strategies. *Frontiers in Chemistry*, **11**, 1135829-1135829, (2023). <https://doi.org/10.3389/FCHEM.2023.1135829/BIBTEX>
- 3 Kant, M. Corrigendum: Overcoming barriers to successfully commercializing carbon dioxide utilization. *Frontiers in Energy Research*, **6**, 375235-375235, (2018). <https://doi.org/10.3389/fenrg.2017.00022>
- 4 Shao, Y., Mirza, M. S. & Wu, X. CO₂ sequestration using calcium-silicate concrete. <https://doi.org/10.1139/L05-105>, **33**, 776-784, (2011). <https://doi.org/10.1139/L05-105>
- 5 Nitopi, S. *et al.* Progress and Perspectives of Electrochemical CO₂ Reduction on Copper in Aqueous Electrolyte. *Chemical Reviews*, **119**, 7610-7672, (2019). <https://doi.org/10.1021/acs.chemrev.8b00705>
- 6 Rahimi, M., Khurram, A., Hatton, T. A. & Gallant, B. Electrochemical carbon capture processes for mitigation of CO₂ emissions. *Chemical Society Reviews*, **51**, 8676-8695, (2022). <https://doi.org/10.1039/D2CS00443G>
- 7 Chen, C., Khosrowabadi Kotyk, J. F. & Sheehan, S. W. Progress toward Commercial Application of Electrochemical Carbon Dioxide Reduction. *Chem*, **4**, 2571-2586, (2018). <https://doi.org/10.1016/j.chempr.2018.08.019>
- 8 Liang, S., Altaf, N., Huang, L., Gao, Y. & Wang, Q. Electrolytic cell design for electrochemical CO₂ reduction. *Journal of CO₂ Utilization*, **35**, 90-105, (2019). <https://doi.org/10.1016/j.jcou.2019.09.007>
- 9 Qiao, J., Liu, Y., Hong, F. & Zhang, J. A review of catalysts for the electroreduction of carbon dioxide to produce low-carbon fuels. Vol. 43, (2014).
- 10 Zhu, Q. *et al.* Carbon dioxide electroreduction to C₂ products over copper-cuprous oxide derived from electrosynthesized copper complex. *Nature Communications*, **10**, (2019). <https://doi.org/10.1038/s41467-019-11599-7>
- 11 Jouny, M., Luc, W. & Jiao, F. General Techno-Economic Analysis of CO₂ Electrolysis Systems. *Industrial and Engineering Chemistry Research*, **57**, 2165-2177, (2018). <https://doi.org/10.1021/acs.iecr.7b03514>
- 12 Lin, R., Guo, J., Li, X., Patel, P. & Seifitokaldani, A. Electrochemical Reactors for CO₂ Conversion. *Catalysts* 2020, Vol. 10, Page 473, **10**, 473-473, (2020). <https://doi.org/10.3390/CATAL10050473>

- 13 Kibria, M. G. *et al.* Electrochemical CO₂ Reduction into Chemical Feedstocks: From Mechanistic Electrocatalysis Models to System Design. *Advanced Materials*, **31**, 1-24, (2019). <https://doi.org:10.1002/adma.201807166>
- 14 Lee, M. Y. *et al.* Current achievements and the future direction of electrochemical CO₂ reduction: A short review. *Critical Reviews in Environmental Science and Technology*, **50**, 769-815, (2020). <https://doi.org:10.1080/10643389.2019.1631991>
- 15 Salvatore, D. & Berlinguette, C. P. Voltage Matters When Reducing CO₂ in an Electrochemical Flow Cell. *ACS Energy Letters*, **5**, 215-220, (2020). <https://doi.org:10.1021/acsenergylett.9b02356>
- 16 Hori, Y. Electrochemical CO₂ Reduction on Metal Electrodes. *Modern Aspects of Electrochemistry*, 89-189, (2008). https://doi.org:10.1007/978-0-387-49489-0_3
- 17 Ouyang, Y., Shi, L., Bai, X., Li, Q. & Wang, J. Breaking scaling relations for efficient CO₂ electrochemical reduction through dual-atom catalysts. *Chemical Science*, **11**, 1807-1813, (2020). <https://doi.org:10.1039/C9SC05236D>
- 18 Abild-Pedersen, F. *et al.* Scaling properties of adsorption energies for hydrogen-containing molecules on transition-metal surfaces. *Physical Review Letters*, **99**, 016105-016105, (2007). <https://doi.org:10.1103/PHYSREVLETT.99.016105/FIGURES/3/MEDIUM>
- 19 Calle-Vallejo, F., Loffreda, D., Koper, M. T. M. & Sautet, P. Introducing structural sensitivity into adsorption–energy scaling relations by means of coordination numbers. *Nature Chemistry* **2015 7:5**, **7**, 403-410, (2015). <https://doi.org:10.1038/nchem.2226>
- 20 Göttle, A. J. & Koper, M. T. M. Proton-coupled electron transfer in the electrocatalysis of CO₂ reduction: prediction of sequential vs. concerted pathways using DFT. *Chemical Science*, **8**, 458-465, (2016). <https://doi.org:10.1039/C6SC02984A>
- 21 Zheng, T. *et al.* Large-Scale and Highly Selective CO₂ Electrocatalytic Reduction on Nickel Single-Atom Catalyst. *Joule*, **3**, 265-278, (2019). <https://doi.org:10.1016/j.joule.2018.10.015>
- 22 Chen, J. G. Electrochemical CO₂ Reduction via Low-Valent Nickel Single-Atom Catalyst. *Joule*, **2**, 587-589, (2018). <https://doi.org:10.1016/j.joule.2018.03.018>
- 23 Lin, S. *et al.* Covalent organic frameworks comprising cobalt porphyrins for catalytic CO₂ reduction in water. *Science*, **349**, 1208-1213, (2015). <https://doi.org:10.1126/science.aac8343>
- 24 Patra, K. K. & Gopinath, C. S. CO₂ electrolysis towards large scale operation: rational catalyst and electrolyte design for efficient flow-cell. *Chemical Communications*, **59**, 6774-6795, (2023). <https://doi.org:10.1039/D3CC01231J>
- 25 Rodriguez, P. & Koper, M. T. M. Electrocatalysis on gold. *Physical Chemistry Chemical Physics*, **16**, 13583-13594, (2014). <https://doi.org:10.1039/C4CP00394B>
- 26 Nitopi, S. *et al.* in *Chemical Reviews*, Vol. 119, 7610-7672, (American Chemical Society, 2019).
- 27 Dinh, C. T. *et al.* CO₂ electroreduction to ethylene via hydroxide-mediated copper catalysis at an abrupt interface. *Science*, **360**, 783-787, (2018). <https://doi.org:10.1126/science.aas9100>

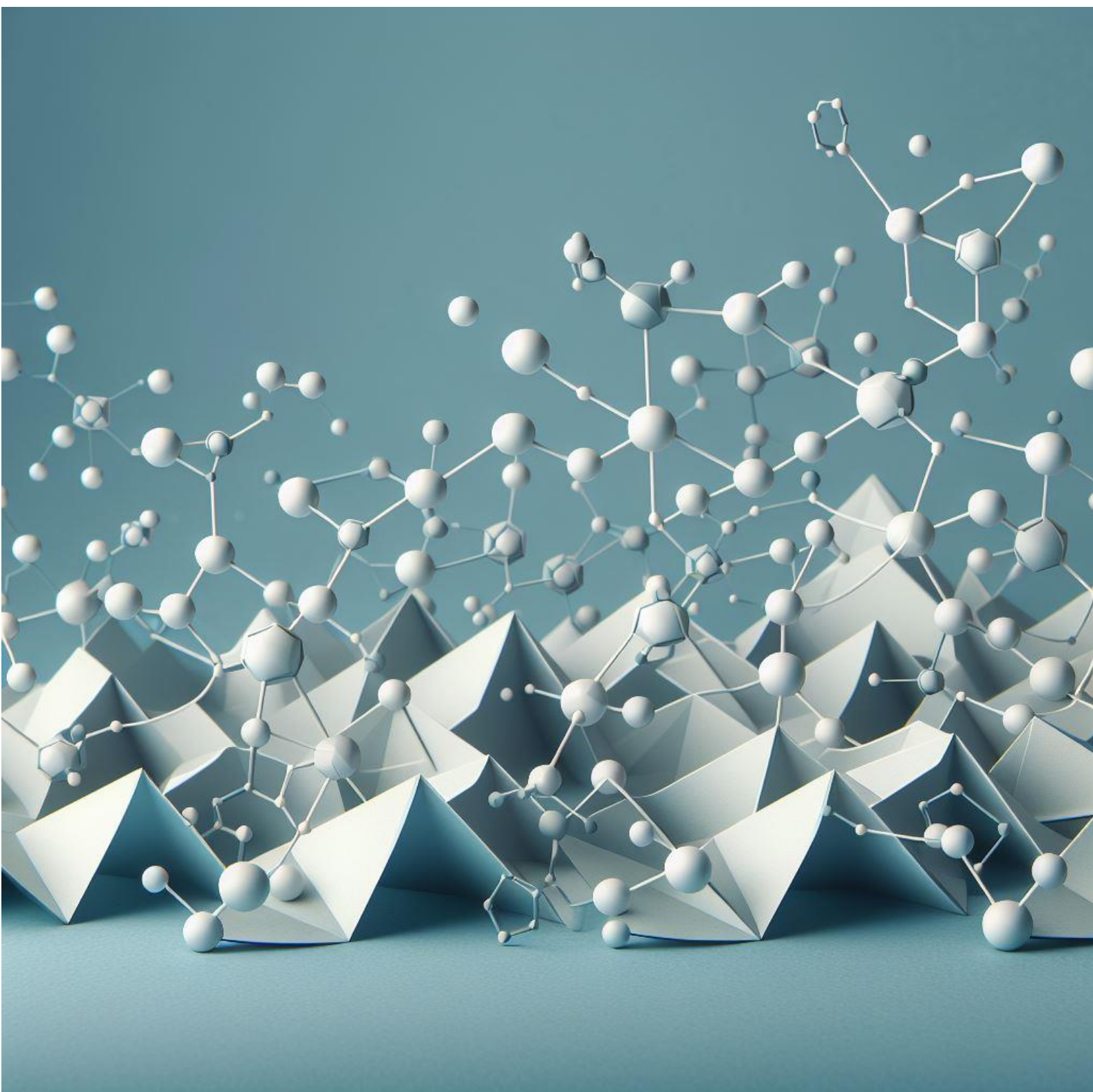
- 28 Man, I. C. *et al.* Universality in Oxygen Evolution Electrocatalysis on Oxide Surfaces. *ChemCatChem*, **3**, 1159-1165, (2011). <https://doi.org/10.1002/cctc.201000397>
- 29 Gao, D., Arán-Ais, R. M., Jeon, H. S. & Roldan Cuenya, B. in *Nature Catalysis*, Vol. 2, 198-210, (Nature Publishing Group, 2019).
- 30 Ross, M. B. *et al.* Designing materials for electrochemical carbon dioxide recycling. *Nature Catalysis*, **2**, 648-658, (2019). <https://doi.org/10.1038/s41929-019-0306-7>
- 31 Wang, X. *et al.* Mechanistic reaction pathways of enhanced ethylene yields during electroreduction of CO₂-CO co-feeds on Cu and Cu-tandem electrocatalysts. *Nature Nanotechnology*, **14**, 1063-1070, (2019). <https://doi.org/10.1038/s41565-019-0551-6>
- 32 Cuellar, N. S. R., Scherer, C., Kaçkar, B., Eisenreich, W. & Huber, C. Two-step electrochemical reduction of CO₂ towards multi-carbon products at high current densities. *Journal of CO₂ Utilization*, **36**, 263-275, (2020). <https://doi.org/10.1016/j.jcou.2019.10.016>
- 33 Chen, C. *et al.* Cu-Ag Tandem Catalysts for High-Rate CO₂ Electrolysis toward Multicarbon. *Joule*, (2020). <https://doi.org/10.1016/j.joule.2020.07.009>
- 34 Lum, Y. & Ager, J. W. Sequential catalysis controls selectivity in electrochemical CO₂ reduction on Cu. *Energy and Environmental Science*, **11**, 2935-2944, (2018). <https://doi.org/10.1039/c8ee01501e>
- 35 Gurudayal, G. *et al.* Sequential Cascade Electrocatalytic Conversion of Carbon Dioxide to C-C Coupled Products. *ACS Applied Energy Materials*, **2**, 4551-4559, (2019). <https://doi.org/10.1021/acsaem.9b00791>
- 36 Theaker, N. *et al.* Heterogeneously catalyzed two-step cascade electrochemical reduction of CO₂ to ethanol. *Electrochimica Acta*, **274**, 1-8, (2018). <https://doi.org/10.1016/j.electacta.2018.04.072>
- 37 Verma, S., Lu, S. & Kenis, P. J. A. Co-electrolysis of CO₂ and glycerol as a pathway to carbon chemicals with improved technoeconomics due to low electricity consumption. *Nature Energy*, **4**, 466-474, (2019). <https://doi.org/10.1038/s41560-019-0374-6>
- 38 Gao, J. *et al.* Selective C-C Coupling in Carbon Dioxide Electroreduction via Efficient Spillover of Intermediates As Supported by Operando Raman Spectroscopy. *Journal of the American Chemical Society*, **141**, 18704-18714, (2019). <https://doi.org/10.1021/jacs.9b07415>
- 39 Morrison, A. R. T., Girichandran, N., Wols, Q. & Kortlever, R. Design of an elevated pressure electrochemical flow cell for CO₂ reduction. *Journal of Applied Electrochemistry*, **1**, 1-10, (2023). <https://doi.org/10.1007/S10800-023-01927-7/FIGURES/8>
- 40 Hou, J., Chang, X., Li, J., Xu, B. & Lu, Q. Correlating CO Coverage and CO Electroreduction on Cu via High-Pressure in Situ Spectroscopic and Reactivity Investigations. *Journal of the American Chemical Society*, **144**, 22202-22211, (2022). <https://doi.org/10.1021/jacs.2c09956>

- 41 Garg, S. *et al.* Advances and challenges in electrochemical CO₂ reduction processes: An engineering and design perspective looking beyond new catalyst materials. *Journal of Materials Chemistry A*, **8**, 1511-1544, (2020). <https://doi.org:10.1039/c9ta13298h>
- 42 Alvarez-Guerra, M., Quintanilla, S. & Irabien, A. Conversion of carbon dioxide into formate using a continuous electrochemical reduction process in a lead cathode. *Chemical Engineering Journal*, **207-208**, 278-284, (2012). <https://doi.org:10.1016/j.cej.2012.06.099>
- 43 Kuhl, K. P., Cave, E. R., Abram, D. N. & Jaramillo, T. F. New insights into the electrochemical reduction of carbon dioxide on metallic copper surfaces. *Energy and Environmental Science*, **5**, 7050-7059, (2012). <https://doi.org:10.1039/c2ee21234j>
- 44 Whipple, D. T., Finke, E. C. & Kenis, P. J. A. Microfluidic reactor for the electrochemical reduction of carbon dioxide: The effect of pH. *Electrochemical and Solid-State Letters*, **13**, 109-111, (2010). <https://doi.org:10.1149/1.3456590>
- 45 Varela, A. S., Kroschel, M., Reier, T. & Strasser, P. Controlling the selectivity of CO₂ electroreduction on copper: The effect of the electrolyte concentration and the importance of the local pH. *Catalysis Today*, **260**, 8-13, (2016). <https://doi.org:10.1016/J.CATTOD.2015.06.009>
- 46 Kas, R. *et al.* Electrochemical CO₂ reduction on Cu₂O-derived copper nanoparticles: controlling the catalytic selectivity of hydrocarbons. *Physical Chemistry Chemical Physics*, **16**, 12194-12201, (2014). <https://doi.org:10.1039/C4CP01520G>
- 47 Vennekötter, J. B., Scheuermann, T., Sengpiel, R. & Wessling, M. The electrolyte matters: Stable systems for high rate electrochemical CO₂ reduction. *Journal of CO₂ Utilization*, **32**, 202-213, (2019). <https://doi.org:10.1016/j.jcou.2019.04.007>
- 48 Monteiro, M. C. O. *et al.* Absence of CO₂ electroreduction on copper, gold and silver electrodes without metal cations in solution. *Nature Catalysis*, **4**, 654-662, (2021). <https://doi.org:10.1038/s41929-021-00655-5>
- 49 Gu, J. *et al.* Modulating electric field distribution by alkali cations for CO₂ electroreduction in strongly acidic medium. *Nature Catalysis* 2022 5:4, **5**, 268-276, (2022). <https://doi.org:10.1038/S41929-022-00761-Y>
- 50 Resasco, J. *et al.* Promoter Effects of Alkali Metal Cations on the Electrochemical Reduction of Carbon Dioxide. *Journal of the American Chemical Society*, **139**, 11277-11287, (2017). https://doi.org:10.1021/JACS.7B06765/SUPPL_FILE/JA7B06765_SI_001.PDF
- 51 Ringe, S. *et al.* Understanding cation effects in electrochemical CO₂ reduction. *Energy & Environmental Science*, **12**, 3001-3014, (2019). <https://doi.org:10.1039/C9EE01341E>
- 52 Singh, M. R., Kwon, Y., Lum, Y., Ager, J. W. & Bell, A. T. Hydrolysis of Electrolyte Cations Enhances the Electrochemical Reduction of CO₂ over Ag and Cu. *Journal of the American Chemical Society*, **138**, 13006-13012, (2016). <https://doi.org:10.1021/jacs.6b07612>

- 53 Kyriacou, G. Z. & Anagnostopoulos, A. K. Influence CO₂ partial pressure and the supporting electrolyte cation on the product distribution in CO₂ electroreduction. *Journal of Applied Electrochemistry*, **23**, 483-486, (1993). <https://doi.org:10.1007/BF00707626>
- 54 Varela, A. S. The importance of pH in controlling the selectivity of the electrochemical CO₂ reduction. *Current Opinion in Green and Sustainable Chemistry*, **26**, 100371-100371, (2020). <https://doi.org:10.1016/J.COOGSC.2020.100371>
- 55 Liu, X., Monteiro, M. C. O. & Koper, M. T. M. Interfacial pH measurements during CO₂ reduction on gold using a rotating ring-disk electrode. *Physical Chemistry Chemical Physics*, **25**, 2897-2906, (2023). <https://doi.org:10.1039/D2CP05515E>
- 56 Kastlunger, G., Heenen, H. H. & Govindarajan, N. Combining First-Principles Kinetics and Experimental Data to Establish Guidelines for Product Selectivity in Electrochemical CO₂ Reduction. *ACS Catalysis*, **13**, 5062-5072, (2023). https://doi.org:10.1021/ACSCATAL.3C00228/ASSET/IMAGES/LARGE/CS3C00228_0005.JPEG
- 57 Gupta, N., Gattrell, M. & MacDougall, B. Calculation for the cathode surface concentrations in the electrochemical reduction of CO₂ in KHCO₃ solutions. *Journal of Applied Electrochemistry*, **36**, 161-172, (2006). <https://doi.org:10.1007/S10800-005-9058-Y/METRICS>
- 58 Liu, X. *et al.* pH effects on the electrochemical reduction of CO(2) towards C2 products on stepped copper. *Nature Communications* 2019 10:1, **10**, 1-10, (2019). <https://doi.org:10.1038/s41467-018-07970-9>
- 59 Hori, Y., Murata, A. & Takahashi, R. Formation of hydrocarbons in the electrochemical reduction of carbon dioxide at a copper electrode in aqueous solution. *Journal of the Chemical Society, Faraday Transactions 1: Physical Chemistry in Condensed Phases*, **85**, 2309-2326, (1989). <https://doi.org:10.1039/F19898502309>
- 60 Clark, E. L. & Bell, A. T. Direct Observation of the Local Reaction Environment during the Electrochemical Reduction of CO₂. *Journal of the American Chemical Society*, **140**, 7012-7020, (2018). https://doi.org:10.1021/JACS.8B04058/ASSET/IMAGES/LARGE/JA-2018-040588_0009.JPEG
- 61 Tan, Y. C., Lee, K. B., Song, H. & Oh, J. Modulating Local CO₂ Concentration as a General Strategy for Enhancing C-C Coupling in CO₂ Electroreduction. *Joule*, **4**, 1104-1120, (2020). <https://doi.org:10.1016/J.JOULE.2020.03.013>
- 62 Hashiba, H., Yotsuhashi, S., Deguchi, M. & Yamada, Y. Systematic Analysis of Electrochemical CO₂ Reduction with Various Reaction Parameters using Combinatorial Reactors. *ACS Combinatorial Science*, **18**, 203-208, (2016). <https://doi.org:10.1021/acscombsci.6b00021>

- 63 Hara, K., Tsuneto, A., Kudo, A. & Sakata, T. Electrochemical Reduction of CO₂ on a Cu Electrode under High Pressure: Factors that Determine the Product Selectivity. *Journal of The Electrochemical Society*, **141**, 2097-2103, (1994). <https://doi.org:10.1149/1.2055067>
- 64 Kas, R., Kortlever, R., Yilmaz, H., Koper, M. T. M. & Mul, G. Manipulating the Hydrocarbon Selectivity of Copper Nanoparticles in CO₂ Electroreduction by Process Conditions. *ChemElectroChem*, **2**, 354-358, (2015). <https://doi.org:10.1002/celec.201402373>
- 65 Wang, L. *et al.* Electrochemical Carbon Monoxide Reduction on Polycrystalline Copper: Effects of Potential, Pressure, and pH on Selectivity toward Multicarbon and Oxygenated Products. *ACS Catalysis*, **8**, 7445-7454, (2018). <https://doi.org:10.1021/acscatal.8b01200>
- 66 Ramdin, M. *et al.* High-Pressure Electrochemical Reduction of CO₂ to Formic Acid/Formate: Effect of pH on the Downstream Separation Process and Economics. *Industrial and Engineering Chemistry Research*, **58**, 22718-22740, (2019). <https://doi.org:10.1021/acs.iecr.9b03970>
- 67 Shen, J. *et al.* Electrocatalytic reduction of carbon dioxide to carbon monoxide and methane at an immobilized cobalt protoporphyrin. *Nature Communications* 2015 6:1, **6**, 1-8, (2015). <https://doi.org:10.1038/ncomms9177>
- 68 Welch, L. M., Vijayaraghavan, M., Greenwell, F., Satherley, J. & Cowan, A. J. Electrochemical carbon dioxide reduction in ionic liquids at high pressure. *Faraday Discussions*, **230**, 331-343, (2021). <https://doi.org:10.1039/D0FD00140F>
- 69 Hara, K., Tsuneto, A., Kudo, A. & Sakata, T. Electrochemical Reduction of CO₂ on a Cu Electrode under High Pressure: Factors that Determine the Product Selectivity. *Journal of the Electrochemical Society*, **141**, 2097-2103, (1994). <https://doi.org:10.1149/1.2055067>
- 70 Li, J. *et al.* Electroreduction of CO₂ to Formate on a Copper-Based Electrocatalyst at High Pressures with High Energy Conversion Efficiency. *Journal of the American Chemical Society*, **142**, 7276-7282, (2020). <https://doi.org:10.1021/jacs.0c00122>

Chapter 2 : Design of an Elevated Pressure Electrochemical Flow Cell for CO₂ Reduction



ABSTRACT

The electrochemical CO₂ reduction reaction (CO₂RR) has been proposed as a sustainable way of closing the carbon cycle while synthesizing useful commodity chemicals. One of the possible routes to scale up the process is the elevated pressure CO₂RR, as this increases the concentration of the poorly soluble CO₂ in aqueous systems. Yet, there are not many studies that focus on this route owing to the inherent challenges with high pressure systems. In this study, a novel high pressure flow cell setup has been designed and validated. The modular design uses a clamp system, which facilitates simple stacking of multiple cell parts while being capable of handling pressures up to 50 bar. The effects of CO₂ pressure on the reaction were investigated on a gold (Au) foil cathode in a 0.1 M KHCO₃ electrolyte. We successfully measured gaseous products produced during high pressure operation using an inline gas chromatograph. We find that the selectivity toward CO₂ reduction products is enhanced while that of H₂ evolution is suppressed as the pressure is increased from 2 to 30 bar. The reported setup provides a robust means to conduct high pressure electrolysis experiments in an easy and safe manner, making this technology more accessible to the electrochemical CO₂RR community.

This chapter is based on the article:

Morrison, A.R.T., Girichandran, N., Wols, Q. *et al.* Design of an Elevated Pressure Electrochemical Flow Cell for CO₂ Reduction. *J Appl Electrochem* 53, 2321–2330 (2023).

<https://doi.org/10.1007/s10800-023-01927-7>.

2.1 Introduction

With climate change and global warming becoming an obvious reality, there is widespread agreement that immediate action is needed to control greenhouse gases emissions. One of the primary greenhouse gases is carbon dioxide (CO_2), a highly stable and therefore difficult molecule to break down. However, under the right conditions there are routes to reduce CO_2 and generate valuable hydrocarbons that can be used as fuel or feedstock for further processing¹. CO_2 can be converted to other chemicals in a variety of processes utilizing thermochemical devices (e.g., reverse water-gas shift reactors)²⁻⁵ or through bioreactors⁶. However, one of the most promising routes is the electrochemical CO_2 reduction reaction (CO_2RR). This process directly utilizes electrical energy to convert CO_2 into useful chemicals and has the potential to be completely sustainable by deriving energy directly from renewable sources like solar, wind, and geothermal⁷.

The CO_2RR has been well studied at the laboratory scale. The developed understanding of reaction mechanisms has allowed significant advances to be made in catalyst development⁸⁻¹¹. However, the large-scale industrial deployment of the CO_2RR is hindered by several factors including, but not limited to, the poor solubility of CO_2 that causes mass transfer limitation and lowers reaction rates, poor product selectivities and unstable electrocatalysts owing to their deactivation or morphological changes during the reaction^{12,13}. Development of catalysts has made several important advances in H-cell type experimental configurations. However, different configurations are required because the H-cell is not an appropriate environment to test catalysts for commercial application where typically, 200 mA/cm^2 partial current density of product is required^{14,15}. Moreover, besides the choice of electrocatalyst, factors such as the

electrolyser design, electrolyte choice, and optimal operating conditions (pH, temperature, pressure, mass transport conditions) play a crucial role in determining the outcome of the reaction¹⁶⁻²⁰. Therefore, there is a need to examine the CO₂RR under more combinations of conditions that are likely to be encountered in scalable and industrially relevant electrolysers, and to test electrocatalytic materials under these operating conditions.

Due to the low solubility of CO₂ in aqueous electrolytes, delivering sufficient CO₂ to the surface of the electrode to avoid mass transport limitations is pivotal for operating CO₂RR at industrial scales. Currently, there are several reactor designs that solve this problem, the most popular being the gas diffusion electrode (GDE) based electrolysers, which deliver gaseous CO₂ through the porous GDE to the catalysts layer that in turn is in contact with the liquid electrolyte^{21,22}. Electrolyser designs such as Taylor flow cells²³, or porous electrode cells²⁴ use a similar concept by providing gaseous CO₂ as directly as possible to the catalyst sites (thereby not depending on dissolved CO₂ from the bulk of the electrolyte). These technologies solve the issue of poor CO₂ solubility by increasing the effective rate of diffusion of CO₂. Alternately, the concentration of CO₂ in the electrolyte can be increased. This can be done by either using non-aqueous electrolytes with higher CO₂ solubilities^{16,25,26} or pressing more CO₂ into the solution by applying an elevated CO₂ pressure²⁷. Elevated pressure electrolysers have been mentioned as one of the more promising routes to industrialize the CO₂RR²⁸. These are two different approaches to CO₂RR reactors. In the GDE design CO₂ can be delivered to (near) the electrode as a gas, and the electrode is a porous membrane assembly. In contrast the high-pressure systems operate with two parallel plate electrodes, and CO₂ is delivered dissolved in the electrolyte. Despite the promise of this type of reactor design, the number of studies that focus on high-pressure CO₂RR is very limited in comparison to GDE based electrolysers. A

possible explanation for this is the challenges that working at elevated pressure poses to the average laboratory team. Here, we report the design of a modular elevated pressure CO₂RR reactor, which can serve as a guide to explore this promising field.

Studying the CO₂RR at elevated pressure has a long history²⁹, and the reactors in previous work on the subject can be divided into two categories: autoclave reactors³⁰⁻³², and larger scale flow cells³³⁻³⁹. The autoclave reactors are essentially normal laboratory scale electrochemical H-cells, or three electrode cells put into a pressurized box. These cells generally have reference electrodes and are operated fully in batch mode with small electrode areas. They have been used to find very high faradaic efficiencies toward both CO, formate and C₂₊ chemicals, dependent on catalyst choice^{30,31,40}. Importantly, they have also been used to demonstrate the potential capability of elevated pressure CO₂RR to deliver on the requirements for a commercial electrolyser, that is 200 mA/cm² partial current density. The larger scale flow cells represent a more industrial kind of reactor and were used to answer questions regarding the scaling up of elevated pressure CO₂ electrolysers. The electrode areas are significantly larger than with the autoclave reactors, with most studies using at least a tenfold higher electrode surface area. The flow cells universally do not have reference electrodes and are operated galvanostatically, which makes it difficult to compare product selectivities and production rates with other systems. Additionally, since the product selectivities and reaction rates are so potential dependent in the CO₂RR, these cell designs can only give limited fundamental insight into the CO₂RR at elevated pressures. A table summarizing the characteristics and obtained results compared with a few other elevated pressure cells from literature can be found in the supplementary information (see **supplementary information (SI) 2.4.5**). High faradaic efficiencies (FE) were obtained in these cells, but

the current densities of the most successful autoclave style cells have never been reached in parallel plate flow reactors ($200 \text{ mA}\cdot\text{cm}^{-2}$ for autoclave and $< 50 \text{ mA}\cdot\text{cm}^{-2}$ for larger flow cells). This shows that scaling up of high-pressure CO_2 electrolyzers is not straightforward. The difficulty in scaling from a small autoclave cell to a large industrial-style cell presents a clear need for an intermediary type of reactor. Furthermore, the challenges in achieving the same order of magnitude current densities in large flow cells as were observed in autoclave cells shows there are parameters of the design which have not been fully understood. The only way to study these parameters is to first develop a laboratory version of such a cell. Such a flexible flow reactor of moderate size with a reference electrode can potentially yield information about how to scale up the elevated pressure CO_2RR . Here, we report on the design of a modular, laboratory size CO_2RR flow reactor and will demonstrate its performance for CO_2RR experiments at elevated pressures. First, the design of the cell is discussed with a special focus on the areas where high pressure presents an interesting design challenge, then the electrochemical behaviour of the reactor is verified, and finally the product characterization capability.

2.2 Experimental Section

2.2.1 Materials

Potassium bicarbonate (KHCO_3 , $\geq 99.95\%$ trace metals basis, $99.7\text{-}100.5\%$ dry basis) was used to prepare both a 0.1 M KHCO_3 anolyte and catholyte. The working electrode used for electrochemical experiments was a gold foil cathode (99.9% , Mateck GmbH) and IrMMO coated titanium foil^{41,42} (MAGNETO special anodes B.V, The Netherlands) was used as the counter electrode. Nafion 117 (Ion Power GmbH) was cleaned in MilliQ water and used as the ion exchange membrane. For testing the reference electrode potential versus pressure, a solution of

0.01 M of $\text{K}_4\text{Fe}(\text{CN})_6 \cdot 3\text{H}_2\text{O}$ ($\geq 99.95\%$ trace metals basis, Sigma Aldrich) and 0.05 M of KNO_3 (ACS reagent, $\geq 99.0\%$, Sigma Aldrich) was used as standard. An ultrapure water purification system (MilliQ IQ 7000, Merck–Millipore, USA) was used as water source for all experiments. All reagents were used without further purification.

2.2.2 Electrochemical Measurements

Electrochemical experiments were conducted using a Bio-Logic SP300 dual-channel potentiostat with an EIS analyser. 1 cm^2 electrodes were secured in place by creating slots in stainless steel endplates (see SI 2.4.1 for an exploded view of the reactor). The PEEK flow plates for the anolyte and catholyte have an internal volume of ($\sim 0.79 \text{ cm}^3$). Nafion 117 served as the separator between the two chambers. For all experiments, a miniaturized leakless Ag/AgCl reference electrode (LF 1.6 – 45 mm, Innovative Instruments, Inc., USA) was used as the reference electrode. The body of the electrode houses the silver wire in a tube made from PEEK with the junction at the end and is described by the manufacturer as non-porous and conductive. The tip at the head is a gold-plated connector. The reference electrode was carefully stored in a 3.5 M KCl solution between experiments and its potential was carefully monitored against a master reference electrode. Since the performance of these electrodes is unknown at elevated pressure, we performed experiments to test their stability at 2, 5, 10, 15, 20, 25, and 30 bar. All potentials are reported versus the Ag/AgCl electrode. Experiments were all conducted at 30 bar or less for safety reasons, although the system was pressure tested up to 50 bar. CO_2RR experiments were conducted at different pressures (2, 5, 15, and 30 bar) by applying a constant current of 10 mA/cm^2 to validate the system. The apparatus is sized for operation up to 200 mA/cm^2 , but this lower current density is selected as a trade-off between testing the system at a stable, well

characterized regime and the desire for high current density. The cell resistance was monitored by carrying out a potentiostatic electrochemical impedance spectroscopy (see SI 2.4.2).

2.2.3 Product analysis

An inline gas chromatograph (CompactGC 4.0, Global Analyzer Solutions, The Netherlands) was used to measure the gaseous products synthesized during the reaction. Gas cylinders (Linde Gas Benelux B.V., The Netherlands) containing custom gas mixtures of different product gases with a range of 50-8000 ppm in CO₂ were used to calibrate the GC. The gas products were analysed every 2 minutes. The GC consists of 2 TCD detectors (one each for CO and H₂) and an FID detector to analyse hydrocarbons (C₁ - C₆). The FID channel comprises of an Rtx-1, 5.00 μm (15 m * 0.32 mm) analytical column, the first TCD channel consists of a Carboxen 1010 (3 m * 0.32 mm) pre-column and a Molsieve 5A (5 m * 0.32 mm) analytical column, and the second TCD channel consists of a Carboxen 1010 (3 m * 0.32 mm) pre-column and a Molsieve 5A (7 m * 0.32 mm) analytical column. They help in the separation of the components before entering the respective channel detectors.

HPLC (Agilent Technologies 1260 Infinity, USA), was used for the analysis of liquid products collected after the completion of the reaction. Standard solutions of the desired chemicals (formic acid >98%, Sigma-Aldrich, USA) were used for the calibration with dissolutions ranging from 0.1 mM to 50 mM. 5 μL of the product sample was injected into a series of Aminex HPX-87H columns (Biorad) which were heated to a temperature of 60°C using a 1 mM H₂SO₄ solution as eluent. A Refractive Index Detector (RID) was used for the detection of the products.

2.3 Results and Discussion

2.3.1 Apparatus Design

The goal of the designed and reported setup is to enable the study of the CO₂RR at different pressures in a cell that can be used to study parameters important for scaling up electrolyser design, while being at a more manageable lab scale. Simultaneously, the design will combine

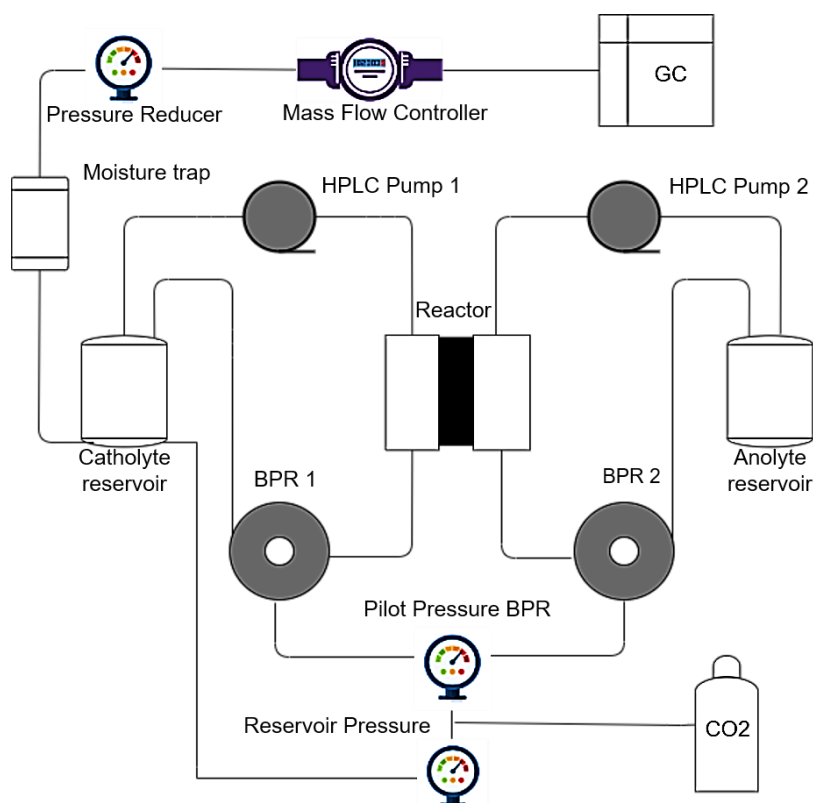


Figure 2.1: A schematic of the experimental setup is presented here to study the CO₂RR at elevated pressures. The system consists of the reactor which has two compartments separated by a membrane, both of which have electrolyte constantly feed into them from separate reservoirs, and a line from the catholyte reservoir into a gas chromatograph for inline product analysis. The pressures of the reactor and the two reservoirs can be controlled independently.

operation at elevated pressure with characterization capabilities typical for a normal lab cell potential measurement via a reference electrode and product characterization via gas chromatography at time scales not significantly different than a standard experiment.

A schematic of the design of the entire system can be found in **Figure 2.1**. The reactor is a membrane-separated parallel plate flow cell with two pressurized external reservoirs. The electrolyte is pumped from the reservoir to the reactor, through a back-pressure regulator, and then back into the external reservoir at a flow rate 25 ml/min. Gas is pressurized into the reservoir at a controlled rate through a pressure controller (Bronkhorst HighTech BV, The Netherlands, and Pressure Control Solutions BV), and the gas outlet is directed to the inline GC. Thus, CO₂ consumed in the reactor is continuously replaced by the gas inlet. Several design choices are discussed below, and for detailed parts of the reactor please see **SI 2.4.1** of the supplementary information.

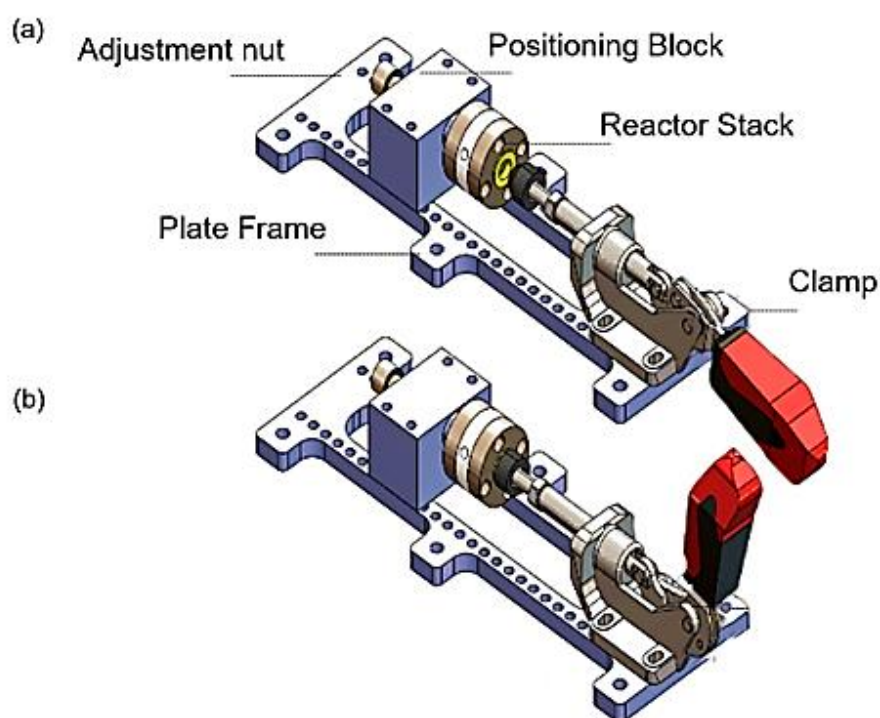


Figure 2.2: Renderings of the mechanical drawings of the reactor and compression system. The system is easy to assemble and disassemble, facilitated by the clamped design, and different segments can be easily added to the reactor stack as required. (a) Closed position, (b) Open position of the clamp.

2.3.2 Reactor Assembly Design

A notable element of the design of the reactor is the clamp system for containing the pressure in the reactor, inspired by Branch et al.⁴³. From our experience, the design of a reactor that relies on nuts and bolts to contain the pressure (or just the electrolyte for atmospheric cells) is extremely time-consuming. In this regard, the clamp element of the design significantly increases the speed of assembly of the reactor. The turnaround time for experiments is extremely important because it will directly influence how many experiments can be performed on an apparatus. The clamp design also allows for flexibility in cell design. If the end plates have adaptors for the linear bearings and the size is compatible, any cell can be inserted into the clamp system and have its pressure contained.

2.3.3 Reference Electrode

The lack of reference electrodes (REs) in high pressure CO₂ electrolyzers indicates that there is a major challenge with adding them to these systems. Indeed, there are costly (compared to standard REs) commercial options available that are meant to be appropriate REs for high pressure systems. The major challenge that justifies the increased costs is the gases dissolved in the electrolyte at high pressure. If the gases infiltrate the reference electrode and the system is depressurized too quickly the gases do not have time to escape, and they can damage the frit or the casing of the electrode. However, the best solution is that high-pressure gases are not allowed to penetrate inside the RE in the first place. For this reason, we tested “leak-free” REs, that showed to avoid these issues at pressures tested here. In order to check the performance and stability, the leak-free Ag/AgCl RE was tested before and after each experiment with respect to a master RE. Open Circuit Voltage (OCV) measurements were carried out to check if the drift in potential was within acceptable limits (max variation $\leq 2\text{-}3\text{ mV}$)⁴⁴. Even though

it is difficult to predict how much drift in potential will occur after each experiment, it is wise to monitor this to ensure the electrode's proper functioning (especially, at higher pressures).

2.3.4 Pressure Regulation

The design of the pressure regulation system has many components that must be considered. For the system to be an elevated pressure CO₂ electrolyser it must be able to deliver electrolyte saturated with CO₂ at a controllable pressure to the cathode surface. This means there will be a part of the system to dissolve CO₂ at the required pressure and transport it to the cathode. Pressing CO₂ into the electrolyte is accomplished by a pressure chamber, but keeping the reactor pressurized presents a slightly different challenge because the system accommodates a divided reactor with a membrane separating catholyte and anolyte. If the pressure is unbalanced, then the membrane will break or stretch and contact one of the electrodes. Therefore, either a mechanically re-enforced membrane must be used, possibly hampering the other important properties of the membrane or the pressure must be balanced. Here, we opted for a dual back pressure regulator in the system. These ensure a balanced pressure across the membrane if the electrolyte is flowing. This is accomplished by piloting the dual back pressure regulator under the same pressure, which means they will enforce the same back pressure at their inlets. The dual back pressure regulator also allows for independent control of the pressure in the reactor and the pressure reservoir. Thus, allowing the separation of the effects of mechanical and gaseous pressure on the CO₂RR. It also allows the reactor to be kept at a pressure high enough to prevent the degasification of the electrolyte in a reactor that is hotter than the reservoir (due to resistive heating at high current density), which will decrease the solubility of CO₂ locally.

2.3.5 Reservoir Sizing

There is a trade-off in deciding the size of the external reservoir. A smaller reservoir will result in more accurate HPLC measurements for quantification of liquid products. A larger reservoir is necessary for longer operating times so that the consumption of water for the CO₂RR does not significantly concentrate the electrolyte over the course of the experiment. Further, in both cases the gas headspace of the reservoir must be minimized to equilibrate GC measurements as quickly as possible. The reservoir was therefore designed to be flexible. In this work it was configured to have 20 ml of electrolyte in total (including electrolyte in the reactor and tubing) to favour longer operation and because quantification of liquid products was less important for these tests. With 20 ml of electrolyte the reactor can continuously operate for 2.5 days at 200 mA/cm² before it consumes 5% of the water in the system. The gas headspace used was 2 ml. Since there are no trade-offs for the gas headspace, this represents the smallest volume which avoided liquid entering the pathway to the GC.

2.3.6 Pump Sizing

The options for pumps that operate in the desired pressure range are relatively small at flow rates interesting in laboratory experiments. There are two factors to consider when selecting pump size. First, the diffusion layer thickness – faster pumping can lead to a thinner diffusion layer and thus faster CO₂RR. To meaningfully study this parameter requires a combination of a very fast pump and a cell with a low volume. The second factor to consider is the rate of consumption of CO₂ in the reactor. The CO₂ concentration falls through the reactor as the reaction proceeds. One of the parameters that can be used to determine by how much this has changed is the flow rate which is set by the pump. The selected pump needed to study the effect of flow rate should be able to pump the liquid fast enough so that the concentration of CO₂

leaving the reactor is close enough to the concentration at the entrance. Then the pump's operational range will cover the area where this effect can be studied well. The pump speed in this work was selected to consider the latter effect because the pump rates to effect diffusion layer thickness are large. The pumps selected are capable of pump speeds up to 50 ml/min, but 25 ml/min during long term operation. At the maximum continuous pumping rate this will be able to keep the CO₂ concentration in the electrolyte in the reaction chamber at more than 95% of the reservoir concentration for currents lower than 500 mA/cm² at pressures of 5 bar and up, allowing for a wide range of operation before consuming the CO₂ in the reactor becomes an issue.

2.3.7 General Operation

The reactor performs well and as expected in general function. Notably, the clamp system is successful in minimizing the turnaround time of experiments. The time to depressurize, disassemble, exchange electrolyte, and reassemble was, at quickest, half an hour, which is superior to several atmospheric cell designs and significantly better than other pressurized systems. The system was pressure tested with hydrostatic pressure up to 50 bar, the eventual desired pressure range, so it will function up to that pressure even though in the following experiments pressures were limited to 30 bar or less.

2.3.8 Effect of Pressure on Reference Electrode Potential

The RE's functioning was tested in a solution of 0.01 M K₄Fe(CN)₆·3H₂O and 0.05 M KNO₃. **Figure 2.3** is a plot of the peak potential of ferrocyanide oxidation versus the reactor pressure (mechanical pressure) and **Figure 2.4** displays the equilibrium potential vs. the reservoir pressure (gas pressure). In both cases there is less than 10 mV drift in potential as pressure above atmospheric is first applied for both mechanical and gas pressure. The potential of the RE first

creeps upwards before stabilizing after the pressure reaches 10 bar, for both the reactor and reservoir pressure. **Figure 2.3** and **Figure 2.4** show that the RE potential does not depend on the applied pressure, either mechanical pressure or with dissolved gases, as otherwise there

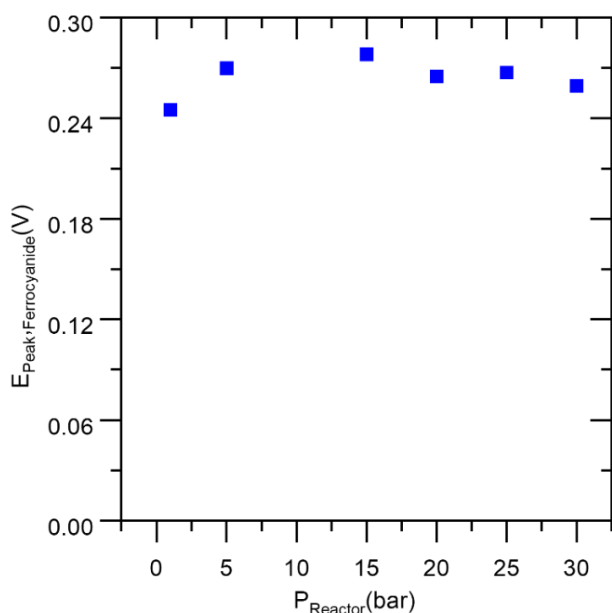


Figure 2.3: Reactor pressure versus peak potential of 0.01 M ferrocyanide oxidation in 0.05 M potassium nitrate. There is a very small increase in the potential from atmospheric pressure to 5 bar, but it is very stable at higher pressures.

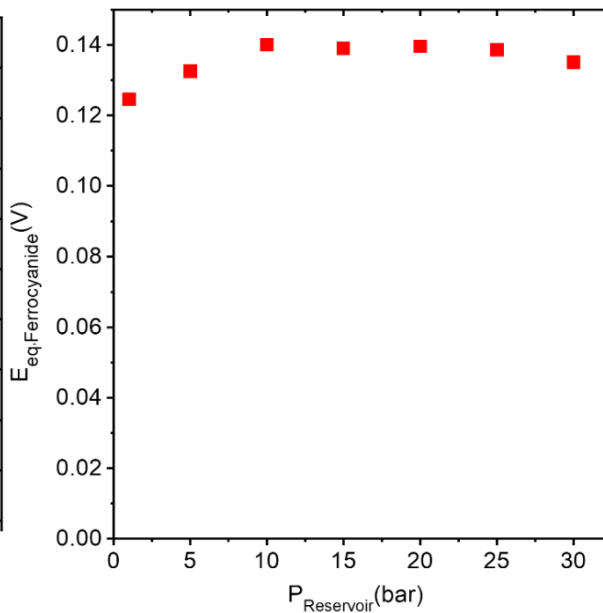


Figure 2.4: Reservoir pressure versus equilibrium potential of 0.1 M ferrocyanide oxidation in 0.005 M potassium nitrate. There is a very small increase in the potential from atmospheric pressure to 10 bar, but it is very stable at higher pressures.

would be a difference in the way that pressure affects these two sets of potentials. No instabilities or potential drifts due to the earlier mentioned crossover of dissolved gasses into the RE were observed. Therefore, the leak-free RE works as it is supposed to and can be used in elevated pressure experiments.

2.3.9 Electrochemical Measurements

Electrochemical tests were performed at several different pressures and across a wide range of electrode voltages. **Figure 2.5** displays the linear sweep voltammograms (LSV) of a polycrystalline Au foil electrode in a 0.1 M KHCO_3 electrolyte at different CO_2 pressures. As shown, increasing the pressure leads to an increase in current density across all potentials, indicating a

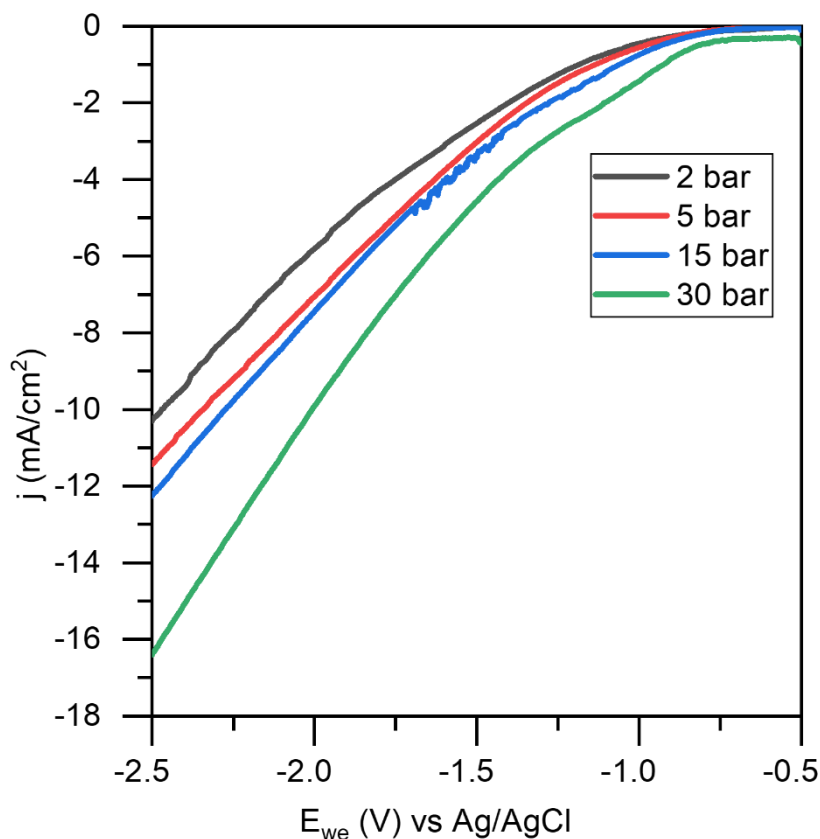


Figure 2.5: LSV polarization curves at 10 mV s^{-1} on an Au foil electrode in a 0.1 M KHCO_3 electrolyte under applied CO_2 pressures of 2, 5, 15, and 30 bar. The current density increases as expected with pressure.

direct relationship between the CO_2RR and the concentration of CO_2 in the electrolyte. Similar behaviour has been reported a silver plate electrode in the work of Federica et al., but without a RE⁴⁵.

The other important element of this experimental setup is product characterization. To test that aspect, chronopotentiometry was carried out at -10 mA cm^{-2} for different pressures (namely 2, 5, 15, and 30 bar) and the faradaic efficiencies of different products were measured. A current density of -10 mA cm^{-2} is specifically chosen as a typical current density observed in CO_2RR studies. The main importance of the experiments is to confirm that we can observe the pressure effect on the CO_2RR . Further optimization of the pressure effect is possible, as can be

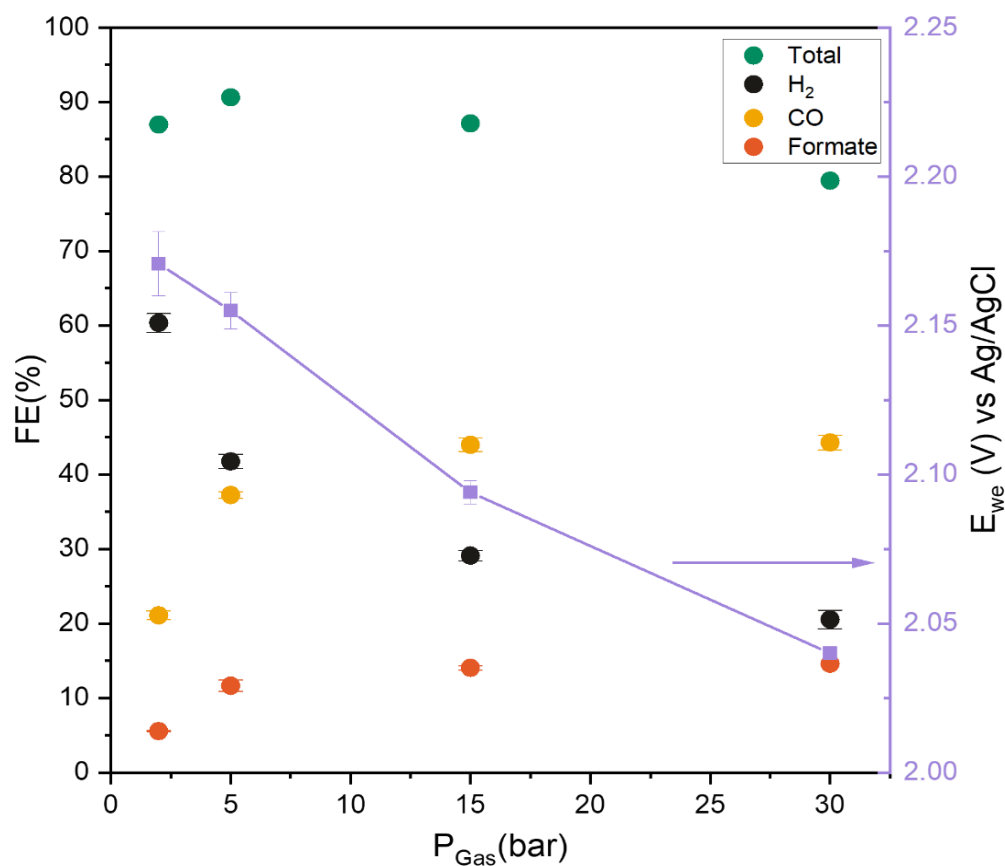


Figure 2.6: Faradaic efficiencies (left axis) of carbon monoxide, hydrogen, formate, and the total FE on Au foil and potential (right axis) at a current density of 10 mA/cm² in a 0.1 M KHCO₃ electrolyte at applied CO₂ pressures of 2, 5, 15, and 30 bar.

seen elsewhere but will be left for future work with this apparatus. The results of the experiments can be seen in **Figure 2.6**. As expected, there is a positive relationship between pressure and the FE for the CO₂RR products while the HER is suppressed. The main products detected include H₂, CO, and formate. As shown, increasing the pressure from 2 to 30 bar decreased the selectivity of H₂ from about 60% to 20% while increasing the selectivity toward CO and formate, with the effect being more drastic at lower applied pressures. This is expected because the concentration of CO₂ increases with a rise in pressure, leading to improved reactant availability and mass transport. Also notable in **Figure 2.6** and more importantly in terms of reactor design, at 5 bar there is 92% closure of the charge balance, which drops to 80% of charge accounted for at 30 bar. The drop in FE at the highest pressure is not completely explained in

our data. However, the charge balance was certainly more difficult to close at higher pressure. Great care needed to be taken to eliminate leaks, since the effect of these is only magnified at high pressure. Additionally, a more stable pressure control system removed pressure oscillations which disrupted measurements more significantly at high pressures. Aside from these, there are other effects which can prevent closing the charge balance completely that are challenging to address: gas permeation (especially H₂) through the Nafion membrane or into the O-rings^{46,47}, several C₂₊ products are more likely to form at higher pressure²⁷ but could be present below the quantification limit, and difficult to detect leaks may still be present. Even if each of these only makes up a couple percentage points, together they could explain the difference between the low-pressure FE and the high-pressure FE. Furthermore, even with the lower FE at high pressure, it is still a charge balance closure that is comparable with several benchmark works in the CO₂RR field⁴⁸⁻⁵¹.

2.3.10 GC Response Time

One of the challenges of operating at high pressure is that it complicates inline GC measurements. The standard functioning of an inline GC involves sampling the headspace above an electrochemical cell at a constant flowrate into a GC⁵². Eventually the concentration in the headspace of the product molecules reaches an equilibrium which can be related to the production rate in the reactor. At elevated pressures the effective volume of the headspace will increase linearly with the pressure. The volume of headspace that is being sampled by the GC (in our

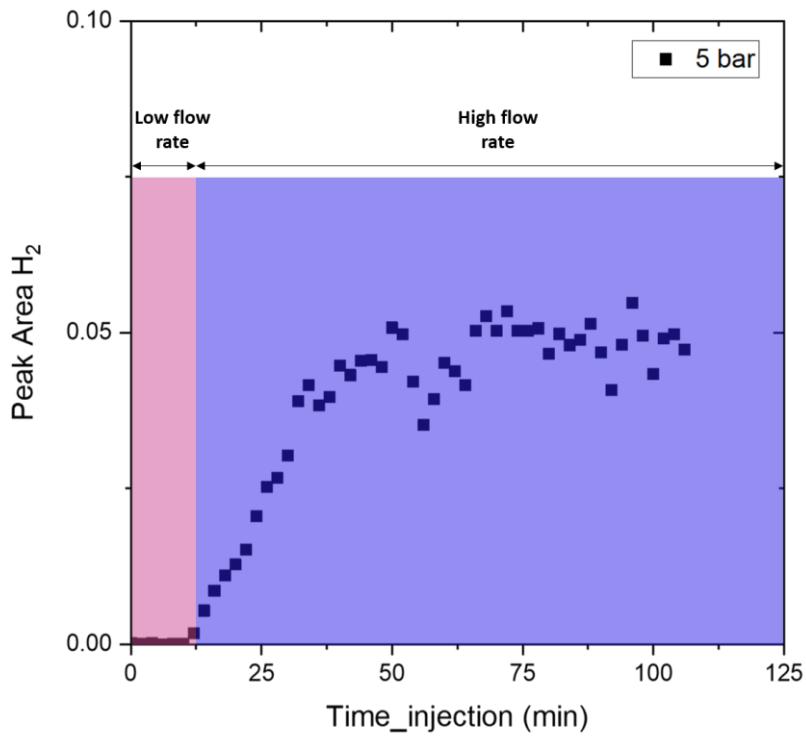


Figure 2.7: A typical switched flow rate GC measurement. The low flow region at the start allows the concentration to quickly build up, while the high flow region at the end maintains the sensitivity of the GC measurement. The effect is to speed up the time it takes the GC measurements to stabilize. The buildup of concentration during the low flow is not seen at the GC due to the low linear velocity at low flow rates.

case 2 ml) is a key factor because of the dynamics that affect GC settling time (the time that it takes the GC signal to be within 5% of the actual concentration in the head space), given by:

$$t_s \approx \frac{3 \cdot V_{h_eff}}{q} \quad (2.1)$$

where t_s is the settling time, V_{h_eff} is the effective volume of headspace (Pressure* V_h), and q is the flowrate of gas from the headspace to the GC. The settling time is thus determined by the flow rate of gas to the GC and the size of the headspace. As can be seen, increasing the pressure, which increases V_{h_eff} , linearly increases the settling time, up to 30 times longer at the highest pressure used here. The obvious solution is to increase the flowrate q to balance the effectively

larger headspace, but this comes with a trade-off. The final concentration of product in the headspace is given by:

$$C_{h_lim} = r/q \tag{2.2}$$

where C_{h_lim} is the limiting value of concentration of the product in the headspace and r is the production rate of the product in the reactor. This means that C_{h_lim} decreases linearly with q , which decreases the sensitivity with which the GC can measure concentration, and thus production rate. The other option is to decrease the volume of the headspace, but this quickly runs into physical constraints. The solution to these issues is to modify the standard in-line GC procedure somewhat. The key observation is that the rate of change of C_h is highest when q is lowest (in absolute terms). Therefore, switching q from a low to high value during the experiment can decrease the settling time, without trading off sensitivity in GC measurements. An example of this procedure can be seen in **Figure 2.7**. If 80% of C_{h_lim} is reached during the low q period, then the settling time can be reduced by 25%, and if 90% of C_{h_lim} is reached then settling time is reduced by 50%. For the details of these calculations, we redirect the interested reader to **SI 2.4.4**. Thus, achieving reasonable settling times (stable readings of the product peaks in the GC reached within 60 minutes for lower pressures and within 100 minutes at the highest pressure) is possible with high pressure reactors, it however does require consideration of all the parameters.

2.3.11 Extended Operation

There are several reasons why extended operation is interesting, including long term testing of electrodes and catalysts for degradation. One of the advantages of having an external reservoir of electrolyte is long continuous operation, as the CO₂RR will consume water (molecules) dur-

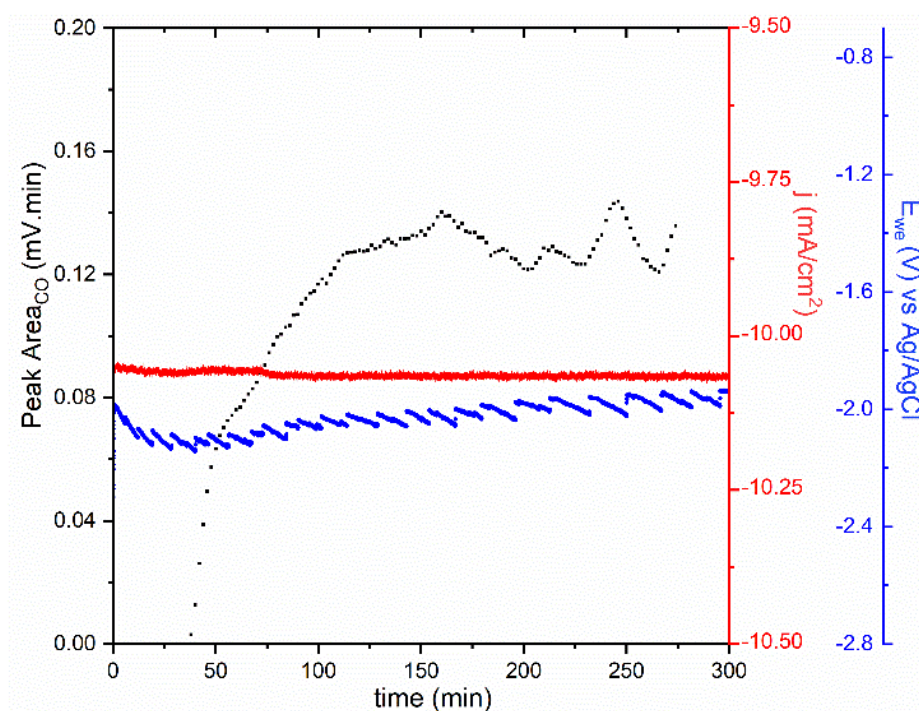


Figure 2.8: An extended operation at 30 bar showing the stability of applied current, recorded potential and GC peak area for CO versus over time. The cell operates here for nearly 5 hours at a current density of 10 mA cm⁻² (actual applied current density - 10.06 mA cm⁻²) and stable electrode potential and CO peak area (after an hour).

ing operation, which will eventually change the concentration of the electrolyte. The system presented here can operate for several hours continuously, as can be seen in **Figure 2.8**.

2.3.12 Conclusions

We have demonstrated the successful design and operation of an elevated pressure divided CO₂RR flow cell to perform experiments that can be considered standard in the field. To achieve this design, minimization of pressure differentials across the dividing membrane by

double back pressure regulators piloted by the same pressure was essential, as well as careful consideration of design parameters such as reservoir and pump sizing. The cell assembly/disassembly time was found to be faster than even some standard atmospheric designs, owing to the quick release clamp design to enclose the pressure inside the reactor (complete turnaround within a half hour).

Electrochemically, the cell performed well and the leakless reference electrode provided a stable reference potential across a range of both reactor and reservoir pressures (stable within 10 mV between 1 and 30 bar). Standard electrochemical experiments, such as linear sweep voltammetry, were successfully performed. Product characterization by in-line GC was possible by utilizing a switching flow rate system, which greatly decreased the settling time, allowing faster measurements (stable readings reached within 60 minutes for lower pressures and within 100 minutes at the highest pressure). The FE for CO₂RR products dramatically increases from close to 26% at 2 bar to about 60 % at 30 bar while H₂ is suppressed, and more importantly 85-90% of the charge balance was closed at lower pressure, dropping only to 82% at 30 bar which is still equivalent to several studies in the literature. The system explained here in detail is successful in its aims and configurable enough to be useful in studying a range of CO₂RR research questions relating to elevated pressure reactors like high current density or CO₂ conversion rate.

2.4 Supporting Information

2.4.1 Exploded View of the Flow Cell

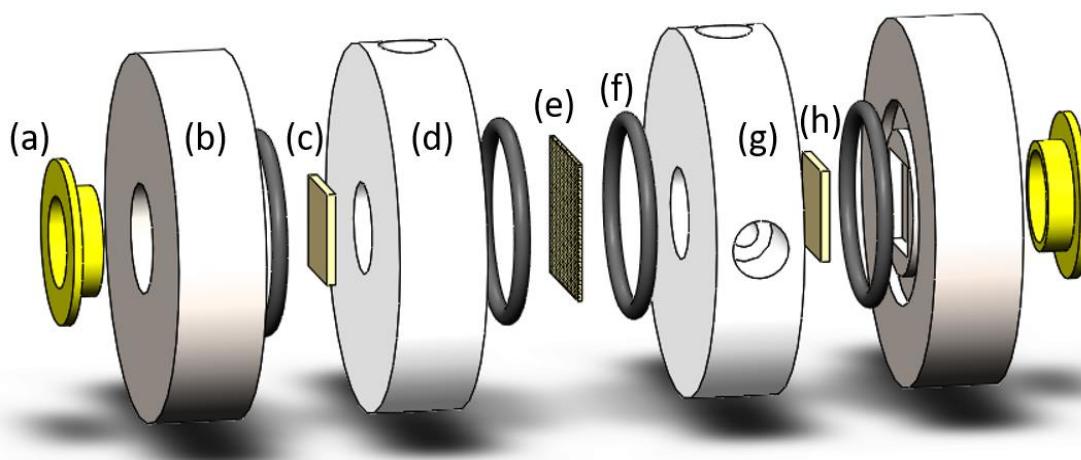


Figure S2-1: Components of the flow cell: (a) Insulation port for clamp to press against, (b) End Plate - Stainless steel, (c) Anode - IrMMO foil, (d) Anode flow plate - PEEK, (e) Membrane - Nafion 117, (f) O ring - Kalrez, (g) Cathode flow plate - PEEK, (h) Cathode - Gold foil.

2.4.2 PEIS at Different Applied Gas Pressures

The impedance measurement was carried out at 0 V, where there is no significant reaction

taking place. The resistance values measured are comparable to the work of Lobaccaro et al.⁵³

and are typical for a such an H-cell configuration.

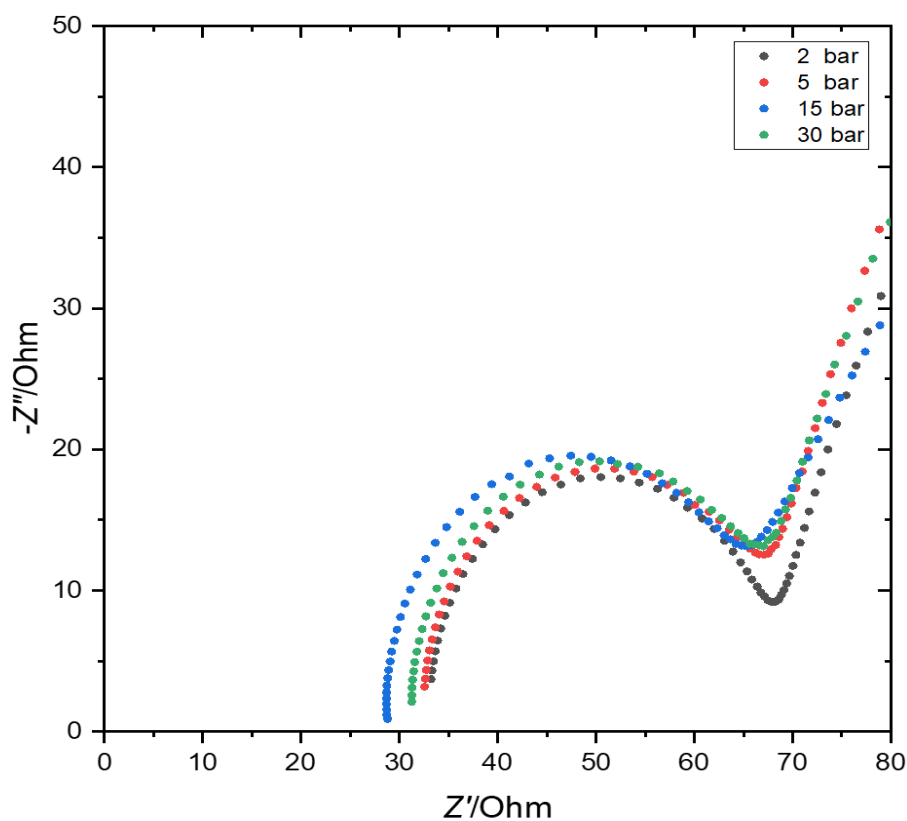


Figure S2-2: Nyquist plots at different pressures recorded at the start of the experiments using an Au foil as WE and Ag/AgCl as RE in a 0.1 M KHCO₃ electrolyte. Frequency range: 50 mHz to 700 kHz.

2.4.3 Reservoir Design

The main body of the reservoir frame is made from Aluminum 5083 which supports the pistons and cylinder in position while the pressure is increased. The pistons are made from PEEK and their main purpose is in sealing the cylinder, making it gas tight. The diameter of the pistons is around 38.05 mm and the use of IDEX O-rings ensures a snug fit in the stainless steel 316 alloy cylinder. The main volume of the reservoir was adjusted using a piece PEEK cylinder that

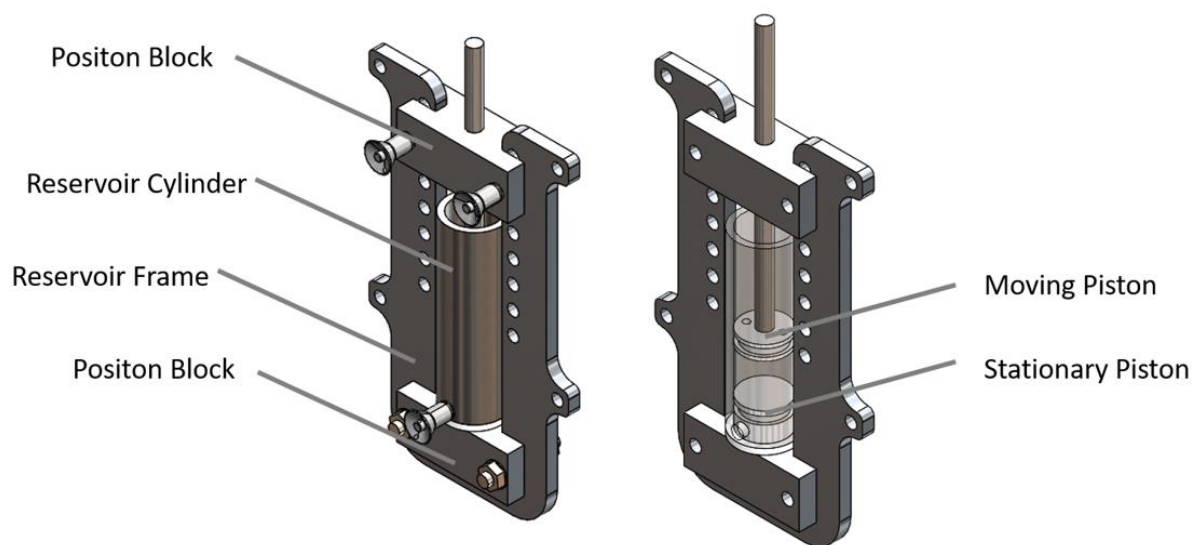


Figure S2-3: A simplified diagram of the gas-liquid reservoir used to pressurize the electrolyte using high-pressure CO₂.

could slide in and out of the cylindrical space. The top piston had four holes to accommodate four tubes namely: the high-pressure gas inlet, a gas outlet to the GC, electrolyte to the reactor, and products from the reactor.

2.4.4 GC Response Time Calculations – Switching Flow Rate Strategy

One of the challenges of operating at high pressure is that it complicates online GC measurements. This is because the added pressure increases the effective volume of the headspace. The headspace will increase linearly with the pressure. The volume of headspace that is being sampled by the GC is a key factor because of the dynamics that affect GC settling time (the time that it takes the GC signal to be within 5% of the final concentration in the head space), which is equal to:

$$t_s \approx \frac{3 \cdot V_{h,eff}}{q} \quad (S1)$$

where t_s is the settling time, $V_{h,eff}$ is the effective volume of headspace ($\text{Pressure} \cdot V_h$), and q is the flowrate of gas from the headspace to the GC. The steps to obtain the above equation is detailed below (equations S2 to S3).

It is also possible to add a delay term, based on the linear velocity of the products from the reactor to the reservoir and from the reservoir to the GC, however this is only significant if the delay is lower than the settling time. This also neglects the time that must be taken after the concentration has reached its equilibrium to ensure the equilibrium has been reached in a real experiment, but this is similar in all conditions. The settling time is thus determined by the flow rate of gas to the GC and the size of the headspace. The flow rate of the gas from the reservoir to the GC also affects the steady-state value, which means that the flow rate determines the sensitivity of the GC measurement. So, while it can be increased to decrease settling time, there is some limit. Similarly, there are practical limits to the size of headspace that can be consistently achieved due to engineering restrictions.

The solution to these issues is to use a switching flow rate to the GC. In the initial period of the experiment a low flow rate can be used. The initial rate must be low enough that pressure cannot build up, but otherwise any rate, as low as possible, is desirable. The low flow rate allows the concentration in the head space to build more quickly than a faster flow rate, but the settling time would be longer because of the higher steady state value. So, switching to the high flow rate after a low flow rate combines the quickly increasing concentration with the low equilibrium concentration of a fast flow rate to decrease the overall time. The trick, then, is to switch to a faster flow rate approximately when you expect that the reservoir concentration will be near the final concentration. To explain why, consider the more general derivation of equation S1. Starting from the simple differential equation representing the flow of products into the head space, and outflow of gases to the GC. The change in amount of the product in the headspace in time will increase at the rate of production and decrease at the rate that the product leaves the headspace:

$$\frac{dn}{dt} = r - c \cdot q \quad (S2)$$

where n is the amount (mol) of gas in the headspace to be measured and c is the concentration in the headspace. Solving this, and converting amount to concentration via volume, V , gives the general solution of:

$$c(t) = \frac{\left(r - e^{-qt/V \cdot (r - c_0 q)} \right)}{q} \quad (S3)$$

Where C_0 is the initial concentration. The final concentration can be seen to be r/q , by taking the limit of eq. S3 as $t \rightarrow \infty$.

Solving for S3 by replacing $C(t) = 0.95 \cdot C_h$ gives equation S1.

The time at which a given target concentration is reached is given by re-arranging eq S3.:

$$t_{tar} = \frac{-V}{q} \ln \left(\frac{r - c_{tar}q}{r - c_0q} \right) \quad (S4)$$

To evaluate how much quicker the two-speed switching strategy is we will allow the concentration to run to a percentage of the final concentration. Consider a high (q_h) and a slow (q_s) flow rate. We will consider q_h equal to 40x q_l (0.2 ml/min and 8 ml/min). The final concentration in question is based on the high flow, and therefore is r/q_h . Concentration reaches 80% when:

$$t_l = \frac{-V}{q_l} \ln \left(\frac{r - 0.8^r/q_h q_l}{r - c_0 q_l} \right) = \frac{-V}{q_l} \ln \left(\frac{r - 0.8 * 0.025r}{r} \right) \quad (S5)$$

$$t_l \approx \frac{0.808V}{q_h} \quad (S6)$$

Then from 80% concentration the time to get to with 5% of the final concentration:

$$t_h = \frac{-V}{q_h} \ln \left(\frac{r - 0.95^r/q_h q_h}{r - 0.8^r/q_h q_h} \right) = \frac{-V}{q_l} \ln \left(\frac{r - 0.025r}{r} \right) \quad (S7)$$

$$t_l \approx \frac{1.38V}{q_h} \quad (S8)$$

And the total time to reach within 5% of the final concentration when the flow rate is switched from 0.02 to 8 ml/min when the headspace concentration reaches 80%:

$$t_{80\%} \approx \frac{2.2V}{q_h} \quad (S9)$$

Of course, when running a real experiment, the final concentration is not known, but by repeated experimentation the final concentration can be estimated accurately, but it will not be exact each time. However, the method is not that sensitive to the exact percentage of final concentration reached. This method will work for a range of stopping points for the slow flow rate.

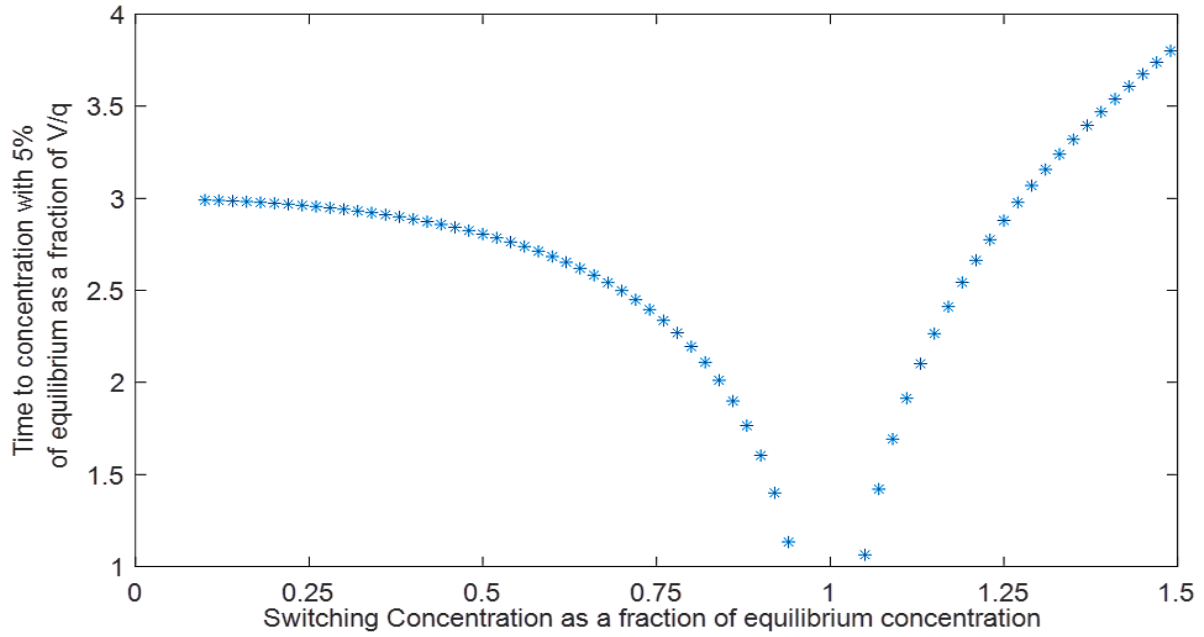


Figure S2-4: The relationship between switching time between slow and high flow and the total time the GC will take to reach with 5% of the final concentration.

In the general case the total time to within 5% of the equilibrium value is $t_p =$

$$\begin{cases} -\left(40 \ln(1 - 0.025p) + \ln\left(\frac{0.05}{1-p}\right)\right) & p < 0.95 \\ -\left(40 \ln(1 - 0.025p) + \ln\left(\frac{-0.05}{1-p}\right)\right) & p > 1.05 \end{cases} \quad (\text{S10})$$

for switching to fast flow at a percentage, p , of the final equilibrium value, this equation has been plotted in figure S4. As can be seen, time will be saved for any value of $p < 1.27$, and a substantial time saving is made if the final concentration can be estimated within $\pm 15\%$.

2.4.5 Comparison of High-Pressure CO₂ Reduction Studies

Table S2-1: Some of the existing notable works on the high-pressure electrochemical CO₂ reduction.

Entry	*P _{CO₂} /bar	T/°C	Current density / mA.cm ⁻²	Electrolyte	Cathode	Cell type	FE _{CO₂} / %	Reference
1	30	ambi-ent	10	0.1 M KHCO ₃	Au foil	Parallel plate Flow	60	This work
2	30	25	12	0.2 M K ₂ SO ₄	Ag plate	Autoclave	67	45
3	30	25	120	0.5 M KHCO ₃	Ni-NC	Autoclave	90	54
4	30	45	6-13	1-ethyl-3-methyl-imidazolium triflate	Zn-Cu	Autoclave	97	55
5	30	25	163	0.1 M KHCO ₃	Ag plate	Autoclave	77	30
6	60		215	0.5 M KHCO ₃	Sn plate	Autoclave	~100	40
7	24.6	60	275	0.5 M K ₂ SO ₄	Ag GDE	GDE	80	39
8	7	25	80-100	7 M KOH	Ag GDE	GDE	85-90	56
9	50	ambi-ent	30	0.5 M KHCO ₃	Sn plate	Parallel plate flow	80	34
10	30	ambi-ent	45	0.1 M KHCO ₃	Sn plate	Parallel plate flow	80	36

2.4.6 Standard Curve of a HPLC Measurement

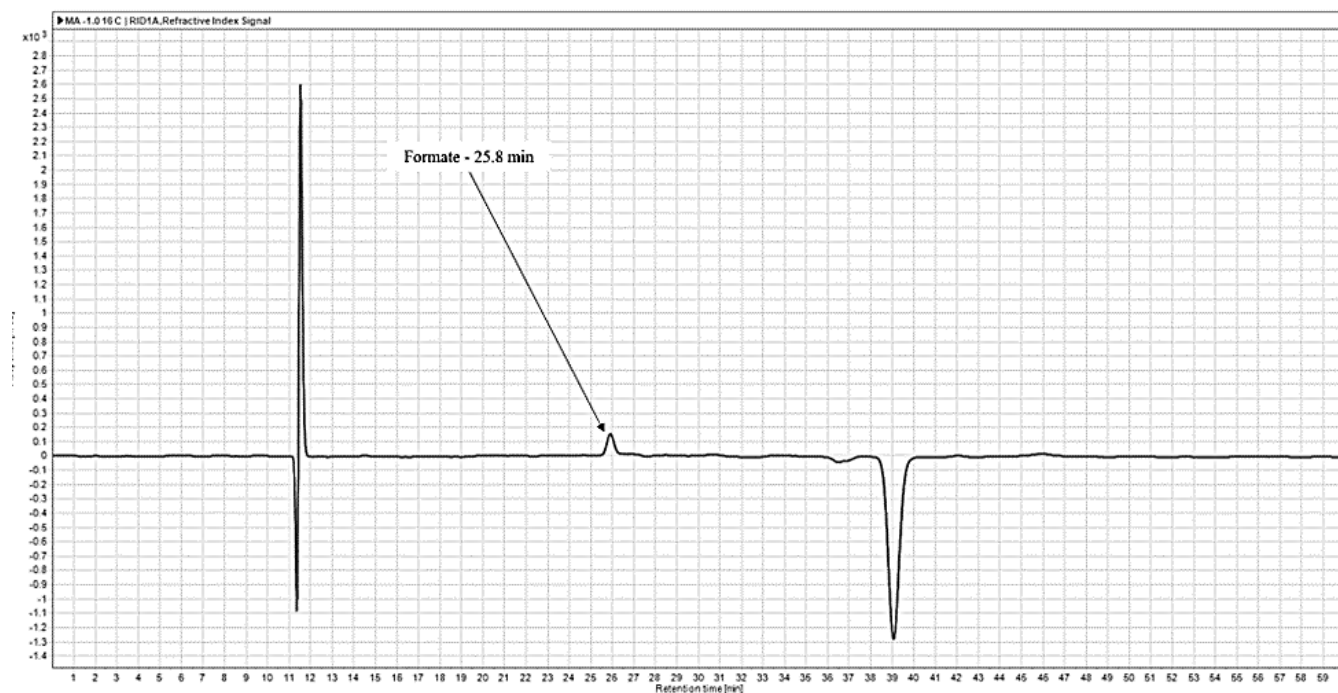


Figure S2-5: Standard HPLC curve for the detection of formate/formic acid. The presence of formic acid (FA) either as an acid or as its conjugate base formate is dependent on pH. Dissolving CO₂ gas at high pressures into 0.1 M KHCO₃ would result in an acidic pH. However, in our system a liquid sample was collected only after depressurizing the system which would result in release of all dissolved excess CO₂ at the pressure studied. Therefore, the electrolyte would revert to an alkaline pH, and we expect formate as the main form of FA. This corresponds with conditions that the standard curve was taken at.

2.4.7 GC Analysis and Faradaic Efficiency Calculations

The GC we use directly utilizes CO₂ as the carrier and we calibrate it using gas mixtures namely, ethylene, CO, CH₄ and H₂ in different concentrations with CO₂ as the bulk gas. The high-pressure gas stream from our reservoir is first sent through a pressure reducer that delivers the gases at a constant pressure of ~ 3 bar to a mass flow controller (MFC, Bronkhorst). Using the MFC we control the volumetric rate to the GC (in our case we switch between two values, 0.2 ml_n/min and 8 ml_n/min to speed up the GC settling time). The columns in the GC have been modified to handle CO₂ as carrier gas and so we don't see CO₂ as a separate but rather it forms the baseline.

$$\text{FE gaseous products} = (n \cdot F \cdot X \cdot \text{molar flow rate}) / I$$

Where, n = number of electrons, F = Faraday's constant (96485 C/mol), X = mole fraction of gaseous product measured by the GC, I = total current applied.

For liquid product analysis, HPLC was used (details are provided in the paper).

$$\text{FE liquid products} = (n \cdot F \cdot C \cdot V) / Q_{\text{tot}}$$

Where, C = concentration derived from HPLC peak integration, V = volume of the catholyte from which the sample is collected for analysis, Q_{tot} = total charge passed during the experiment.

2.5 References

- 1 Pei, Y., Zhong, H. & Jin, F. A brief review of electrocatalytic reduction of CO₂—Materials, reaction conditions, and devices. *Energy Science and Engineering*, 1012-1032, (2021). <https://doi.org:10.1002/ese3.935>
- 2 Schlautmann, R. *et al.* Renewable Power-to-Gas: A Technical and Economic Evaluation of Three Demo Sites Within the STORE&GO Project. *Chemie-Ingenieur-Technik*, **93**, 568-579, (2021). <https://doi.org:10.1002/CITE.202000187>
- 3 Bailera, M., Lisbona, P., Romeo, L. M. & Espatolero, S. Power to Gas projects review: Lab, pilot and demo plants for storing renewable energy and CO₂. *Renewable and Sustainable Energy Reviews*, **69**, 292-312, (2017). <https://doi.org:10.1016/J.RSER.2016.11.130>
- 4 Perathoner, S. & Centi, G. A New Scenario for Green & Sustainable Chemical Production. *Journal of the Chinese Chemical Society*, **61**, 719-730, (2014). <https://doi.org:10.1002/JCCS.201400080>
- 5 Galadima, A. & Muraza, O. From synthesis gas production to methanol synthesis and potential upgrade to gasoline range hydrocarbons: A review. *Journal of Natural Gas Science and Engineering*, **25**, 303-316, (2015). <https://doi.org:10.1016/J.JNGSE.2015.05.012>
- 6 Goli, A. *et al.* An overview of biological processes and their potential for CO₂ capture. *Journal of Environmental Management*, **183**, 41-58, (2016). <https://doi.org:10.1016/J.JENVMAN.2016.08.054>
- 7 Brewis, I., Shahzad, R.-F., Field, R. W., Jedidi, A. & Rasul, S. Combining experimental and theoretical insights for reduction of CO₂ to multi-carbon compounds. *Discover Chemical Engineering*, **2**, (2022). <https://doi.org:10.1007/s43938-022-00009-y>
- 8 Kortlever, R., Shen, J., Schouten, K. J. P., Calle-Vallejo, F. & Koper, M. T. M. Catalysts and Reaction Pathways for the Electrochemical Reduction of Carbon Dioxide. *Journal of Physical Chemistry Letters*, **6**, 4073-4082, (2015). https://doi.org:10.1021/ACS.JPCLETT.5B01559/ASSET/IMAGES/MEDIUM/JZ-2015-01559C_0005.GIF
- 9 Hatsukade, T., Kuhl, K. P., Cave, E. R., Abram, D. N. & Jaramillo, T. F. Insights into the electrocatalytic reduction of CO₂ on metallic silver surfaces. *Physical Chemistry Chemical Physics*, **16**, 13814-13819, (2014). <https://doi.org:10.1039/C4CP00692E>
- 10 Feaster, J. T. *et al.* Understanding Selectivity for the Electrochemical Reduction of Carbon Dioxide to Formic Acid and Carbon Monoxide on Metal Electrodes. *ACS Catalysis*, **7**, 4822-4827, (2017). https://doi.org:10.1021/ACSCATAL.7B00687/SUPPL_FILE/CS7B00687_SI_001.PDF

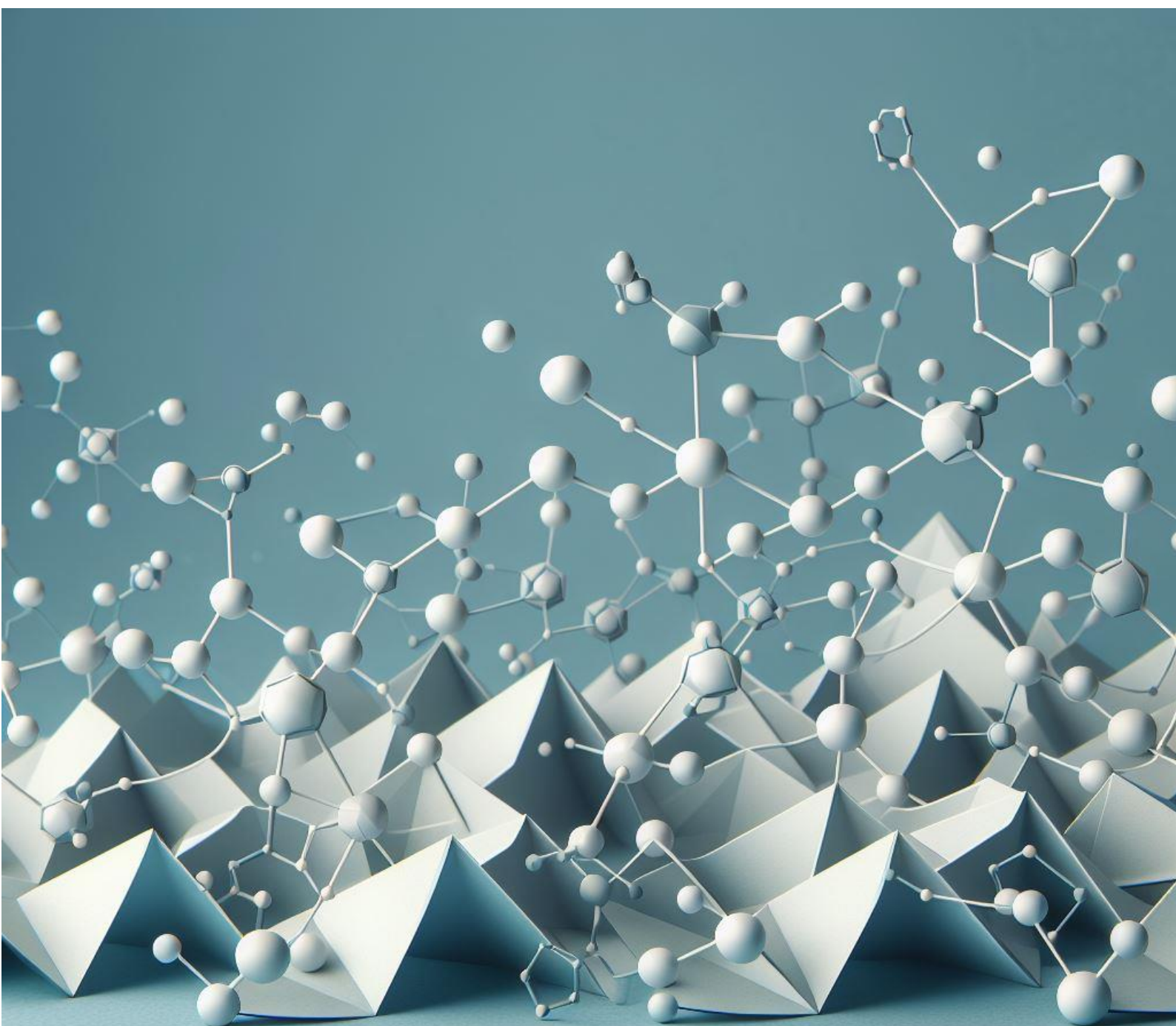
- 11 Zhu, M. *et al.* Structure-Tunable Copper-Indium Catalysts for Highly Selective CO₂ Electroreduction to CO or HCOOH. *ChemSusChem*, **12**, 3955-3959, (2019). <https://doi.org:10.1002/CSSC.201901884>
- 12 Garg, S. *et al.* Advances and challenges in electrochemical CO₂ reduction processes: An engineering and design perspective looking beyond new catalyst materials. *Journal of Materials Chemistry A*, **8**, 1511-1544, (2020). <https://doi.org:10.1039/c9ta13298h>
- 13 Van Daele, K. *et al.* Sn-Based Electrocatalyst Stability: A Crucial Piece to the Puzzle for the Electrochemical CO₂ Reduction toward Formic Acid. *ACS Energy Letters*, **6**, 4317-4327, (2021). https://doi.org:10.1021/ACSENERGYLETT.1C02049/SUPPL_FILE/NZ1C02049_SI_001.PDF
- 14 Jouny, M., Luc, W. & Jiao, F. General Techno-Economic Analysis of CO₂ Electrolysis Systems. *Industrial and Engineering Chemistry Research*, **57**, 2165-2177, (2018). <https://doi.org:10.1021/acs.iecr.7b03514>
- 15 Verma, S., Kim, B., Jhong, H. R. M., Ma, S. & Kenis, P. J. A. A Gross-Margin Model for Defining Technoeconomic Benchmarks in the Electroreduction of CO₂. *ChemSusChem*, **9**, 1972-1979, (2016). <https://doi.org:10.1002/CSSC.201600394>
- 16 Moura de Salles Pupo, M. & Kortlever, R. Electrolyte Effects on the Electrochemical Reduction of CO₂. *ChemPhysChem*, **20**, 2926-2935, (2019). <https://doi.org:10.1002/CPHC.201900680>
- 17 Kas, R., Kortlever, R., Yilmaz, H., Koper, M. T. M. & Mul, G. Manipulating the Hydrocarbon Selectivity of Copper Nanoparticles in CO₂ Electroreduction by Process Conditions. *ChemElectroChem*, **2**, 354-358, (2015). <https://doi.org:10.1002/celec.201402373>
- 18 Gupta, N., Gattrell, M. & MacDougall, B. Calculation for the cathode surface concentrations in the electrochemical reduction of CO₂ in KHCO₃ solutions. *Journal of Applied Electrochemistry*, **36**, 161-172, (2006). <https://doi.org:10.1007/S10800-005-9058-Y/METRICS>
- 19 Liang, S., Altaf, N., Huang, L., Gao, Y. & Wang, Q. Electrolytic cell design for electrochemical CO₂ reduction. *Journal of CO₂ Utilization*, **35**, 90-105, (2019). <https://doi.org:https://doi.org/10.1016/j.jcou.2019.09.00710.1016/j.jcou.2019.09.007>
- 20 Endrődi, B. *et al.* Continuous-flow electroreduction of carbon dioxide. *Progress in Energy and Combustion Science*, **62**, 133-154, (2017). <https://doi.org:10.1016/j.pecs.2017.05.005>
- 21 Higgins, D., Hahn, C., Xiang, C., Jaramillo, T. F. & Weber, A. Z. Gas-Diffusion Electrodes for Carbon Dioxide Reduction: A New Paradigm. *ACS Energy Letters*, **4**, 317-324, (2019). <https://doi.org:10.1021/acsenergylett.8b02035>
- 22 Del Castillo, A. *et al.* Sn nanoparticles on gas diffusion electrodes: Synthesis, characterization and use for continuous CO₂ electroreduction to formate. *Journal of CO₂ Utilization*, **18**, 222-228, (2017). <https://doi.org:10.1016/j.jcou.2017.01.021>

- 23 Zhang, F., Chen, C., Tang, Y. & Cheng, Z. CO₂ reduction in a microchannel electrochemical reactor with gas-liquid segmented flow. *Chemical Engineering Journal*, **392**, 124798-124798, (2020). <https://doi.org:10.1016/j.cej.2020.124798>
- 24 Vedharathinam, V. *et al.* Using a 3D Porous Flow-Through Electrode Geometry for High-Rate Electrochemical Reduction of CO₂ to CO in Ionic Liquid. *ACS Catalysis*, **9**, 10605-10611, (2019). <https://doi.org:10.1021/acscatal.9b03201>
- 25 Zhang, X. *et al.* Electrochemical Reduction of Carbon Dioxide to Formic Acid in Ionic Liquid [Emim][N(CN)₂]/Water System. *Electrochimica Acta*, **247**, 281-287, (2017). <https://doi.org:10.1016/J.ELECTACTA.2017.06.112>
- 26 Tomita, Y., Teruya, S., Koga, O. & Hori, Y. Electrochemical Reduction of Carbon Dioxide at a Platinum Electrode in Acetonitrile-Water Mixtures. *Journal of The Electrochemical Society*, **147**, 4164-4164, (2000). <https://doi.org:10.1149/1.1394035/XML>
- 27 Hara, K. & Sakata, T. Large Current Density CO₂ Reduction under High Pressure Using Gas Diffusion Electrodes. *Bulletin of the Chemical Society of Japan*, **70**, 571-576, (1997). <https://doi.org:10.1246/BCSJ.70.571>
- 28 Jones, J. P., Prakash, G. K. S. & Olah, G. A. Electrochemical CO₂ Reduction: Recent Advances and Current Trends. *Israel Journal of Chemistry*, **54**, 1451-1466, (2014). <https://doi.org:10.1002/IJCH.201400081>
- 29 Fischer, F. & Prziza, O. Über die elektrolytische Reduktion von unter Druck gelöstem Kohlendioxyd und Kohlenoxyd. *Berichte der deutschen chemischen Gesellschaft*, **47**, 256-260, (1914). <https://doi.org:10.1002/CBER.19140470137>
- 30 Hara, K., Kudo, A. & Sakata, T. Electrochemical reduction of carbon dioxide under high pressure on various electrodes in an aqueous electrolyte. *Journal of Electroanalytical Chemistry*, **391**, 141-147, (1995). [https://doi.org:10.1016/0022-0728\(95\)03935-A](https://doi.org:10.1016/0022-0728(95)03935-A)
- 31 Hara, K., Tsuneto, A., Kudo, A. & Sakata, T. Electrochemical Reduction of CO₂ on a Cu Electrode under High Pressure: Factors that Determine the Product Selectivity. *Journal of the Electrochemical Society*, **141**, 2097-2103, (1994). <https://doi.org:10.1149/1.2055067>
- 32 Li, J. & Prentice, G. Electrochemical synthesis of methanol from CO₂ in high-pressure electrolyte. *Journal of The Electrochemical Society*, **144**, 4284-4288, (1997). <https://doi.org:10.1149/1.1838179>
- 33 Ramdin, M. *et al.* High pressure electrochemical reduction of CO₂ to formic acid/formate: A comparison between bipolar membranes and cation exchange membranes. *Industrial and Engineering Chemistry Research*, **58**, 1834-1847, (2019). <https://doi.org:10.1021/ACS.IECR.8B04944>
- 34 Ramdin, M. *et al.* High-Pressure Electrochemical Reduction of CO₂ to Formic Acid/Formate: Effect of pH on the Downstream Separation Process and Economics. *Industrial and*

- Engineering Chemistry Research, 58, 22718-22740, (2019).
<https://doi.org:10.1021/acs.iecr.9b03970>
- 35 Endrödi, B. *et al.* Multilayer Electrolyzer Stack Converts Carbon Dioxide to Gas Products at High Pressure with High Efficiency. ACS Energy Letters, 4, 1770-1777, (2019).
https://doi.org:10.1021/ACSENERGYLETT.9B01142/ASSET/IMAGES/LARGE/NZ-2019-01142C_0007.JPEG
- 36 Proietto, F., Schiavo, B., Galia, A. & Scialdone, O. Electrochemical conversion of CO₂ to HCOOH at tin cathode in a pressurized undivided filter-press cell. Electrochimica Acta, 277, 30-40, (2018). <https://doi.org:10.1016/j.electacta.2018.04.159>
- 37 Scialdone, O. *et al.* Electrochemical reduction of carbon dioxide to formic acid at a tin cathode in divided and undivided cells: effect of carbon dioxide pressure and other operating parameters. Electrochimica Acta, 199, 332-341, (2016).
<https://doi.org:10.1016/J.ELECTACTA.2016.02.079>
- 38 Dufek, E. J., Lister, T. E. & Stone, S. G. Sampling dynamics for pressurized electrochemical cells. Journal of Applied Electrochemistry, 44, 849-855, (2014).
<https://doi.org:10.1007/S10800-014-0693-Z/METRICS>
- 39 Dufek, E. J., Lister, T. E., Stone, S. G. & McIlwain, M. E. Operation of a Pressurized System for Continuous Reduction of CO₂. Journal of The Electrochemical Society, 159, F514-F517, (2012). <https://doi.org:10.1149/2.011209JES/XML>
- 40 Todoroki, M., Hara, K., Kudo, A. & Sakata, T. Electrochemical reduction of high pressure CO₂ at Pb, Hg and In electrodes in an aqueous KHCO₃ solution. Journal of Electroanalytical Chemistry, 394, 199-203, (1995). [https://doi.org:10.1016/0022-0728\(95\)04010-L](https://doi.org:10.1016/0022-0728(95)04010-L)
- 41 Rühl, M. *et al.* Stabilization of an iridium oxygen evolution catalyst by titanium oxides. Journal of Physics: Energy, 3, 034006-034006, (2021). <https://doi.org:10.1088/2515-7655/ABBD34>
- 42 Gu, X. K., Camayang, J. C. A., Samira, S. & Nikolla, E. Oxygen evolution electrocatalysis using mixed metal oxides under acidic conditions: Challenges and opportunities. Journal of Catalysis, 388, 130-140, (2020). <https://doi.org:10.1016/J.JCAT.2020.05.008>
- 43 Branch, J. *et al.* Plastic Reactor Suitable for High Pressure and Supercritical Fluid Electrochemistry. Journal of The Electrochemical Society, 164, H375-H381, (2017).
<https://doi.org:10.1149/2.1051706JES/XML>
- 44 Reference Electrodes Influence Electrochemical Measurements Gamry Instruments, <<https://www.gamry.com/application-notes/instrumentation/reference-electrodes/>> (
- 45 Proietto, F., Berche, F., Galia, A. & Scialdone, O. Electrochemical conversion of pressurized CO₂ at simple silver-based cathodes in undivided cells: study of the effect of pressure and other operative parameters. Journal of Applied Electrochemistry, 51, 267-282, (2021).
<https://doi.org:10.1007/S10800-020-01505-1/FIGURES/6>

- 46 Bernt, M., Schröter, J., Möckl, M. & Gasteiger, H. A. Analysis of Gas Permeation Phenomena in a PEM Water Electrolyzer Operated at High Pressure and High Current Density. *Journal of The Electrochemical Society*, **167**, 124502-124502, (2020). <https://doi.org:10.1149/1945-7111/ABAA68>
- 47 Sartory, M. *et al.* Theoretical and experimental analysis of an asymmetric high pressure PEM water electrolyser up to 155 bar. *International Journal of Hydrogen Energy*, **42**, 30493-30508, (2017). <https://doi.org:10.1016/J.IJHYDENE.2017.10.112>
- 48 Kuhl, K. P., Cave, E. R., Abram, D. N. & Jaramillo, T. F. New insights into the electrochemical reduction of carbon dioxide on metallic copper surfaces. *Energy and Environmental Science*, **5**, 7050-7059, (2012). <https://doi.org:10.1039/c2ee21234j>
- 49 Pander, J. E., Ren, D. & Yeo, B. S. Practices for the collection and reporting of electrocatalytic performance and mechanistic information for the CO₂ reduction reaction. *Catalysis Science and Technology*, **7**, 5820-5832, (2017). <https://doi.org:10.1039/c7cy01785e>
- 50 Möller, T. *et al.* Electrocatalytic CO₂ Reduction on CuO_x Nanocubes: Tracking the Evolution of Chemical State, Geometric Structure, and Catalytic Selectivity using Operando Spectroscopy. *Angewandte Chemie International Edition*, **59**, 17974-17983, (2020). <https://doi.org:10.1002/ANIE.202007136>
- 51 Pavesi, D. *et al.* CO₂ electroreduction on bimetallic Pd-In nanoparticles. *Catalysis Science & Technology*, **10**, 4264-4270, (2020). <https://doi.org:10.1039/D0CY00831A>
- 52 Dufek, E. J., Lister, T. E. & McIlwain, M. E. Bench-scale electrochemical system for generation of CO and syn-gas. *Journal of Applied Electrochemistry*, **41**, 623-631, (2011). <https://doi.org:10.1007/S10800-011-0271-6/METRICS>
- 53 Lobaccaro, P. *et al.* Effects of temperature and gas-liquid mass transfer on the operation of small electrochemical cells for the quantitative evaluation of CO₂ reduction electrocatalysts. *Physical Chemistry Chemical Physics*, **18**, 26777-26785, (2016). <https://doi.org:10.1039/C6CP05287H>
- 54 Proietto, F. *et al.* High-pressure synthesis of CO and syngas from CO₂ reduction using Ni-N-doped porous carbon electrocatalyst. *Chemical Engineering Journal*, **429**, 132251-132251, (2022). <https://doi.org:10.1016/j.cej.2021.132251>
- 55 Pardal, T. *et al.* Syngas production by electrochemical CO₂ reduction in an ionic liquid based-electrolyte. *Journal of CO₂ Utilization*, **18**, 62-72, (2017). <https://doi.org:10.1016/J.JCOU.2017.01.007>
- 56 Gabardo, C. M. *et al.* Combined high alkalinity and pressurization enable efficient CO₂ electroreduction to CO. *Energy & Environmental Science*, **11**, 2531-2539, (2018). <https://doi.org:10.1039/C8EE01684D>

Chapter 3 : Electrochemical CO₂ Reduction on a Copper Foam Electrode at Elevated Pressures



Abstract

Electrochemical CO₂ reduction is a promising way of closing the carbon cycle while synthesizing useful commodity chemicals and fuels. One of the possible routes to scale up the process is CO₂ reduction at elevated pressure, as this is a way to increase the concentration of poorly soluble CO₂ in aqueous systems. Yet, not many studies focus on this route, owing to the inherent challenges with high-pressure systems, such as leaks, product quantification, and ease of operation. In this study, we use a high-pressure flow cell setup to investigate the impact of CO₂ pressure on the electrochemical performance of a copper foam electrode for CO₂ reduction within a pressure range of 1 to 25 bar. Our initial findings using a 0.5 M potassium bicarbonate (KHCO₃) electrolyte show a consistent improvement in selectivity towards CO₂ reduction products, with HCOOH being the dominant product. By conducting a systematic exploration of operating parameters including applied current density, applied CO₂ pressure, cation effect, and electrolyte concentration, the selectivity towards formate (HCOOH) is optimized, achieving a remarkable 70% faradaic efficiency (FE) under moderate conditions of 25 bar in a 0.5 M caesium bicarbonate (CsHCO₃) electrolyte. Additionally, we report the synthesis of iso/2 - propanol with a FE of 11 % at the 25 bar in 0.5 M KHCO₃ which is the highest reported selectivity towards isopropanol on copper using a bicarbonate system.

This chapter is based on the article:

Girichandran, N. *et al.* Electrochemical CO₂ Reduction on a Copper Foam Electrode at Elevated Pressures. *Chem Eng*, Volume 487, 150478 (2024).

<https://doi.org/10.1016/j.cej.2024.150478>

3.1 Introduction

Striving for carbon neutrality remains a worldwide ambition in mitigating climate change as global temperatures continue to rise with each passing year¹. The electrochemical CO₂ reduction reaction (CO₂RR) has received ample interest as a potential power-to-chemical technology². Its main advantages are the possibility to produce a wide range of useful products and the relatively mild process conditions. Many promising catalysts have been identified for CO₂RR, which are typically classified based on their selectivity towards different products^{3,4}. Among these, copper is the only known catalyst that produces a blend of hydrocarbons, alcohols, and aldehydes^{5,6} directly from CO₂. Yet, the CO₂RR on copper suffers from a limited product selectivity⁶⁻⁹.

A challenge that pertains to the CO₂RR is the poor solubility of CO₂ in aqueous electrolytes (~33 mM in water¹⁰). This results in poor conversion rates and limits CO₂ reduction selectivity due to the competition with the hydrogen evolution reaction (HER) in the same potential window. One interesting way of increasing the CO₂ concentration is by increasing the amount of dissolved CO₂ using elevated pressures¹¹⁻¹⁴. Pressurizing CO₂ into the electrolyte has been reported to enhance the CO₂RR by improving the selectivity and partial current densities towards CO₂ reduction products¹³⁻¹⁶, while pressurizing in general could enable better integration of the CO₂RR with upstream and downstream operations¹⁷. Additionally, it offers the chance to work at increased temperatures, given that higher temperatures result in decreased CO₂ solubility, potentially benefiting reaction kinetics¹⁸. Recent studies suggest that the CO₂ reduction reaction (CO₂RR) performance can be modified by manipulating the operating pressure. The catalytic performance is altered through multiple mechanisms, for instance through changing thermodynamics of the reaction, balance of the carbonate buffer reactions

($\text{CO}_2/\text{HCO}_3^-/\text{CO}_3^{2-}$), and the extent of CO_2 coverage and coverage of reaction intermediates on the catalyst surface¹⁹⁻²¹. The rate of CO_2RR has also been shown to diminish below a pressure of 1 atm while H_2 evolution dominates²². Recently, Lamaison et al. reported a boost in the CO partial current density to $-286 \text{ mA}\cdot\text{cm}^{-2}$ at a CO_2 pressure of 9.5 atm on an Ag-Zn alloy dendrite catalyst that was well above its mass transport limited current density of $-30 \text{ mA}\cdot\text{cm}^{-2}$ at 1 atm²³. Hashiba et al., reported a boost in the synthesis of CH_4 with a stable suppression of H_2 evolution at elevated CO_2 pressures²⁴. In a recent study by Ramdin et al., formate selectivity was increased to 90% with a $j > 30 \text{ mA}\cdot\text{cm}^{-2}$ at a pressure of 50 bar²⁵. Even with these promising results, there is still very limited research on high-pressure CO_2RR , with most studies focusing on the production of C_1 products such as CO and formic acid on metallic electrodes such as silver, gold, and tin^{12,26-30}.

In contrast, only a handful of studies have investigated elevated pressure CO_2RR on copper electrodes in aqueous electrolytes. These studies have been, for the most part, restricted to flat planar electrodes in autoclave type reactors³¹⁻³⁴. For example, a recent study by Li et al. using a (111) oriented Cu_2O film on a copper foil reported a high FE_{HCOOH} of 98% at a high CO_2 pressure of 60 atm³³. A more recent study by Huang et al., reported an 84% formate FE at 50 bar CO_2 pressure using a polypyrrole-coated copper (CuPPy) electrode. While these studies show the potential of using a pressurized CO_2 feed to achieve high product selectivities using tailor made catalysts, yet they do so at extreme pressure conditions (≥ 50 bar). However, recent studies have shown that using moderate pressures up to 25 bar is beneficial as it involves low operational and capital costs^{35,36}. To the best of our knowledge, there are very limited studies performed on the electrochemical CO_2RR performance of copper in this operating pressure window of 1-25 bar.

Therefore, we here report a systematic study on the influence of pressure on a polished copper foam electrode in a custom-built flow cell¹¹. The effect of different operating parameters, including, applied current density, cation size and electrolyte concentration, is investigated. We show that the coupled use of pressurized CO₂ and Cu foam electrode offers a notable improvement in the formate selectivity while unlocking new C-C coupled pathways towards higher alcohols.

3.2 Experimental Section

3.2.1 Materials

An ultrapure water purification system (MilliQ IQ 7000, Merck–Millipore, USA) was used as water source for all experiments. Potassium and cesium bicarbonate (KHCO₃, ≥ 99.95% trace metals basis, 99.7–100.5% dry basis, and CsHCO₃ 99.9%, metals basis, Sigma) were used to prepare 0.5, 1, and 2 M catholytes. 1 M potassium hydroxide (KOH pellets, ACS reagent, Emsure) was used as the anolyte. The working electrode used for electrochemical experiments was a copper foam (99.8–99.9%, Recemat BV) and nickel foam (99.9%, Recemat BV) served as the counter electrode. Nafion 117 (Ion Power GmbH) was cleaned in MilliQ water and used as the ion exchange membrane. Hydrochloric acid (ACS reagent, 37%, Sigma), acetone (Technical Grade, assay ≥ 99%, VWR Chemicals) and phosphoric acid (85% VLSI, Technic) were used for cleaning and preparation of the electrodes. Sulfuric acid (95–97%, ACS reagent,

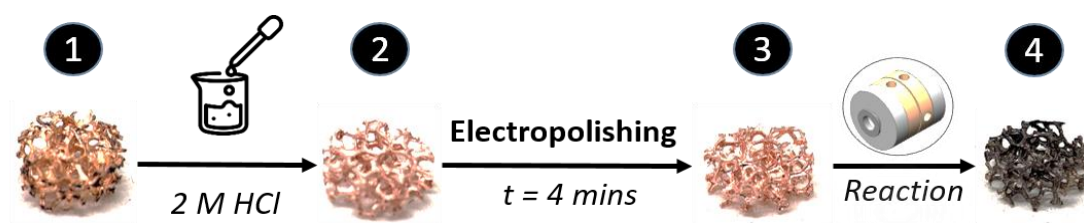


Figure 3.1: Images of the copper foam electrode at different stages in the experimental procedure: (1) as received, (2) After a 2 M HCl acid wash, (3) after electropolishing in phosphoric acid, (4) after electrochemical CO₂ reduction.

Honeywell), DMSO (ACS reagent, $\geq 99.9\%$, Sigma), phenol (ACS reagent, 99.0-100.5%, Sigma), and D₂O (99.9 atom% D, Sigma) were used for liquid product analysis. All reagents were used without further purification.

3.2.2 Electrochemical Measurements

The electrochemical performance of the copper foam electrodes at different pressures were assessed using chronopotentiometry experiments by applying current densities and measuring the potentials. Chronopotentiometry was employed because recent studies have demonstrated that notable changes in the immediate surroundings near the catalyst surface based on the current density³⁷. Consequently, in this context, we aim to investigate how these changes might influence product selectivity. A custom-made flow cell with a continuous gas product measurement and stackable clamp design was used to conduct the experiments, as detailed in our previous work¹¹. In brief, the setup was designed with flexibility and ease of operation in mind and can handle pressures up to 50 bar while functioning in a continuous mode including inline gas product analysis. A Biologic BP300 potentiostat was used for all CO₂RR experiments. Nickel foam and a miniaturized leakless Ag/AgCl reference electrode (LF 1.6–45 mm, Innovative Instruments, Inc., USA) served as the anode and reference electrode respectively. 0.5, 1 or 2 M KHCO₃ or CsHCO₃ was used as the catholyte while 1 M KOH was used as the anolyte. The cathode and anode chambers were separated using a Nafion 117 membrane. Before each experiment the catholyte was purged with CO₂ at the desired pressure in an external reservoir for 30 minutes (for schematics of the setup, please see **Figure S 3-1**). The CO₂RR was performed at ambient temperature and at four different gas pressures; 1, 5, 10, and 25 bar. The reactor pressure was held slightly higher (≥ 5 bar) compared to the gas pressure to prevent dissolved gases from escaping the electrolyte due to ohmic heating near the electrode. Also, having a

higher upstream pressure on the back pressure regulator helps with quicker discharge of dissolved gases into the headspace as the circulated electrolyte enters the reservoir.

3.2.3 Electrode preparation

For each experiment a freshly cut copper and nickel foam electrode was used. Images of the copper foam electrode at different stages in the experimental procedure are depicted in **Figure 3.1**. Copper foam was cut in the shape of a cylinder with a diameter of 1 cm and thickness of 0.4 cm. Prior to each experiment the copper foam was first sonicated in acetone for 10 minutes followed by washing with 2 M HCl for 5 minutes³⁸. Afterwards it was rinsed with ultrapure water and dried under argon flow, before putting it in a two-electrode electrochemical cell, where it was electropolished in 85% phosphoric acid using a carbon rod as counter and reference electrode by applying a potential of 2.1V for 4 minutes. A similar cleaning procedure was performed on the nickel foam except for the electropolishing step.

3.2.4 Characterization

Scanning Electron Microscopy (SEM, Jeol JSM 6500F) images were taken prior and after the experiments to understand the changes incurred to the copper foam during the experiment. An energy dispersive X-ray spectrometry detector (Ultradry, Thermofischer, USA) enabled detection of chemical elemental composition. X-Ray Diffraction (XRD) patterns were obtained using a Bruker D8 Advance diffractometer (Bruker, USA) Bragg-Brentano geometry with graphite monochromator and Vantec position sensitive detector (Co K α radiation. Divergence slit var12, scatter screen height 8 mm, 40 kV 40 mA).

The surface chemistry of the electrodes was studied using a Thermo ScientificTM K-AlphaTM spectrometer (Thermoscientific, USA). The monochromated aluminum K α radiation, with a photon energy of 1486.7 eV, was used to generate a monochromated X-ray with a spot size of

400 μm . The X-ray photoelectron spectroscopy (XPS) data were acquired before and after the experiments. To compensate for the differential charging, a flood gun was employed. High-resolution scans were acquired with a step size of 0.1 eV. The XPS spectra obtained were analysed using the CasaXPS software.

3.3 Results and Discussion

3.3.1 Effect of Pressure and Current Density on CO₂ Electroreduction

The influence of pressure on the CO₂RR on copper foam electrodes (ECSA = 3.3 cm² (SI 3.4.4)) was studied using the previously described cell at different applied current densities (j) (Figure 3.2). As a base case, a pressure of 1 bar of CO₂ was applied and the electrochemical performance was measured at -30, -40, -50, and -60 mA (j = -9.1, -12.1, -15.2, and -18.2 mA/cm²). H₂ is the dominating product at all applied current densities with the FE_{H₂} > 70 %. The main CO₂RR products observed are formate (HCOOH), methane (CH₄), ethylene (C₂H₄) and carbon monoxide (CO), with a combined FE < 30 %. This relatively poor performance is explained by the poor CO₂ solubility in aqueous electrolytes at 1 bar. Remarkably, at the highest pressure studied in this work (25 bar), the trend is reversed with CO₂RR products reaching a total FE > 70% at the expense of hydrogen production, which is suppressed to less than 30% (see SI 3.4.9 for details regarding all the products). It is interesting to note that with an increase in pressure from 1 to 10 bar, the most preferred CO₂RR product is HCOOH followed by CO, while we only observe trace amounts of ethylene at higher current densities. However, at 25 bar, apart from HCOOH and CO, the most preferred products are oxygenates (alcohols) with trace amounts of hydrocarbons.

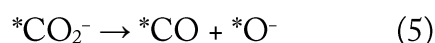
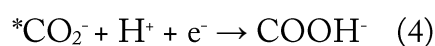
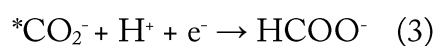
To rule out that differences in observed CO₂RR performance arise from catalyst morphology and compositional changes, we performed characterizations prior to and after electrochemical measurements. The surface morphology of the used copper foam electrodes, as visualized with SEM, does not exhibit any substantial changes to the electrodes prior to the experiment (SI 3.4.5). Similarly, XRD measurements show no changes in the crystal structures of the copper foam post electrochemical measurements (SI 3.4.8). The copper foam is polycrystalline in nature with the most dominant facets being Cu (100) and Cu (111)³⁹. This also dismisses any contributions to the observed performance due to changes in the catalyst crystal structure. The deconvoluted XPS C 1s and Cu 2p spectra for pure copper foam and after experiments at 5 bar, 10 bar, and 25 bar are shown in supplementary information SI 3.4.6 and SI 3.4.7. We mainly observe that after the electrochemical experiments trace amounts of various carbon species are present on the copper surface. In situ XPS studies on copper during CO₂ reduction have reported the formation of carbon species (specifically via the C₁ pathway)⁴⁰. Previous studies have shown that the formation of carbon mainly occurs in bicarbonate systems and surfaces with less defects (polished electrodes)⁴¹.

At 25 bar, HCOOH is the favoured product at all current densities with the highest FE_{HCOOH} of ~57% at -9.1 mA/cm². With more negative current densities at 25 bar, there is a decline in HCOOH production with a simultaneous increase in FE_{H₂} and FE_{CO}. The initial step in the CO₂RR is believed to be the formation of a carboxylate intermediate *CO₂⁻ anion radical^{7,42,43},



which can bind to the copper surface through either C, O, both O's, or both C and O^{44,45}. The formation of HCOOH occurs through either a hydride or proton coupled electron transfer

(PCET) reaction when $^*\text{CO}_2^-$ is bound with a C or O atom to the copper surface, as demonstrated in the following equations:



Irina et al. suggest that the reaction proceeds via the carboxylate intermediate ($-\text{CO}_2^-$), which is stabilized on the electrode surface due to an interplay of its electrostatic interactions with the hydrated metal cations, strong covalency of the carbon atom towards the surface, and the polarization forces present near the electrode⁴⁶. Further cathodic activation (applying more negative currents/potentials) results in the weakening of the C-Cu bond and C-O bond, with simultaneous stabilization of the O-Cu bond. At this stage, either step (2) or (3) can result in the formation of HCOO^- or direct formation of CO with further protonation (this is true for near neutral or alkaline conditions). Another possibility is the interaction between a proton and the exposed O atom of the $^*\text{CO}_2^-$ anion radical giving rise to a carboxyl intermediate⁴⁷ (step 4), which can lead to both CO and HCOO^- . Recent studies on copper catalysts indicate that the HCOOH pathway is favoured on Cu (111)⁴⁶ and Cu (200)⁴⁸ surfaces. The increase in HCOOH production with increasing pressure has been recently reported and is ascribed to an increase in CO_2 coverage^{34,49} with a simultaneous drop in surface water coverage that serves as the main proton donor⁵⁰. The formation of HCOOH requires the least protons per carbon atom among the different liquid products which explains its increased formation relative to more hydrogenated CO_2RR products.

The shift in selectivity from HCOOH to CO and subsequently to hydrocarbons as the cathodic current density increases is attributed to a transition from a thermodynamics to a kinetics-mediated pathway⁵¹. Another crucial factor to consider is the interfacial pH, which affects the pathways towards HCOOH and CO differently. This becomes particularly evident at 25 bar (Figure 3.2d) when the current density is increased from -9.1 to -18.2 mA/cm², resulting in an increase in CO production, with a decline in FE_{HCOOH}, and a simultaneous increase in H₂ formation. This observation is explained by the interplay between the flux of CO₂ (concentration

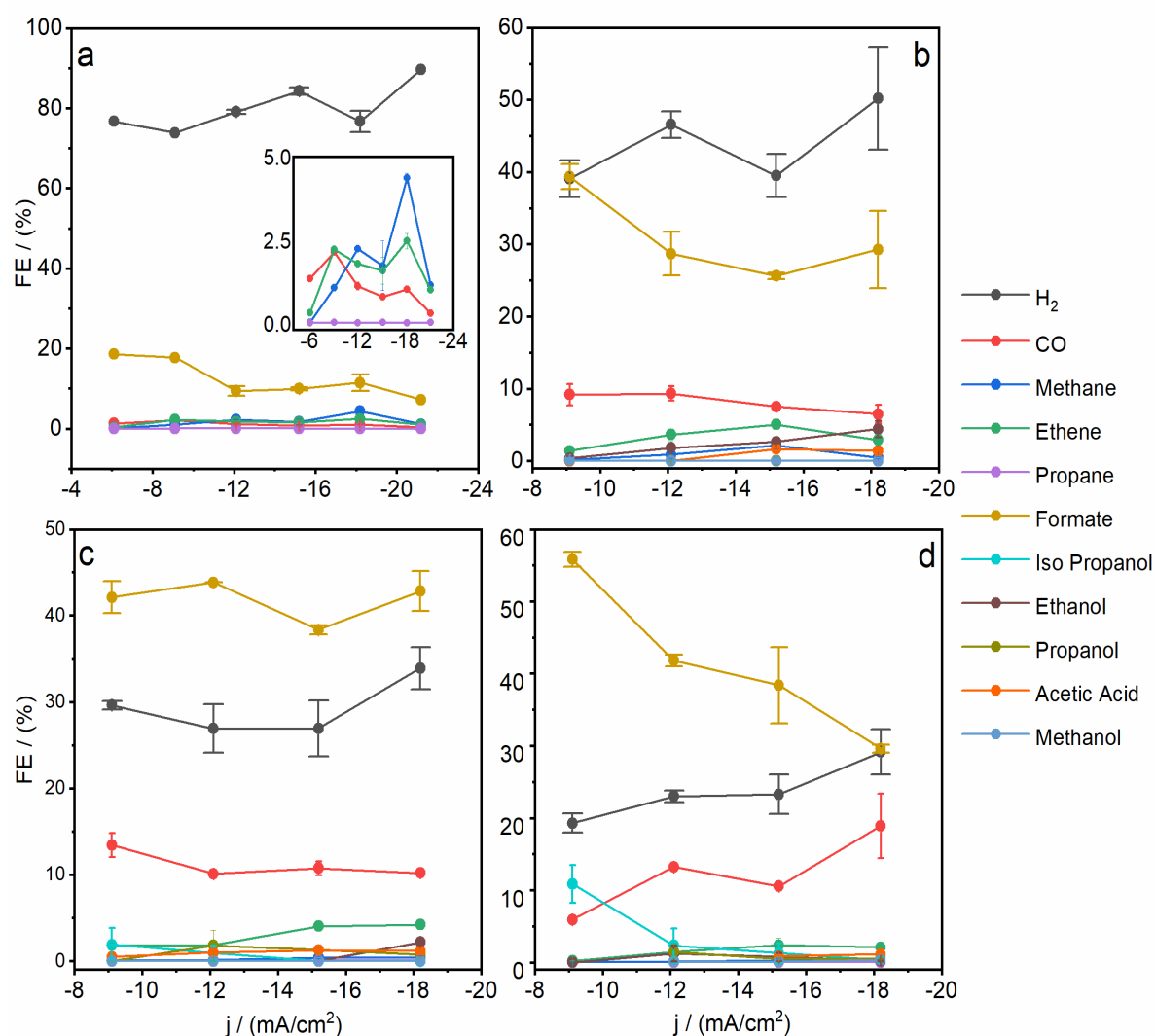
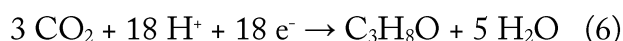


Figure 3.2: Faradaic efficiency towards product at varying applied current densities at a) 1 bar, b) 5 bar, c) 10 bar, and d) 25 bar CO₂ pressure using a Cu foam in a 0.5 M KHCO₃ electrolyte. The exact faradaic efficiency values can be found in

SI 3.4.9.

in the bulk) and the pH at the electrode surface, that increases with increasing current densities³². At -18.2 mA/cm², reducing the pressure from 25 bar to 1 bar follows a volcano like trend for C₂₊ species, with the FE peaking at 5 bar for ethylene and 10 bar for ethanol (SI 3.4.9). This can be attributed to the fact that at 25 bar, there is a higher amount of CO₂ available to react with the generated OH⁻ ions at the electrode surface, effectively buffering the interfacial pH. However, as the pressure decreases, the concentration of CO₂ (and consequently the CO₂ flux to the surface) diminishes, leading to a weaker pH buffering effect. Additionally, the presence of a higher amount of surface water⁵⁰ at lower pressures compared to higher pressures contributes to an increased amount of adsorbed hydrogen on the electrocatalytic surface, promoting the formation of more reduced products from CO₂.

Interestingly, we observe the formation of Iso/2-propanol (IPA) at 10 bar and 25 bar. The FE_{IPA} peaks at ~11% with applying 25 bar and -9.1 mA/cm² and drops to a mere 0.7% at -18.2 mA/cm² (Figure 3.2d). 2-propanol is an uncommon product for CO₂RR on copper electrodes as it requires the transfer of 18 electrons:



Although the exact mechanism behind the formation of 2-propanol on copper is still unclear, a possible pathway is explained below based on our experimental results and the mechanistic studies conducted by Garcia et al.⁵² and Kun et al.⁵³. *CO species (equation 1) can dimerize via a C-C coupling following an initial electron transfer and a proton transfer to give a reduced dimer species (*CO-COH) which can rearrange and reduce further to give rise to a C₂ enol intermediate (*C₂H₃O, a precursor to ethanol). At the lower current densities, a higher surface *CO density, that occurs at higher pressures, can promote interactions between the enol intermediate with adjacent *CO species. Further proton coupled electron transfers then result in the

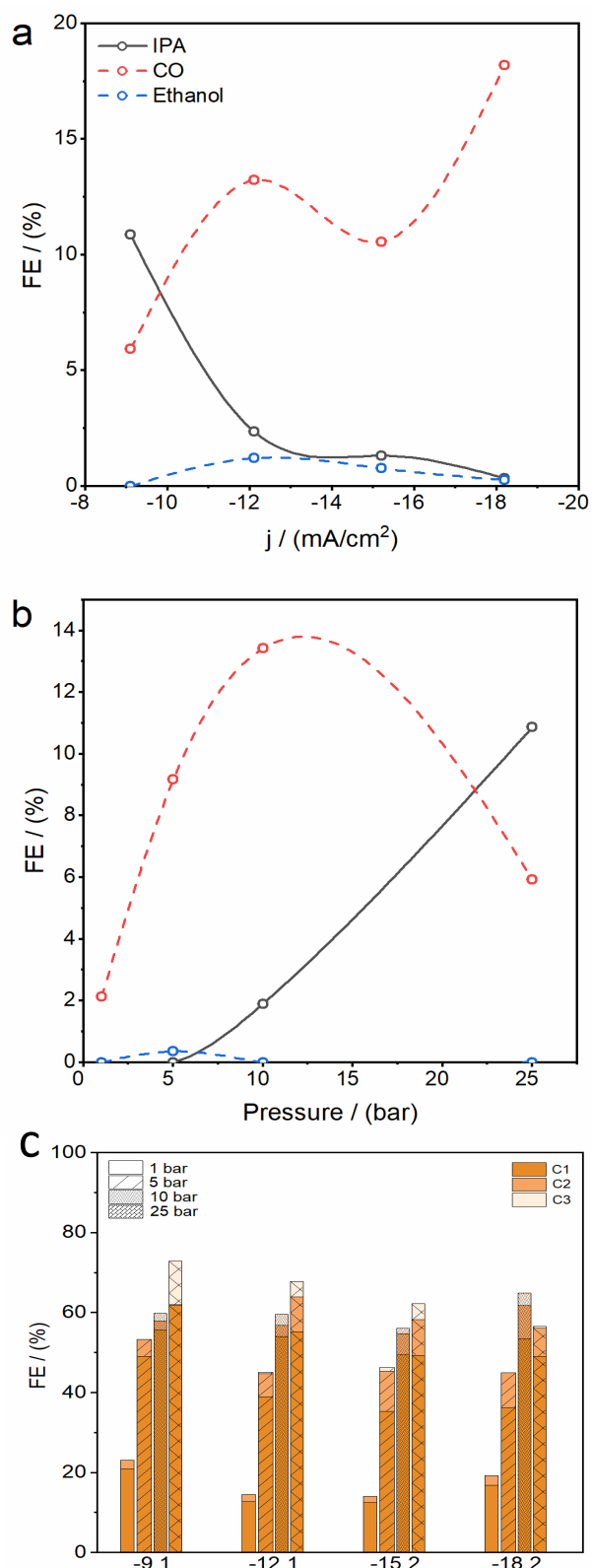


Figure 3.3: a) Relationship between FE_{IPA} , FE_{CO} , and FE_{EtOH} versus applied current densities at $P = 25$ bar, b) Relationship between FE_{IPA} , FE_{CO} , and FE_{EtOH} versus CO_2 pressure at $j = -9.1$ mA/cm², c) C_1 , C_2 and C_3 product FE versus applied current densities under $PCO_2 = 1, 5, 10, 25$ bar. All experiments were carried out in 0.5 M $KHCO_3$ (For error bars see **Figure 3.2** and **SI 3.4.9**)

formation of a C_3 enol species that can give rise to 2-propanol mimicking the pathway of ethanol formation from the C_2 enol intermediate. The low amounts of ethanol at all tested conditions (especially at higher pressures) are assumed to be due to its consumption at the copper electrode to produce 2-propanol.

To provide a general understanding, the reader is guided through the trends in FE_{IPA} , FE_{CO} and FE_{EtOH} below. When the current density is increased (going from -9.1 to -18.2 mA/cm²) at a pressure of 25 bar, a gradual rise in FE_{CO} is observed, while FE_{EtOH} initially rises to 0.8% before dropping to 0.3%. At the same time, as the current density becomes more negative, FE_{IPA} decreases from 11% to zero. Notably, at -9.1 mA/cm², where the most 2-propanol is observed (as shown in **Figure 3.3a**), ethanol is not detected. This is similar to the results reported by Kun et al.⁵³, where an increase in FE_{IPA} was observed at the expense of FE_{EtOH} and FE_{CO} . Also, at -9.1 mA/cm², there is an initial increase in CO production when the pressure is

raised from 1 bar, which then decreases to about 5.9% as the pressure reaches 25 bar (Figure 3.3b). A similar pattern is seen for FE_{EtOH} . Alongside this, FE_{IPA} shows an opposite trend to that of FE_{CO} and FE_{EtOH} , increasing from 1.9% at 10 bar to 11% at 25 bar.

A broad overview of the trends in total C_1 , C_2 , and C_3 product distributions over the entire range of applied current densities under different CO_2 pressures is shown in Fig. 3c. Furthermore, the partial current densities of $HCOOH$, CO and H_2 versus applied current densities at all pressures are provided in the SI 3.4.14.

3.3.2 Effect of Cation at Elevated Pressure

An interesting parameter to consider is the cation effect that has a substantial effect on the electrochemical CO_2 reduction performance at ambient pressures. In fact, a recent study by Monteiro et al., claimed the absence of any CO_2 reduction on Ag, Au, and Cu electrodes without cations⁵⁴. While the exact mechanism is still debated, previous studies have demonstrated that larger cations like Cs^+ can boost CO_2RR activity by inducing changes to the local pH⁵⁵,

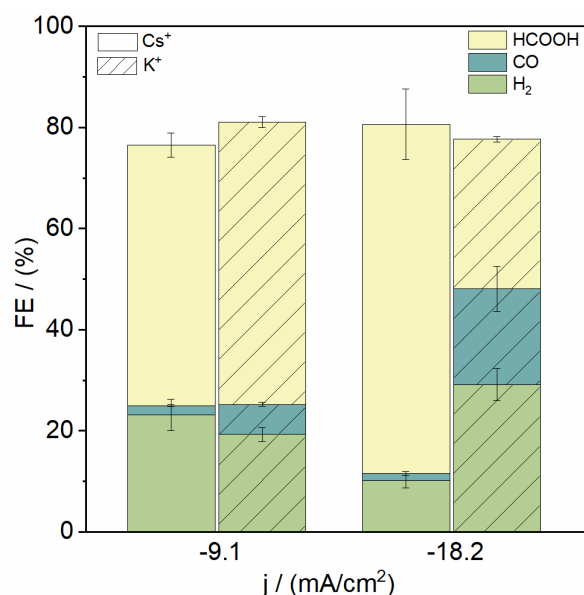


Figure 3.4: FE of H_2 , CO , and $HCOOH$ versus current density (-9.1 and -18.2 mA/cm²) at $P = 25$ bar in 0.5 M $KHCO_3$ and $CsHCO_3$.

the interfacial electric field close to the electrode surface^{56,57}, stabilizing various reaction intermediates⁵⁸, or by modifying the structure of surface bound water⁵⁹. While these studies have been mainly restricted to ambient pressures, combining these effects with the increased CO_2 concentrations at high pressures, could lead to further selectivity enhancements. To probe this, experiments were carried out to investigate the influence of cation

size toward CO₂ reduction performance (at 25 bar, -9.1 and -18.2 mA/cm²) using a 0.5 M CsHCO₃ electrolyte.

The selectivities towards CO, H₂, and formate as a function of cation choice are shown in **Figure 3.4**. 2-propanol has been omitted as it was not present while using 0.5 M CsHCO₃ at either of the studied current densities. The results show that there is not a significant difference in FE_{HCOOH} at -9.1 mA/cm² between K⁺ and Cs⁺, with only a slight increase observed with K⁺ (FE_{HCOOH} = 55% compared to 51% for Cs⁺). However, at -18.2 mA/cm², the FE of HCOOH increases significantly from approximately 30% with KHCO₃ to 70% with CsHCO₃, more than doubling in value. Moreover, the production of hydrogen is suppressed to 10%. Cations with a smaller hydration shell such as Cs⁺ have been shown to be more concentrated at the electrode surface under reduction conditions than cations such as K⁺ with a bigger hydration radius⁵⁶. Mechanistic studies at ambient pressure also report that Cs⁺ can stabilize negatively charged reaction intermediates such as *CO₂⁻ (a common precursor to both HCOOH and CO)⁴⁷ much more strongly than K⁺⁵⁴. Here, the interplay of the above enhancement effects of Cs⁺ combined with the increased concentrations of CO₂ at high pressure explain the notable increase in the selectivity and partial current density towards HCOOH.

3.3.3 Effect of Electrolyte Concentration at Elevated Pressure

The CO₂ electrochemical reduction activity was further investigated by studying the effects of electrolyte concentration with 0.5, 1 M and 2 M KHCO₃ and CsHCO₃ at 25 bar and -9.1 mA/cm² (**Figure 3.5a**). The motivation behind these experiments was to understand the impact of electrolyte concentration on the reduction activity as studies at ambient pressure have shown that the [CO₂]/[cation] ratio can have a significant impact on the performance of a copper electrode⁶⁰. The major factors dictating the observed behaviour are a loss of CO₂ to the salting

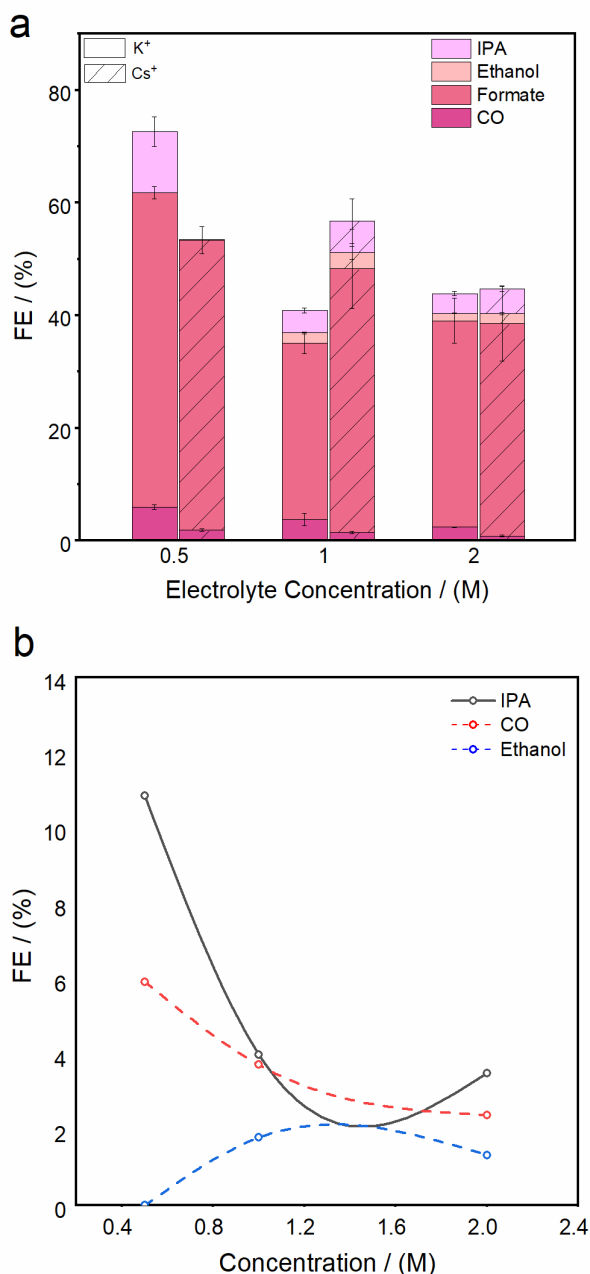


Figure 3.5: a) FE of CO, ethanol, HCOOH, and iso propanol (IPA) versus electrolyte concentration (0.5, 1, and 2 M) at $P = 25$ bar and -9.1 mA/cm², b) Relationship between FE_{IPA} , FE_{CO} , and FE_{EtOH} versus $KHCO_3$ concentration at $j = -9.1$ mA/cm² and $P = 25$ bar.

out effect, a decrease in local pH due to the stronger buffering effect of a higher bicarbonate concentration, a drop in the electric field affecting the stability of CO₂RR intermediates, and an increased CO₂ mass transport limitation due to the adsorption of cations on the electrode surface owing to an increased cation/ [CO₂] ratio. According to Ramdin et al., a moderate electrolyte concentration exists that works best for high pressure CO₂ reduction to formic acid¹⁴.

Figure 3.5a shows that the FE_{HCOOH} decreases with an increase in concentration for both the electrolytes (KHCO₃ and CsHCO₃). Interestingly, there is a decline in FE_{CO} and FE_{IPA} when increasing the electrolyte concentration from 0.5 to 2 M with a simultaneous increase in FE_{EtOH} reaching a maximum value of 1.8 % at 1 M before decreasing to 1.3% for 2 M. The

decrease in FE_{CO} can be attributed to the decrease in local interfacial pH (though less significant at higher pressure) with an increase in electrolyte (therefore, [HCO₃⁻]) concentration, which also results in slightly higher amounts of H₂ and CH₄ (see SI 3.4.10). The trends shown in **Figure 3.5**, for the different KHCO₃ concentrations, further illustrate that the variation in

FE_{IPA} is closely tied to the changes in FE_{CO} and FE_{EtOH} , similar to the patterns presented in **Figure 3.3a** and **Figure 3.3b**. This emphasizes the existence of a pathway towards 2-propanol that mimics ethanol formation⁴¹. For $CsHCO_3$, the trends for FE_{HCOOH} , FE_{CO} , and FE_{EtOH} are like that of $KHCO_3$, however there are some notable differences. The ethanol selectivity increases from 0.1% for 0.5 M to 2.9% for 1 M $CsHCO_3$ before dropping to 1.8% at 2 M. Moreover, the amount of CO is lower at all the studied $CsHCO_3$ concentrations while 2-propanol only appears at 1 M concentration indicating a different optimum for Cs^+ compared to K^+ .

3.3.4 Conclusions

We report a systematic investigation of the effects of pressure, current density, cation size, and electrolyte concentration on the electrochemical CO_2 reduction using a copper foam electrode. At 25 bar, the electrode shows a remarkable selectivity of 70% for formate in 0.5 M $CsHCO_3$ with j_{HCOOH} of -12.7 mA/cm^2 . Furthermore, we report the formation of the uncommon product 2-propanol, with a FE of 11% in 0.5 M $KHCO_3$ at 25 bar, which is the highest reported selectivity for this product under moderate pressures on a polished copper foam. The conducted experiments shed light on the idea that electrolyte engineering coupled with the right operating conditions can be a viable option to enhance the selectivity towards profitable products such as formate on a simple copper electrode⁶¹. Moreover, a pressurized CO_2 feed can potentially unlock new C-C coupling pathways on copper and pave the way towards the production of elusive higher CO_2 reduction products. This also questions whether newly developed catalysts should be tested under elevated pressure conditions.

3.4 Supplementary Information

3.4.1 Schematics of the High-Pressure Setup

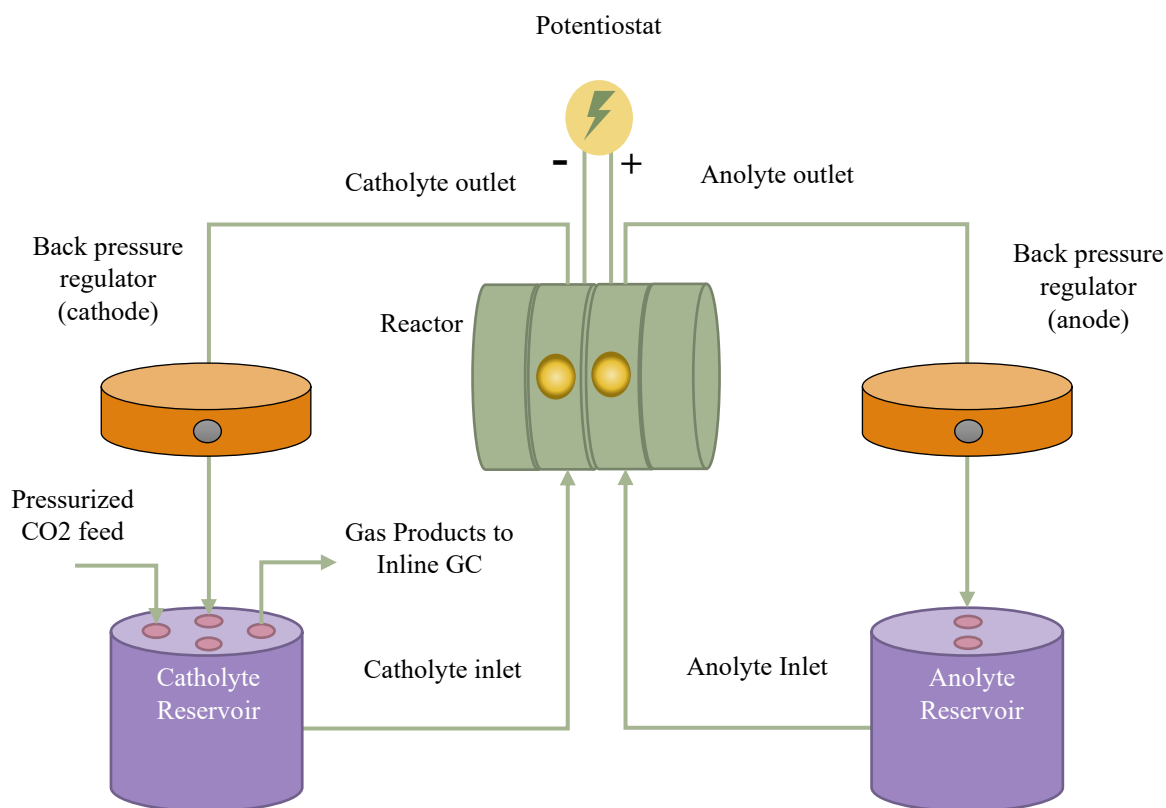


Figure S 3-1: A schematic representation of the high-pressure setup used in this study.

The reactor is a membrane separated parallel plate flow cell with two pressurized external reservoirs. The electrolyte is pumped from the reservoir to the reactor, through a back-pressure regulator, and then back into the external reservoir at a flow rate of 25 ml/min using HPLC pump. Gas is pressurized into the reservoir at a controlled rate through a pressure controller (Bronkhorst High-Tech BV, The Netherlands), and the gas outlet is directed to the inline GC. Thus, CO₂ consumed in the reactor is continuously replaced by the gas inlet. For further details regarding design choices and detailed information please refer to our previous work¹¹.

3.4.2 Product Analysis

Gas Products - For measuring the gaseous products generated during the reaction, an inline gas chromatograph (CompactGC 4.0, Global Analyzer Solutions, The Netherlands) was used. To calibrate the GC, gas cylinders (Linde Gas Benelux B.V., The Netherlands) containing custom gas mixtures of different product gases with CO₂ concentrations ranging from 50 to 8000 ppm were employed. The gas products were analyzed at regular intervals of 2 minutes. The GC system comprises two TCD detectors, one for CO and one for H₂, along with an FID detector used for hydrocarbon analysis (C1 - C6). The FID channel is equipped with an Rtx-1, 5.00 μm (15 m * 0.32 mm) analytical column. The first TCD channel consists of a Carboxen 1010 (3 m * 0.32 mm) pre-column and a Molsieve 5A (5 m * 0.32 mm) analytical column, while the second TCD channel comprises a Carboxen 1010 (3 m * 0.32 mm) pre-column and a Molsieve 5A (7 m * 0.32 mm) analytical column. These components aid in separating the constituents before reaching their respective channel detectors.

Liquid Products - The liquid products (major products – formate, intermediate products - isopropanol/2-propanol, minor products – acetate) obtained after the reaction were analyzed using an Agilent Technologies 1260 Infinity HPLC system from the USA. To calibrate the system, standard solutions of the desired chemicals (Sigma-Aldrich, USA, >98% formic acid) were prepared with concentrations ranging from 0.1 mM to 50 mM. Each analysis involved injecting 5 μL of the product sample onto two Aminex HPX-87H columns (Biorad) in series, which were heated to 60°C. A 1 mM H₂SO₄ solution was used as the eluent. The products were then detected using a Refractive Index Detector (RID).

To cross check and detect intermediate and minor products present in the electrolyte samples like ethanol, 1-propanol, isopropanol, acetaldehyde, ethylene glycol and propionaldehyde, ^1H NMR (400 MHz Agilent, USA), equipped with the built-in software OpenVnmrJ (University of Oregon, USA) was used. NMR samples were prepared by combining 630 μL of the catholyte solution with 70 μL of D_2O (99.9 atom % D, Sigma Aldrich, USA), and 30 μL of a freshly prepared mixture containing 50 mM phenol (Sigma Aldrich, USA) and 10 mM DMSO (Sigma Aldrich, USA) as internal standards. The solution was transferred to 5 mm NMR tubes (Norell Select, USA). The tubes were first properly cleaned using an in-house setup with acetone and dried at 80 $^{\circ}\text{C}$ before preparing the samples. Water suppression was carried out to obtain a clearer spectrum.

3.4.3 Faradaic Efficiency Calculation

We use a gas chromatography (GC) system that directly employs CO₂ as the carrier gas. To calibrate the system, we employ gas mixtures comprising of ethylene, CO, CH₄, and H₂ at varying concentrations, with CO₂ serving as the predominant gas. The high-pressure gas stream originating from our reservoir is subjected to pressure reduction, resulting in a constant pressure level of approximately 2-3 bar. Subsequently, the gases are delivered to a mass flow controller (MFC, Bronkhorst), enabling precise regulation of the volumetric flow rate to the GC. In our case, we alternate between two distinct values, specifically 0.2 ml/min and 8 ml/min, to expedite the GC's settling time¹¹. The faradaic efficiencies of gaseous products are calculated via the following equation:

$$\text{FE gaseous products} = (n \cdot F \cdot X \cdot \text{molar flow rate}) / I$$

Where, n = number of electrons, F = Faraday's constant (96485 C/mol), X = mole fraction of gaseous product measured by the GC, I = total current applied.

Regarding the analysis of liquid products, we employed high-performance liquid chromatography (HPLC) and H-NMR techniques. Detailed information regarding this matter can be found within the supplementary information section. To calculate the faradaic efficiency of liquid products, we employed the subsequent equation:

$$\text{FE liquid products} = (n \cdot F \cdot C \cdot V) / Q_{\text{tot}}$$

Where, C = concentration derived from HPLC peak integration, V = volume of the catholyte from which the sample is collected for analysis, Q_{tot} = total charge passed during the experiment.

3.4.4 Electrochemical Surface Area Measurements

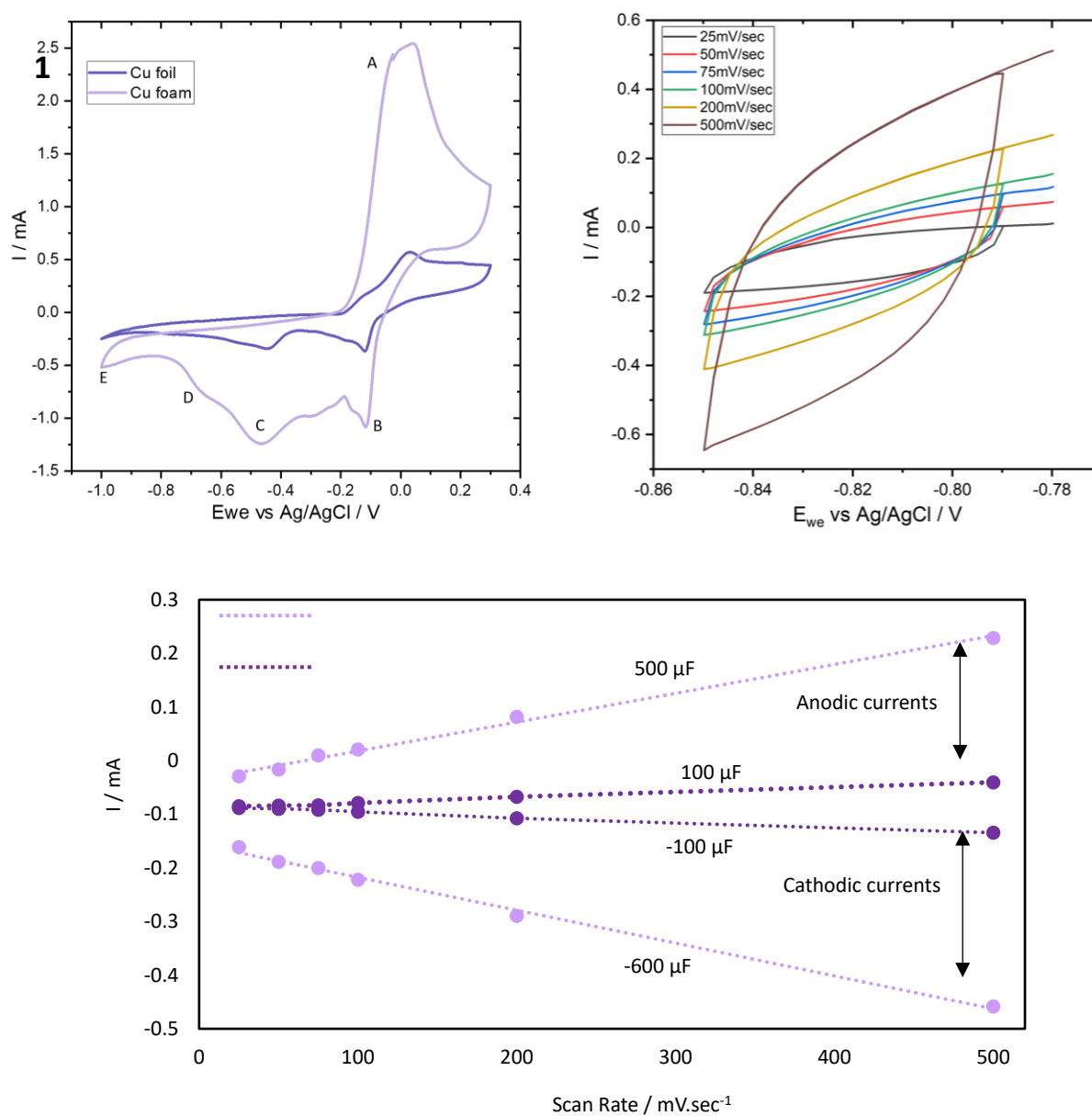


Figure S 3-2: 1) CV scans of a polished copper foil and copper foam (A - copper hydroxide formation, B – copper redeposition, C – Cu(II) to Cu(I), D – Cu(I) to Cu(0), E – HER), 2) CVs of copper foam versus scan rate in 0.5M KHCO₃, 3) linear fitting of anodic and cathodic capacitive currents of the foil and foam electrodes vs. scan rate.

- Average differential capacitance of copper foam – 550 μF
- Average differential capacitance of copper foil – 100 μF
- Geometric area of copper foil – 0.6 cm^2
- Specific Capacitance copper foil – 166.67 $\mu\text{F}/\text{cm}^2$
- ECSA copper foam – 3.3 cm^2

3.4.5 SEM images of Copper Foam Pre and Post Experiment

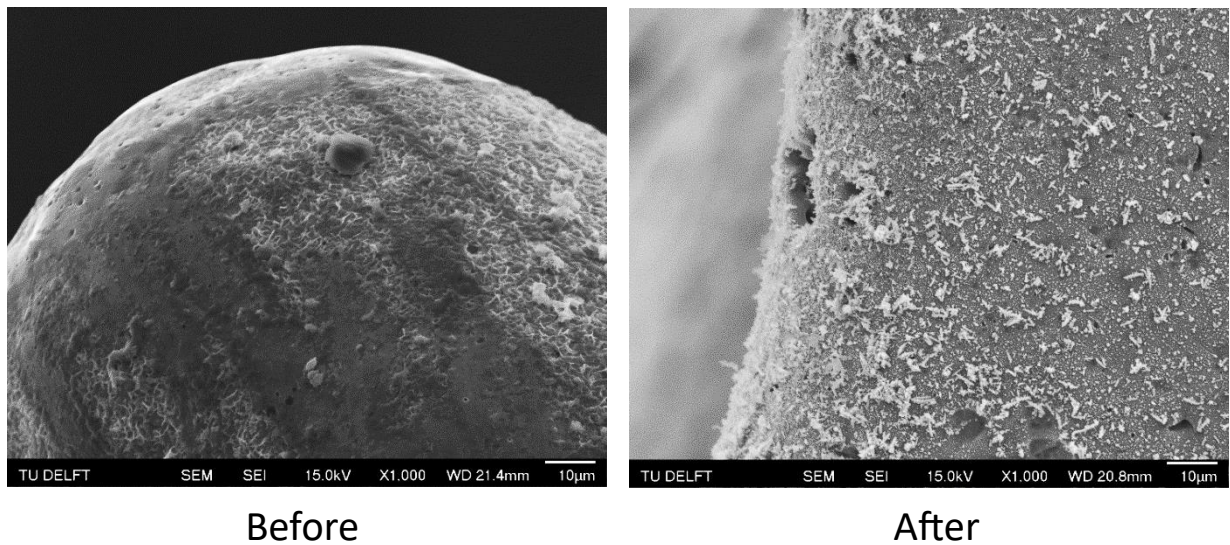


Figure S 3-3: SEM images of the clean Cu foam before experiment and used Cu foam after experiment at 25 bar and -9.1 mA/cm^2 .

There is not a significant difference between the fresh and used copper foam except for an increase amount of surface oxides after stopping the reaction. This is expected to be due to the sudden removal of reduction conditions and exposure to atmosphere.

3.4.6 XPS Spectra Carbon Species

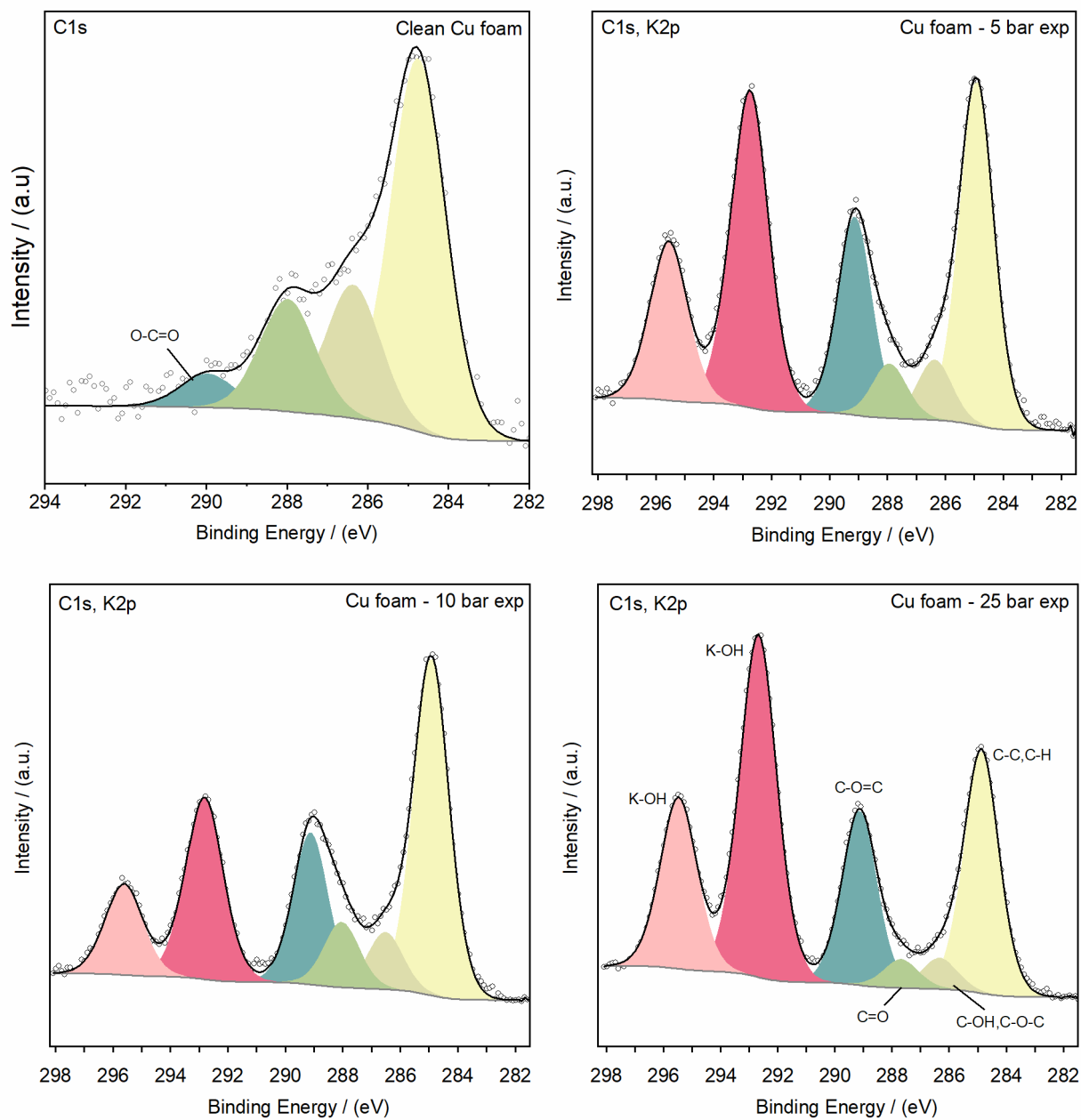


Figure S 3-4: The deconvoluted C1s peaks of clean and used Cu foams at 5, 10, and 25 bar, $j = -9.1 \text{ mA/cm}^2$.

3.4.7 XPS Spectra Copper Species

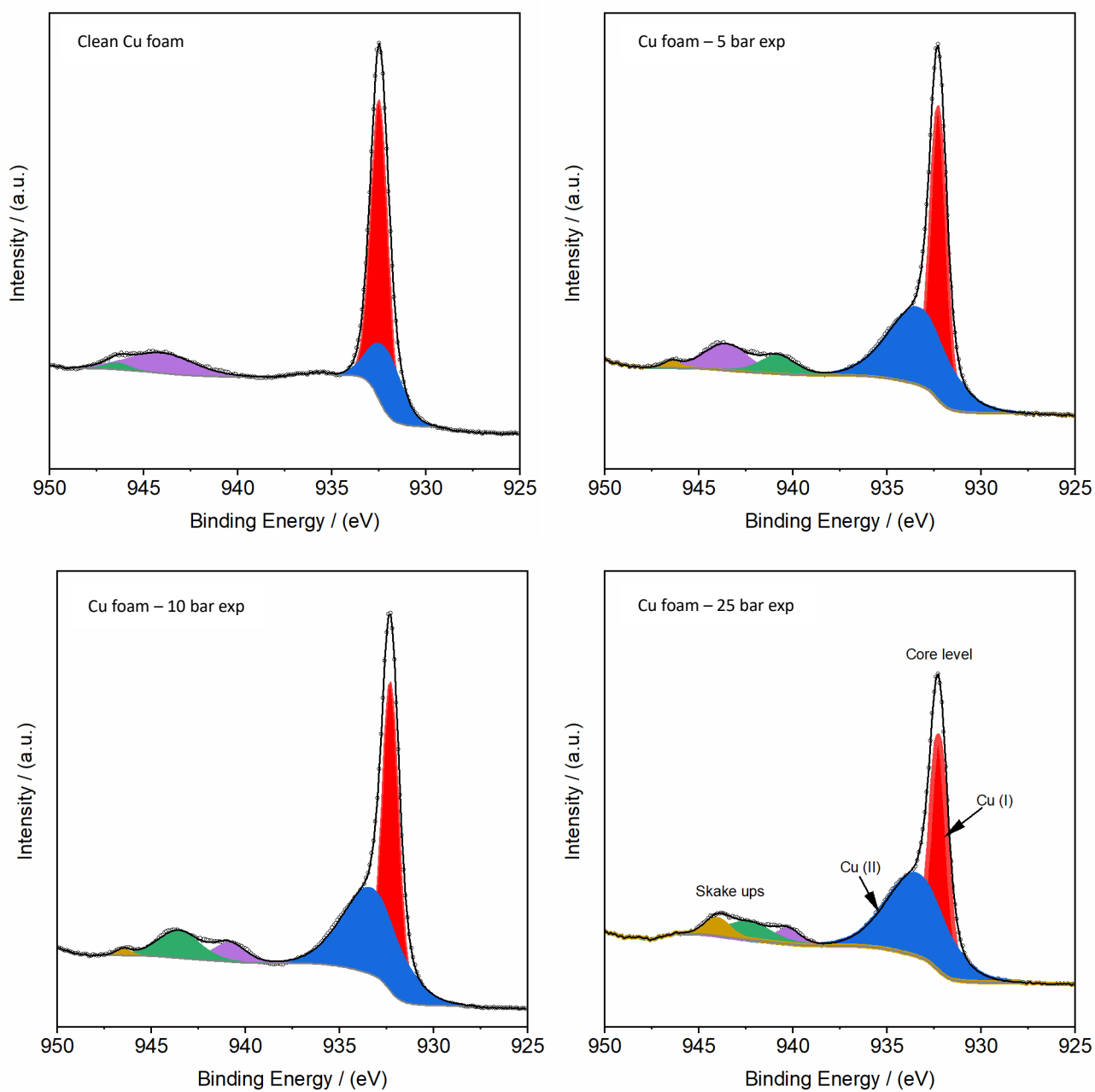


Figure S 3-5: The deconvoluted Cu_{2p_{3/2}} peaks of clean and used Cu foams at 5, 10, and 25 bar, $j = -9.1 \text{ mA/cm}^2$.

3.4.8 X-Ray Diffraction Spectra

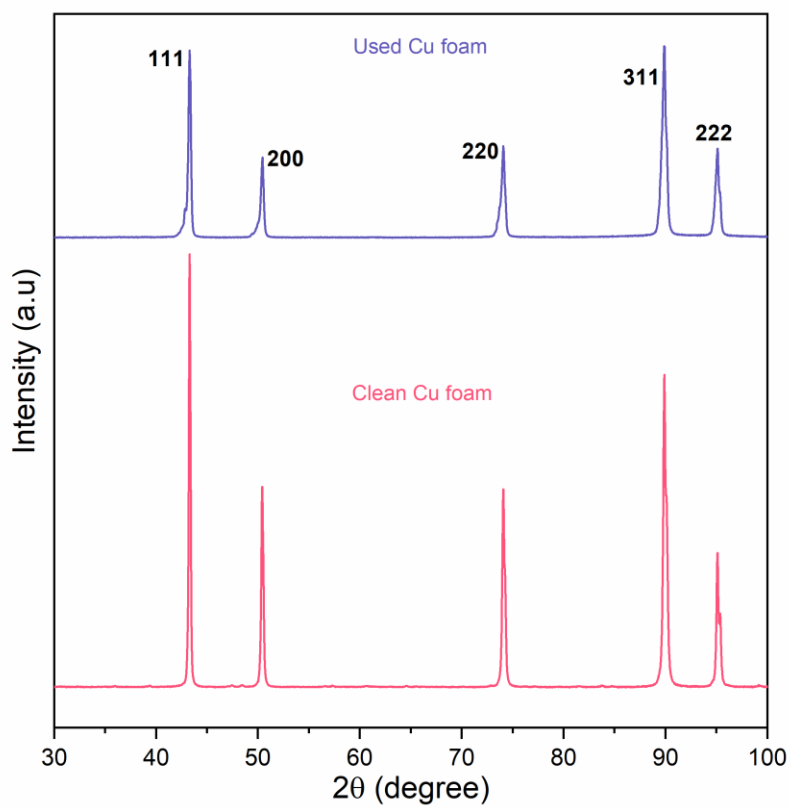


Figure S 3-6: XRD spectra of clean and used Cu foams before and after experiment at 25 bar, $j = -9.1\text{mA}/\text{cm}^2$.

3.4.9 Faradaic Efficiency of Products – 0.5M KHCO₃

Table S 3-1: Faradaic Efficiency of all products at 1 bar

j (mA/cm ²)	-9.1	-12.1	-15.2	-18.2
H ₂	73.9	79.8	84.3	76.7
CO	2.1	1.1	0.8	1.0
Formate	17.7	9.4	9.9	11.5
CH ₄	1.1	2.2	1.7	4.4
C ₂ H ₄	2.2	1.8	1.6	2.5
C ₃ H ₈	0.01	0.01	0.01	0.01
Ethanol				
Acetic Acid				
Acetaldehyde				
Methanol				
Iso / 2 - Propanol				
Propanol				
Propionaldehyde				
V _{RHE}	-0.99	-1.07	-1.15	-1.31
Total FE ~ (%)	96.97	94.31	98.32	95.99

Table S 3-2: Faradaic Efficiency of all products at 5 bar

j (mA/cm ²)	H ₂	CO	Formate	CH ₄	C ₂ H ₄	C ₃ H ₈	Ethanol	Acetic Acid	Acetaldehyde	Methanol	Iso / 2 - Propanol	Propanol	Propionaldehyde	VRHE	Total FE ~ (%)
-9.1	39.1	9.2	39.4	0.1	1.4	0.02	0.35			0.1				-1.03	89.61
-12.1	46.6	9.3	28.7	0.9	3.6	0.03	0.18		0.4			0.3		-1.13	90.03
-15.2	40	7.5	25.6	2.2	5.0	0.04	0.23	1.7	0.7			0.9		-1.18	83.3
-18.2	50.2	6.5	29.3	0.5	2.9	0.02	4.4	1.4						-1.23	95.16

Table S 3-3: Faradaic Efficiency of all products at 10 bar

j (mA/cm ²)	H ₂	CO	Formate	CH ₄	C ₂ H ₄	C ₃ H ₈	Ethanol	Acetic Acid	Acetaldehyde	Methanol	Iso / 2 - Propanol	Propanol	Propionaldehyde	V _{RHE}	Total FE ~ (%)
-9.1	29.6	13.4	42.1	0.1	1.8	0.03		0.5			1.9			-1.01	89.44
-12.1	26.9	10.1	43.8	0.1	1.8	0.03		0.9			0.9	1.8		-1.08	86.46
-15.2	26.9	10.7	38.3	0.4	4.02	0.04		1.3				1.3		-1.19	82.97
-18.2	33.9	10.2	42.8	0.4	4.2	0.03	2.2	1.1	0.8	0.05		0.8	2.3	-1.25	98.81

Table S 3-4: Faradaic Efficiency of all products at 25 bar

j (mA/cm ²)	H ₂	CO	Formate	CH ₄	C ₂ H ₄	C ₃ H ₈	Ethanol	Acetic Acid	Acetaldehyde	Methanol	Iso / 2 - Propanol	Propanol	Propionaldehyde	V _{RHE}	Total FE ~ (%)
-9.1	19.3	5.9	55.9	0.03	0.2						11			-0.95	92.18
-12.1	22.9	13.2	41.8	0.13	1.5	0.02				0.04	4.7	1.5		-1.09	85.79
-15.2	23.3	10.5	38.4	0.3	2.4	0.03	0.76	0.83		0.12	2.6	0.5	0.8	-1.18	80.54
-18.2	29.1	18.9	29.6	0.2	2.1	0.03	0.26	1.13	0.384	0.37		0.4		-1.27	82.27

3.4.10 Faradaic Efficiency of Products – Cation Effect and Electrolyte Concentration

Table S 3-5: Faradaic Efficiency of all products at 25 bar, 0.5M CsHCO₃

Table S 3-6: Faradaic Efficiency of all products at 25 bar, -9.1mA/cm², 1M KHCO₃, 2M KHCO₃

j (mA/cm ²)	-9.1	-18.2
H ₂	23.1	10.1
CO	1.85	1.47
Formate	51.5	70
CH ₄	0.53	0.2
C ₂ H ₄	1.75	1.34
C ₃ H ₈	0.11	0.05
Ethanol	0.1	0.8
Acetic Acid		
Acetaldehyde		0.15
Methanol	0.09	0.03
Iso / 2 - Propanol		0.99
Propanol	0.53	0.52
Propionaldehyde		
V _{RHE}	-1.05	-1.25
Total FE (%)	79.6	85.65

Concentration	H ₂	CO	Formate	CH ₄	C ₂ H ₄	C ₃ H ₈	Ethanol	Acetic Acid	Acetaldehyde	Methanol	Iso / 2 - Propanol	Propanol	Propionaldehy de	V _{RHE}	Total FE ~ (%)
1M	35.75	3.73	31.35	0.21	0.51	0.05	1.8				3.99			-0.93	77.4
2M	30.1	2.4	36.62	0.12	0.22	0.03	1.33				3.51			-0.88	74.34

Table S 3-7: Faradaic Efficiency of all products at 25 bar, -9.1mA/cm², 1M CsHCO₃, 2M CsHCO₃

Concentration	H ₂	CO	Formate	CH ₄	C ₂ H ₄	C ₃ H ₈	Ethanol	Acetic Acid	Acetaldehyde	Methanol	Iso / 2 - Propanol	Propanol	Propionaldehy de	V _{RHE}	Total FE ~ (%)
1M	28.45	1.5	46.76	0.45	1.66	0.12	2.85				5.67	0.69		-0.92	88.15
2M	28.28	0.8	37.7	0.7	0.64	0.14	1.8				4.36			-0.88	74

3.4.11 Reference Plot for HPLC

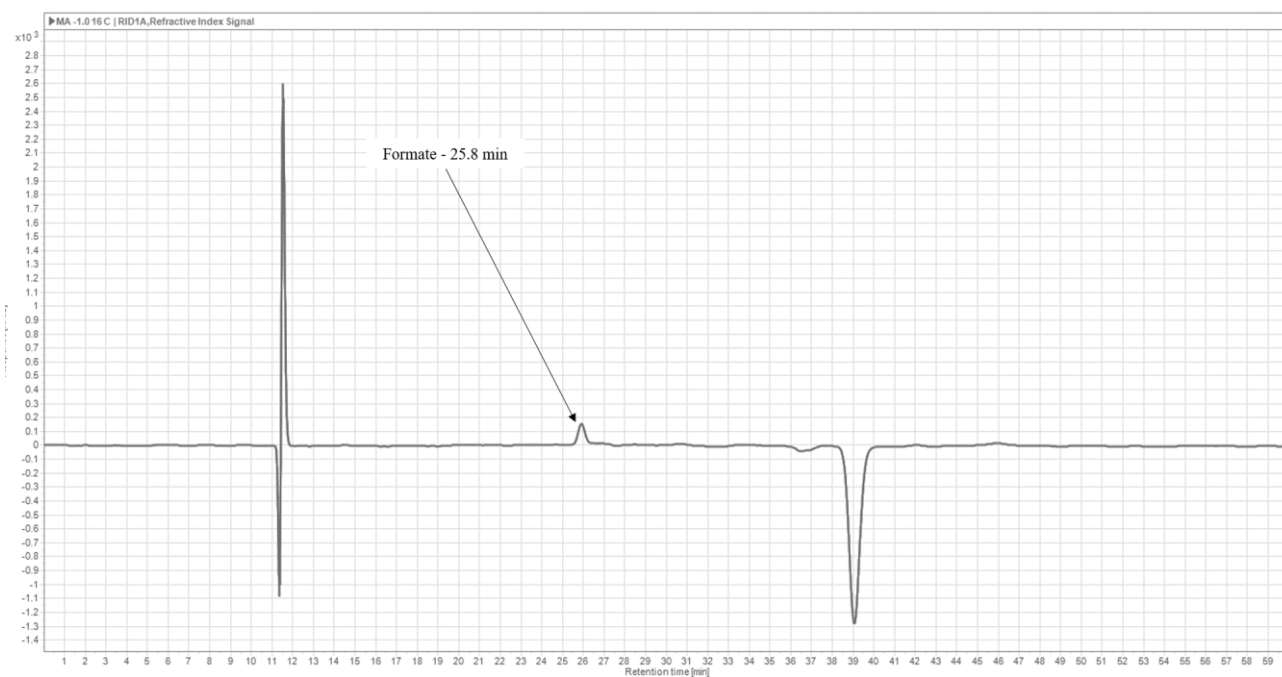


Figure S 3-7: Standard HPLC curve for the detection of formate/formic acid. Formic acid (FA) exists in either its acidic or formate form, depending on the pH. When we dissolve CO₂ gas at high pressures into a 0.5 M KHCO₃ solution, it becomes acidic. However, in our experiment, we collected a liquid sample after depressurizing the system, which releases the excess CO₂ and would shift the pH back to alkaline. We expect formate to be the primary form of FA under these conditions, matching the conditions of our standard curve.

3.4.12 NMR Calibrated Component Peaks with a Sample Experimental Peak for 2-Propanol

NMR Values			Assignment	
Chemical Shift	1H Splitting	J coupling	Probed Nucleus	Name
9.54	s		CH2O	Formaldehyde
8.12	s		CHOOH	Formic acid
6.77	d		Phenol	Internal Standard
5.86	m		CH2CHCH2OH	Allyl alcohol
5.13	d	1.65	CH2CHCH2OH	Allyl Alcohol
3.87	hept	6.21	(CH3)2CHOH	2-Propanol
3.52	s		OHCH2CH2OH	Ethylene glycol
3.51	q	7.08	CH3CH2OH	Ethanol
3.41	t	6.64	CH3CH2CHOH	n-Propanol
3.21	s		CH3OH	Methanol
2.57	s		DMSO	Internal Standard
2.08	s		CH3COCH3	Acetone
1.93	s		CH3COOCH2CH3	Ethyl acetate
1.45	m	5.56	CH3CH2CH(OH)2	Propionaldehyde
1.18	d	5.20	CH3CH2(OH)2	Acetaldehyde
1.02	t	7.16	CH3CH2OH	Ethanol

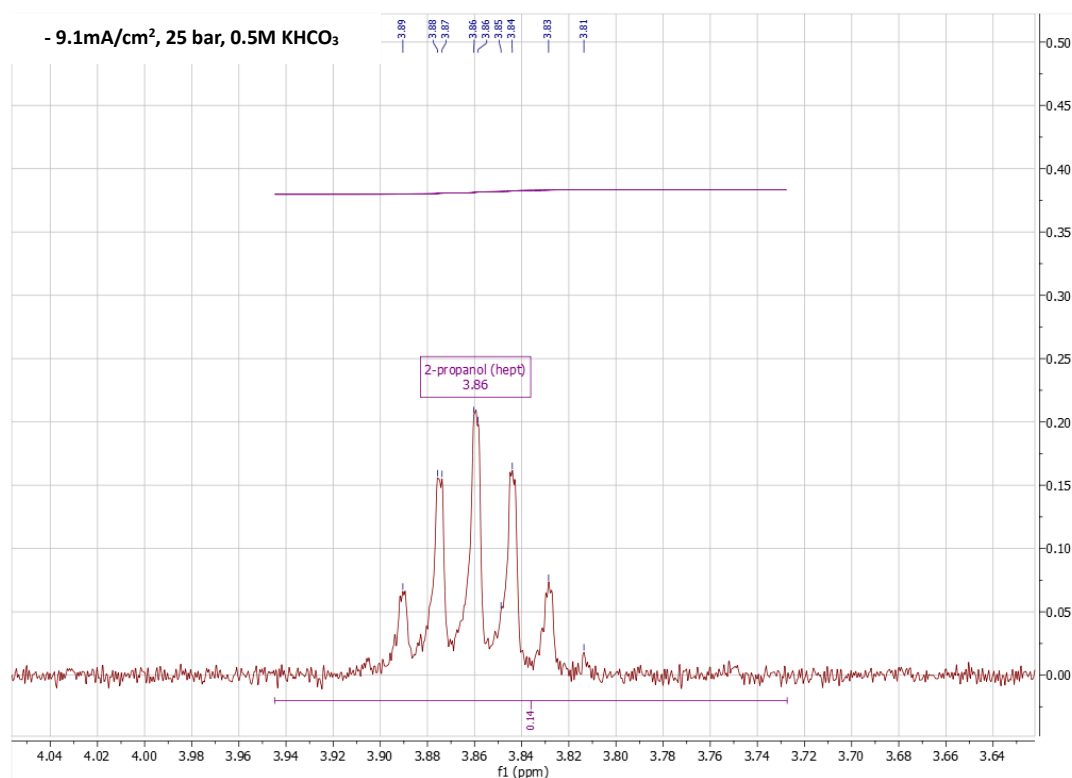


Figure S 3-8: NMR plot with the peak of 2-propanol, for an experiment conducted at $-9.1\text{mA}/\text{cm}^2$ and 25 bar in 0.5 M KHCO_3 .

3.4.13 Comparison of High-Pressure CO₂ Reduction Studies on Copper based Electrodes

Table S 3-8: Comparison of different high-pressure studies to this work.

No	pCO ₂	*Product	j _{product} / mA cm ⁻²	Electrolyte	Cathode	Cell type	FE _{CO} _{2RR} / %	Reference
1	30 atm	HCOO ⁻	87.5	0.1 M KHCO ₃	Polished Cu foil	Autoclave	53.7	³¹
2	60 atm	HCOO ⁻	5.7	0.5 M KHCO ₃	SW-Cu ₂ O/Cu	Autoclave	98.2	³³
3	20 atm	HCOO ⁻	22	0.5 M KHCO ₃	Cu-TPP	Autoclave	22	⁶²
4	45 atm	HCOO ⁻	1.06	0.5 M KHCO ₃	Polished Cu foil	Autoclave	53.1	³³
5	9 atm	HCOO ⁻	30	0.5 M KCl	Strip-shaped Cu	Autoclave	60	⁶³
6	9 atm	HCOO ⁻	-	0.5 M KHCO ₃	Oxide derived Cu np	Autoclave	20.8	⁶⁴
7	50 bar	HCOO ⁻	95	0.5 M KHCO ₃	Cu np	H cell	68.1	³⁴
8	50 bar	HCOO ⁻	169	1 M KHCO ₃	CuPPy	Flow cell	84.7	³⁴
9	10 bar	2-propanol	59	1M CsHCO ₃	CO ₂ -10-Cu ₉₄ Ag ₆ alloy	Autoclave	56.7	⁵³
10	25 bar	HCOO ⁻	12.7	0.5 M CsHCO ₃	Polished Cu foam	Flow cell	70	<u>This work</u>
11	25 bar	2-propanol	1	0.5 M KHCO ₃	Polished Cu foam	Flow cell	10.9	<u>This work</u>

*Mainly on studies that report HCOO⁻ and 2-propanol production from copper-based electrodes

3.4.14 Partial Current Densities of H₂, CO, and HCOOH in 0.5M KHCO₃

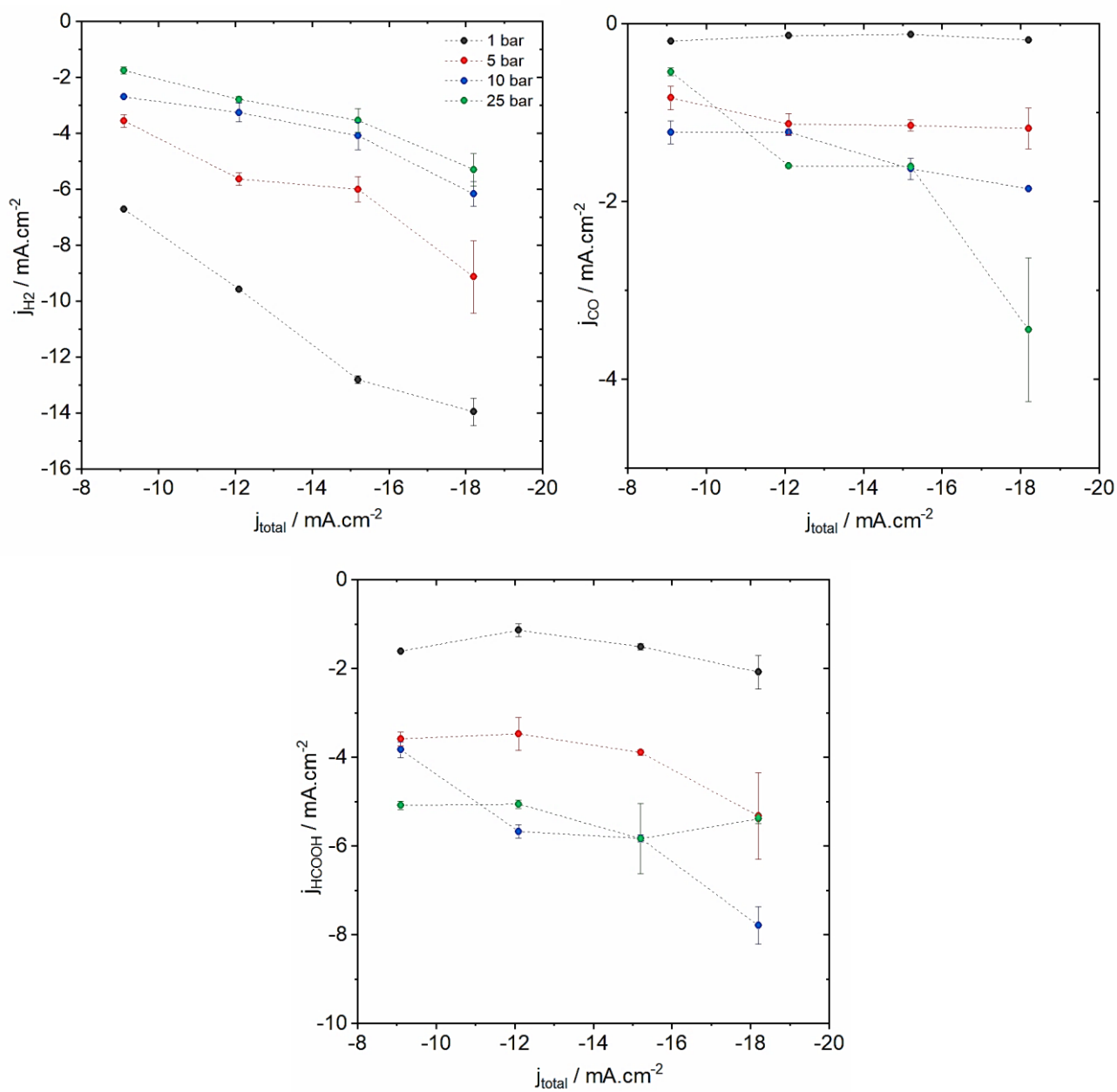


Figure S 3-9: Partial current densities versus applied current densities of H₂, CO, and HCOOH in 0.5 M KHCO₃ at 1, 5, 10, and 25 bar.

3.5 References

- 1 Pörtner, H. O. *et al.* IPCC, 2022: summary for policymakers. *Climate Change 2022 – Impacts, Adaptation and Vulnerability*, (2022). <https://doi.org:10.1017/9781009325844.001>
- 2 Wyndorps, J., Ostovari, H. & von der Assen, N. Is electrochemical CO₂ reduction the future technology for power-to-chemicals? An environmental comparison with H₂-based pathways. *Sustainable Energy & Fuels*, **5**, 5748-5761, (2021). <https://doi.org:10.1039/D1SE00975C>
- 3 Kibria, M. G. *et al.* Electrochemical CO₂ Reduction into Chemical Feedstocks: From Mechanistic Electrocatalysis Models to System Design. *Advanced Materials*, **31**, 1-24, (2019). <https://doi.org:10.1002/adma.201807166>
- 4 Pei, Y., Zhong, H. & Jin, F. A brief review of electrocatalytic reduction of CO₂—Materials, reaction conditions, and devices. *Energy Science and Engineering*, 1012-1032, (2021). <https://doi.org:10.1002/ese3.935>
- 5 Hori, Y., Kikuchi, K. & Suzuki, S. Production of CO and CH₄ in electrochemical reduction of CO₂ at metal electrodes in aqueous hydrogencarbonate solution. *Chemistry Letters*, **14**, 1695-1698, (1985). <https://doi.org:10.1246/CL.1985.1695>
- 6 Kuhl, K. P., Cave, E. R., Abram, D. N. & Jaramillo, T. F. New insights into the electrochemical reduction of carbon dioxide on metallic copper surfaces. *Energy and Environmental Science*, **5**, 7050-7059, (2012). <https://doi.org:10.1039/c2ee21234j>
- 7 Gattrell, M., Gupta, N. & Co, A. A review of the aqueous electrochemical reduction of CO₂ to hydrocarbons at copper. *Journal of Electroanalytical Chemistry*, **594**, 1-19, (2006). <https://doi.org:10.1016/j.jelechem.2006.05.013>
- 8 Asperti, S., Hendrikx, R., Gonzalez-Garcia, Y. & Kortlever, R. Benchmarking the Electrochemical CO₂ Reduction on Polycrystalline Copper Foils: The Importance of Microstructure Versus Applied Potential. *ChemCatChem*, **14**, e202200540-e202200540, (2022). <https://doi.org:10.1002/CCTC.202200540>
- 9 Nitopi, S. *et al.* Progress and Perspectives of Electrochemical CO₂ Reduction on Copper in Aqueous Electrolyte. *Chemical Reviews*, **119**, 7610-7672, (2019). <https://doi.org:10.1021/acs.chemrev.8b00705>
- 10 Li, J., Guo, J. & Dai, H. Probing dissolved CO₂(aq) in aqueous solutions for CO₂ electroreduction and storage. *Science Advances*, **8**, (2022). <https://doi.org:10.1126/sciadv.abo0399>
- 11 Morrison, A. R. T., Girichandran, N., Wols, Q. & Kortlever, R. Design of an elevated pressure electrochemical flow cell for CO₂ reduction. *Journal of Applied Electrochemistry*, **1**, 1-10, (2023). <https://doi.org:10.1007/S10800-023-01927-7/FIGURES/8>

- 12 Proietto, F., Schiavo, B., Galia, A. & Scialdone, O. Electrochemical conversion of CO₂ to HCOOH at tin cathode in a pressurized undivided filter-press cell. *Electrochimica Acta*, **277**, 30-40, (2018). <https://doi.org:10.1016/j.electacta.2018.04.159>
- 13 Proietto, F. *et al.* High-pressure synthesis of CO and syngas from CO₂ reduction using Ni-N-doped porous carbon electrocatalyst. *Chemical Engineering Journal*, **429**, 132251-132251, (2022). <https://doi.org:10.1016/j.cej.2021.132251>
- 14 Ramdin, M. *et al.* High-Pressure Electrochemical Reduction of CO₂ to Formic Acid/Formate: Effect of pH on the Downstream Separation Process and Economics. *Industrial and Engineering Chemistry Research*, **58**, 22718-22740, (2019). <https://doi.org:10.1021/acs.iecr.9b03970>
- 15 Hiejima, Y. *et al.* Electrochemical carboxylation of α -chloroethylbenzene in ionic liquids compressed with carbon dioxide. *Physical Chemistry Chemical Physics*, **12**, 1953-1957, (2010). <https://doi.org:10.1039/B920413J>
- 16 Messias, S. *et al.* Electrochemical production of syngas from CO₂ at pressures up to 30 bar in electrolytes containing ionic liquid. *Reaction Chemistry & Engineering*, **4**, 1982-1990, (2019). <https://doi.org:10.1039/C9RE00271E>
- 17 Snyder, B. F., Layne, M. & Dismukes, D. E. A cash flow model of an integrated industrial CCS-EOR project in a petrochemical corridor: A case study in Louisiana. *International Journal of Greenhouse Gas Control*, **93**, 102885-102885, (2020). <https://doi.org:10.1016/J.IJGGC.2019.102885>
- 18 Proietto, F., Rinicella, R., Galia, A. & Scialdone, O. Electrochemical conversion of CO₂ to formic acid using a Sn based cathode: Combined effect of temperature and pressure. *Journal of CO₂ Utilization*, **67**, 102338-102338, (2023). <https://doi.org:10.1016/J.JCOU.2022.102338>
- 19 Hara, K., Tsuneto, A., Kudo, A. & Sakata, T. Change in the product selectivity for the electrochemical CO₂ reduction by adsorption of sulfide ion on metal electrodes. *Journal of Electroanalytical Chemistry*, **434**, 239-243, (1997). [https://doi.org:10.1016/S0022-0728\(97\)00045-4](https://doi.org:10.1016/S0022-0728(97)00045-4)
- 20 Hori, Y., Wakebe, H., Tsukamoto, T. & Koga, O. Electrocatalytic process of CO selectivity in electrochemical reduction of CO₂ at metal electrodes in aqueous media. *Electrochimica Acta*, **39**, 1833-1839, (1994). [https://doi.org:10.1016/0013-4686\(94\)85172-7](https://doi.org:10.1016/0013-4686(94)85172-7)
- 21 Carroll, J. J., Slupsky, J. D. & Mather, A. E. The Solubility of Carbon Dioxide in Water at Low Pressure. *Journal of Physical and Chemical Reference Data*, **20**, 1201-1209, (1991). <https://doi.org:10.1063/1.555900>
- 22 Kyriacou, G. Z. & Anagnostopoulos, A. K. Influence CO₂ partial pressure and the supporting electrolyte cation on the product distribution in CO₂ electroreduction. *Journal of Applied Electrochemistry*, **23**, 483-486, (1993). <https://doi.org:10.1007/BF00707626>

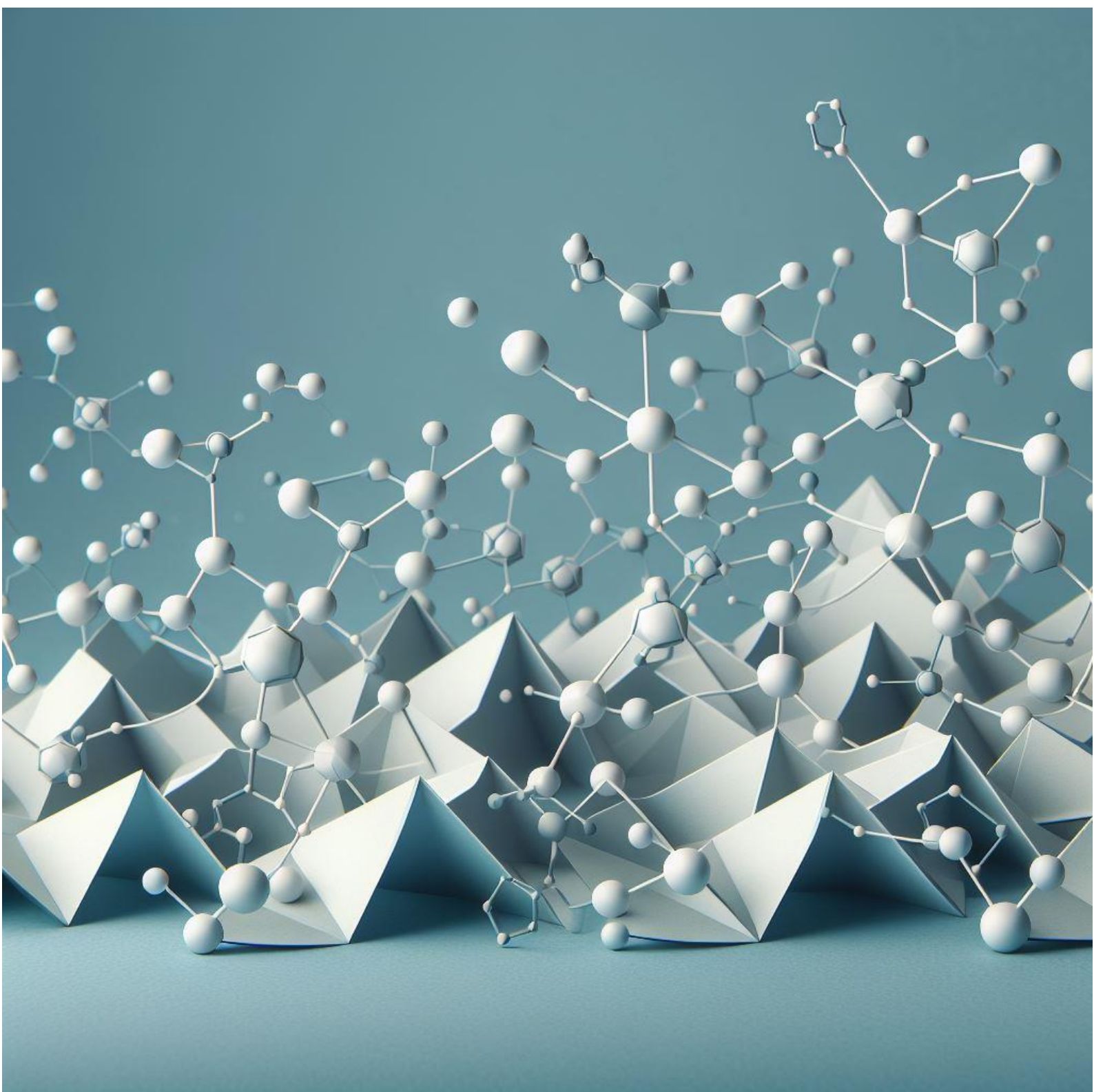
- 23 Lamaison, S. *et al.* High-Current-Density CO₂-to-CO Electroreduction on Ag-Alloyed Zn Dendrites at Elevated Pressure. *Joule*, **4**, 395-406, (2020). <https://doi.org/10.1016/j.joule.2019.11.014>
- 24 Hashiba, H., Yotsuhashi, S., Deguchi, M. & Yamada, Y. Systematic Analysis of Electrochemical CO₂ Reduction with Various Reaction Parameters using Combinatorial Reactors. *ACS combinatorial science*, **18**, 203-208, (2016). <https://doi.org/10.1021/ACSCOMBSCI.6B00021>
- 25 Ramdin, M. *et al.* High pressure electrochemical reduction of CO₂ to formic acid/formate: A comparison between bipolar membranes and cation exchange membranes. *Industrial and Engineering Chemistry Research*, **58**, 1834-1847, (2019). <https://doi.org/10.1021/ACS.IECR.8B04944>
- 26 Scialdone, O. *et al.* Electrochemical reduction of carbon dioxide to formic acid at a tin cathode in divided and undivided cells: effect of carbon dioxide pressure and other operating parameters. *Electrochimica Acta*, **199**, 332-341, (2016). <https://doi.org/10.1016/J.ELECTACTA.2016.02.079>
- 27 Proietto, F., Berche, F., Galia, A. & Scialdone, O. Electrochemical conversion of pressurized CO₂ at simple silver-based cathodes in undivided cells: study of the effect of pressure and other operative parameters. *Journal of Applied Electrochemistry*, **51**, 267-282, (2021). <https://doi.org/10.1007/S10800-020-01505-1/FIGURES/6>
- 28 Gabardo, C. M. *et al.* Combined high alkalinity and pressurization enable efficient CO₂ electroreduction to CO. *Energy & Environmental Science*, **11**, 2531-2539, (2018). <https://doi.org/10.1039/C8EE01684D>
- 29 Dufek, E. J., Lister, T. E., Stone, S. G. & McIlwain, M. E. Operation of a Pressurized System for Continuous Reduction of CO₂. *Journal of The Electrochemical Society*, **159**, F514-F517, (2012). <https://doi.org/10.1149/2.011209JES/XML>
- 30 Todoroki, M., Hara, K., Kudo, A. & Sakata, T. Electrochemical reduction of high pressure CO₂ at Pb, Hg and In electrodes in an aqueous KHCO₃ solution. *Journal of Electroanalytical Chemistry*, **394**, 199-203, (1995). [https://doi.org/10.1016/0022-0728\(95\)04010-L](https://doi.org/10.1016/0022-0728(95)04010-L)
- 31 Hara, K., Kudo, A. & Sakata, T. Electrochemical reduction of carbon dioxide under high pressure on various electrodes in an aqueous electrolyte. *Journal of Electroanalytical Chemistry*, **391**, 141-147, (1995). [https://doi.org/10.1016/0022-0728\(95\)03935-A](https://doi.org/10.1016/0022-0728(95)03935-A)
- 32 Hara, K., Tsuneto, A., Kudo, A. & Sakata, T. Electrochemical Reduction of CO₂ on a Cu Electrode under High Pressure: Factors that Determine the Product Selectivity. *Journal of The Electrochemical Society*, **141**, 2097-2103, (1994). <https://doi.org/10.1149/1.2055067>
- 33 Li, J. *et al.* Electroreduction of CO₂ to Formate on a Copper-Based Electrocatalyst at High Pressures with High Energy Conversion Efficiency. *Journal of the American Chemical Society*, **142**, 7276-7282, (2020). <https://doi.org/10.1021/jacs.0c00122>

- 34 Huang, L. *et al.* Pressure dependence in aqueous-based electrochemical CO₂ reduction. *Nature Communications* 2023 14:1, **14**, 1-11, (2023). <https://doi.org:10.1038/s41467-023-38775-0>
- 35 Proietto, F., Galia, A. & Scialdone, O. Towards the Electrochemical Conversion of CO₂ to Formic Acid at an Applicative Scale: Technical and Economic Analysis of Most Promising Routes. *ChemElectroChem*, **8**, 2169-2179, (2021). <https://doi.org:10.1002/celec.202100213>
- 36 Sabatino, S., Galia, A., Saracco, G. & Scialdone, O. Development of an Electrochemical Process for the Simultaneous Treatment of Wastewater and the Conversion of Carbon Dioxide to Higher Value Products. *ChemElectroChem*, **4**, 150-159, (2017). <https://doi.org:10.1002/CELC.201600475>
- 37 Yang, K., Kas, R. & Smith, W. A. In Situ Infrared Spectroscopy Reveals Persistent Alkalinity near Electrode Surfaces during CO₂ Electroreduction. (2019). <https://doi.org:10.1021/jacs.9b07000>
- 38 Urbain, F. *et al.* Tailoring Copper Foam with Silver Dendrite Catalysts for Highly Selective Carbon Dioxide Conversion into Carbon Monoxide. *ACS Applied Materials and Interfaces*, **10**, 43650-43660, (2018). <https://doi.org:10.1021/acsami.8b15379>
- 39 Zhang, Q. *et al.* Self-Assembly of Graphene-Encapsulated Cu Composites for Nonenzymatic Glucose Sensing. *ACS Omega*, **3**, 3420-3428, (2018). https://doi.org:10.1021/ACSOMEGA.7B01197/ASSET/IMAGES/LARGE/AO-2017-01197B_0007.JPEG
- 40 DeWulf, D. W., Jin, T. & Bard, A. J. Electrochemical and Surface Studies of Carbon Dioxide Reduction to Methane and Ethylene at Copper Electrodes in Aqueous Solutions. *Journal of The Electrochemical Society*, **136**, 1686-1691, (1989). <https://doi.org:10.1149/1.2096993/XML>
- 41 Xiang, K. *et al.* A strategy to eliminate carbon deposition on a copper electrode in order to enhance its stability in CO₂ RR catalysis by introducing crystal defects. *Electrochemistry Communications*, **102**, 72-77, (2019). <https://doi.org:10.1016/j.elecom.2019.04.001>
- 42 Hori, Y. Electrochemical CO₂ Reduction on Metal Electrodes. *Modern Aspects of Electrochemistry*, 89-189, (2008). https://doi.org:10.1007/978-0-387-49489-0_3
- 43 Li, C. W. & Kanan, M. W. CO₂ reduction at low overpotential on Cu electrodes resulting from the reduction of thick Cu₂O films. *Journal of the American Chemical Society*, **134**, 7231-7234, (2012). https://doi.org:10.1021/JA3010978/SUPPL_FILE/JA3010978_SI_001.PDF
- 44 Aresta, M. & Angelini, A. The carbon dioxide molecule and the effects of its interaction with electrophiles and nucleophiles. *Carbon Dioxide and Organometallics*, **53**, 1-38, (2015). https://doi.org:10.1007/3418_2015_93/SCHEMES/4
- 45 Gibson, D. H. Carbon dioxide coordination chemistry: metal complexes and surface-bound species. What relationships? *Coordination Chemistry Reviews*, **185-186**, 335-355, (1999). [https://doi.org:10.1016/S0010-8545\(99\)00021-1](https://doi.org:10.1016/S0010-8545(99)00021-1)

- 46 Chernyshova, I. V., Somasundaran, P. & Ponnuram, S. On the origin of the elusive first intermediate of CO₂ electroreduction. *Proceedings of the National Academy of Sciences of the United States of America*, **115**, E9261-E9270, (2018). https://doi.org/10.1073/PNAS.1802256115/SUPPL_FILE/PNAS.1802256115.SAPP.PDF
- 47 García-Muelas, R. *et al.* Origin of the Selective Electroreduction of Carbon Dioxide to Formate by Chalcogen Modified Copper. *Journal of Physical Chemistry Letters*, **9**, 7153-7159, (2018). <https://doi.org/10.1021/acs.jpcllett.8b03212>
- 48 Sen, S., Liu, D. & Palmore, G. T. R. Electrochemical reduction of CO₂ at copper nanofoams. *ACS Catalysis*, **4**, 3091-3095, (2014). <https://doi.org/10.1021/cs500522g>
- 49 Morrison, A. R. T. *et al.* Surface Coverage as an Important Parameter for Predicting Selectivity Trends in Electrochemical CO₂ Reduction. *Journal of Physical Chemistry C*, **126**, 11927-11936, (2022). https://doi.org/10.1021/ACS.JPCC.2C00520/ASSET/IMAGES/LARGE/JP2C00520_0005.JPEG
- 50 Hou, J., Chang, X., Li, J., Xu, B. & Lu, Q. Correlating CO Coverage and CO Electroreduction on Cu via High-Pressure in Situ Spectroscopic and Reactivity Investigations. *Journal of the American Chemical Society*, **144**, 22202-22211, (2022). <https://doi.org/10.1021/jacs.2c09956>
- 51 Su, D. J. *et al.* Kinetic Understanding of Catalytic Selectivity and Product Distribution of Electrochemical Carbon Dioxide Reduction Reaction. *JACS Au*, (2023). https://doi.org/10.1021/JACSAU.3C00002/ASSET/IMAGES/LARGE/AU3C00002_0009.JPEG
- 52 Sergio Pablo-García *et al.* Mechanistic routes toward C₃ products in copper-catalysed CO₂ electroreduction. *Catalysis Science & Technology*, **12**, (2022/01/26). <https://doi.org/10.1039/D1CY01423D>
- 53 Qi, K. *et al.* Unlocking direct CO₂ electrolysis to C₃ products via electrolyte supersaturation. *Nature Catalysis*, (2023). <https://doi.org/10.1038/s41929-023-00938-z>
- 54 Monteiro, M. C. O. *et al.* Absence of CO₂ electroreduction on copper, gold and silver electrodes without metal cations in solution. *Nature Catalysis*, **4**, 654-662, (2021). <https://doi.org/10.1038/s41929-021-00655-5>
- 55 Singh, M. R., Kwon, Y., Lum, Y., Ager, J. W. & Bell, A. T. Hydrolysis of Electrolyte Cations Enhances the Electrochemical Reduction of CO₂ over Ag and Cu. *Journal of the American Chemical Society*, **138**, 13006-13012, (2016). <https://doi.org/10.1021/jacs.6b07612>
- 56 Ringe, S. *et al.* Understanding cation effects in electrochemical CO₂ reduction. *Energy & Environmental Science*, **12**, 3001-3014, (2019). <https://doi.org/10.1039/C9EE01341E>
- 57 Gu, J. *et al.* Modulating electric field distribution by alkali cations for CO₂ electroreduction in strongly acidic medium. *Nature Catalysis* **2022** 5:4, **5**, 268-276, (2022). <https://doi.org/10.1038/S41929-022-00761-Y>

- 58 Resasco, J. *et al.* Promoter Effects of Alkali Metal Cations on the Electrochemical Reduction of Carbon Dioxide. *Journal of the American Chemical Society*, **139**, 11277-11287, (2017). https://doi.org:10.1021/JACS.7B06765/SUPPL_FILE/JA7B06765_SI_001.PDF
- 59 Li, J., Li, X., Gunathunge, C. M. & Waegele, M. M. Hydrogen bonding steers the product selectivity of electrocatalytic CO reduction. *Proceedings of the National Academy of Sciences of the United States of America*, **116**, 9220-9229, (2019). https://doi.org:10.1073/PNAS.1900761116/SUPPL_FILE/PNAS.1900761116.SAPP.PDF
- 60 Zhong, H., Fujii, K. & Nakano, Y. Effect of KHCO₃ Concentration on Electrochemical Reduction of CO₂ on Copper Electrode. *Journal of The Electrochemical Society*, **164**, F923-F927, (2017). <https://doi.org:10.1149/2.0601709JES/XML>
- 61 Lv, X., Liu, Z., Yang, C., Ji, Y. & Zheng, G. Tuning Structures and Microenvironments of Cu-Based Catalysts for Sustainable CO₂ and CO Electroreduction. *Accounts of Materials Research*, (2022). <https://doi.org:10.1021/accountsmr.2c00216>
- 62 Sonoyama, N., Kirii, M. & Sakata, T. Electrochemical reduction of CO₂ at metal-porphyrin supported gas diffusion electrodes under high pressure CO₂. **1**, 213-216, (1999).
- 63 Hashiba, H., Yotsuhashi, S., Deguchi, M. & Yamada, Y. Systematic Analysis of Electrochemical CO₂ Reduction with Various Reaction Parameters using Combinatorial Reactors. *ACS Combinatorial Science*, **18**, 203-208, (2016). <https://doi.org:10.1021/acscombsci.6b00021>
- 64 Kas, R., Kortlever, R., Yilmaz, H., Koper, M. T. M. & Mul, G. Manipulating the Hydrocarbon Selectivity of Copper Nanoparticles in CO₂ Electroreduction by Process Conditions. *ChemElectroChem*, **2**, 354-358, (2015). <https://doi.org:10.1002/celec.201402373>

Chapter 4 : Elevated Pressure Cascade
Electrocatalytic Conversion of CO₂ to C₃
Products



Abstract

Recent progress in the electroreduction of CO_2 has led to notable breakthroughs in generating C_2 compounds such as ethylene and ethanol. Nevertheless, the direct formation of C_3 products encounters significant limitations due to the $\text{C}_2\text{-C}_1$ coupling reaction, posing a considerable challenge to improving their faradaic efficiency. Here, we present a design for an elevated pressure cascade catalytic reactor to convert CO_2 to a liquid C_3 product in a two-step electrochemical process. At 25 bar pressure, by regulating the potential of the cascade system and the electrolyte flow rate we report a 40% selectivity for 2-propanol from the copper electrode. Upstream silver converts CO_2 to CO which is further reduced on a downstream copper electrode. In the cascade mode (with both silver and copper catalysts active), the $\text{C}_3\text{:C}_2$ oxygenate ratio significantly increases to 6.92 compared to the non-cascade mode (Cu only active) with a modest ratio of 0.62. In conclusion, our cascade catalytic reactor represents a notable step forward in CO_2 electroreduction, exhibiting a meaningful improvement in C_3 selectivity.

4.1 Introduction

Cascade catalysis is a multistep process involving multiple catalysts where a reactant is first converted to an intermediate product on one catalyst that gets consumed on another catalyst to give the desired product. One of the most common examples of this process is photosynthesis in plants where enzymes catalyse the reactions¹. Photosynthesis involves a light-mediated step where water is oxidized photo catalytically followed by a reduction of CO₂ to carbohydrates that consumes the intermediate hydrogen species, making it a perfect example of a cascade catalytic process. One of the primary focusses in electrochemical CO₂ reduction (CO₂RR) research has been the development of suitable catalysts to produce valuable products such as formic acid, CO, ethylene, ethanol, and propanol. However, especially to produce multicarbon products, the optimization of a single catalyst is limited by scaling relations that prevent the optimization of every individual step in the entire reaction mechanism^{2,3}. Cascading has been demonstrated as an interesting alternative approach to produce products that arise from CO as a primary intermediate^{4,5}.

Cascading in CO₂ electroreduction generally consists of the combination of CO₂ reduction to CO with CO electroreduction to hydrocarbon products. Theaker et al. used silver and copper electrodes in two separate reactors to produce ethanol from CO₂ via CO as the intermediate⁵. The conversion of CO was poor (<10%) due to CO being diluted between the reactors owing to mixing with other components and due to its poor solubility in water. In a study using gold and copper interdigitated cascaded electrodes within a single reactor, Lum et al. showed that CO formed on gold, spills over via diffusion to copper thereby increasing its concentration well beyond its solubility limit⁶. This resulted in an enhanced synthesis of C-C coupled products

from CO₂. Interestingly, the obtained amounts of oxygenates (ethanol) was higher than that of hydrocarbons (ethylene), which is consistent with a recent study on high-pressure CO reduction on copper that highlights the importance of achieving a high CO coverage to obtain higher reduction liquid products⁷. In a different interpretation of the same concept using their custom setup, Gurudayal et al. employed convection to aid the transport of CO formed on a silver electrode to a downstream copper electrode⁸. By controlling the flow rate and applied potential an optimal ratio of oxygenates to hydrocarbons was achieved. Yet, the most prominently observed products were restricted to the commonly reported ethanol, formic acid with small amounts of acetate and acetaldehyde. Synthesis of three carbon products like propanol was still challenging pointing to suboptimal reaction conditions.

Theoretical studies predict that the coverage of the key intermediates *CO and *H on a copper surface, and therefore the product distribution, is contingent upon factors such as surface morphology, applied potential, and importantly, the applied pressure^{7,9-13}. The main benefits of pressurization are that it negates the solubility limitations of CO₂ and CO in aqueous media and thereby increases the surface coverage of the reactants and intermediates on copper, resulting in enhanced production of higher carbon products such as alcohols, and aldehydes⁷. Higher surface coverages of *CO on the surface of copper can significantly decrease the binding energies for *CO and other key intermediate species, paving the way towards uncommon products^{7,12}. For instance, in a recent study using a supersaturated CO₂ electrolyte, Kun et al. reported an enhanced production of 2-propanol/iso-propanol (IPA) with a selectivity of 56% on a silver-copper alloy catalyst prepared under similar supersaturated conditions¹⁴. Moreover, in our own previous work (Chapter 3) using high pressure for CO₂RR on a copper foam electrode we

observed the production of 2-propanol with a selectivity of 11%. The low amounts of C₃ products observed in atmospheric pressure cascade CO₂ electroreduction could be an indication of poor surface coverages of *CO and other reactant species¹⁴. This hypothesis is further supported by the prediction of Sandberg et al. that the *CO and *H coverage impacts the surface dimerization and hydrogenation rate¹².

We posit that applying elevated CO₂ pressure to a cascade catalytic system composed of an upstream silver and downstream copper electrode, can enable and enhance unique C-C coupled pathways towards elusive higher alcohols like 2-propanol. To test this hypothesis, we have designed a novel high pressure electrochemical reactor for cascade CO₂ reduction. Using this setup, we aim to deliver a sufficiently concentrated supply of the reaction intermediate (CO) to the copper electrode. At a pressure of 25 bar, by tuning the potential of the cascade system and flow rate of the electrolyte, we report a 2-propanol selectivity of 40% from a copper electrode. Furthermore, the C₃:C₂ oxygenates (main considered products – for C₃: 2-propanol, and for C₂: ethanol, acetaldehyde, ethylene glycol) ratio reaches a significant 6.92 for the cascade mode (with both silver and copper as active catalysts) compared to a mere 0.62 for the non-cascade mode with only Cu as the active catalyst.

4.2 Experimental

4.2.1 Materials

0.1 M potassium bicarbonate (KHCO₃, ≥ 99.95% trace metals basis, Sigma Aldrich), and 0.1 M cesium bicarbonate (CsHCO₃, 99.9% purity, Sigma Aldrich) were used to prepare the catholyte and anolyte. Silver foil (Ag, 1mm thick, >99.95%, GoodFellow), and copper foil (Cu, 1mm thick, 99.999% trace metal basis, Sigma Aldrich) served as the two working electrodes, while

IrMMO foil was the anode. Nafion 117 (Ion Power GmbH) was cleaned in MilliQ water (18M Ω .cm at 25°C) and used as the ion exchange membrane. HCl (ACS reagent, 37%, Sigma), acetone (Technical Grade, assay \geq 99%, VWR Chemicals), and H₃PO₄ (85% VLSI, Technic) were used for cleaning and preparation of the electrodes. H₂SO₄ (95-97%, ACS reagent, Honeywell), DMSO (ACS reagent, \geq 99.9%, Sigma), phenol (ACS reagent, 99.0-100.5%, Sigma), and D₂O (99.9 atom% D, Sigma) were used for liquid product analysis. An ultrapure water purification system (MilliQ IQ 7000, Merck–Millipore, USA) was used as water source for all experiments. All reagents were used without further purification.

4.2.2 Electrochemical Apparatus and Measurement

The schematic of the entire setup is shown in SI 4.5.1. The details of the custom designed cascade reactor housing two working electrodes (Ag and Cu) are given in the results section. A modular clamp system secures the reactor in place and seals the stack leak tight without the need for any nuts and bolts. The catholyte and anolyte are circulated through the reactor using two HPLC pumps (Knauer AZURA P4.1 S with 50 ml pump heads). The outlets from the reactor are connected to external reservoirs through back pressure regulators (Equilibar). The cathode side reservoir is equipped with two inlets – one for the pressurized CO₂ feed and the other coming from the back pressure regulator. An outlet from the reservoir is connected to the pump, while another outlet carries the gaseous stream to an inline GC. In-depth details regarding the assembly can be found in our previous work (section 2.3.1)¹⁵.

Electrochemical experiments were carried out in the custom-designed high-pressure flow setup, using a BioLogic BP300 dual channel potentiostat with EIS analyser. The reactor was operated in a bipotentiostatic mode, offering independent control of the Ag and Cu electrodes against

the Ag/AgCl reference electrode (LF 1.6–45 mm, Innovative Instruments Inc., USA). The operation of the two working electrodes and the electrical connections to the external potentiostat were established in a manner similar to that proposed by Gurudayal et al.⁸. Gas products were analysed every 2 minutes using an in-line gas chromatograph (CompactGC 4.0, Global Analyzer Solutions, The Netherlands). Liquid products were collected at the end of the electrochemical experiments and analysed using high-pressure liquid chromatography (HPLC, Agilent Technologies 1260 Infinity, USA). To cross check and detect intermediate and minor products present in the electrolyte samples ¹H-NMR was used (400 MHz Agilent, USA), with the built-in software OpenVnmrJ (University of Oregon, USA). Further details regarding product analysis are provided in SI 4.5.2.

4.2.3 Electrode Preparation

Ag and Cu foils were cut into pieces of 1.1 cm × 0.6 cm (exposed area in the reactor was 0.6 cm²). Ag pieces were first mechanically sanded with P1000 and P1200 sandpaper after which the foils were mechanically polished with 3 μ and 1 μ diamond suspension to a mirror-like finish, devoid of any visible major scratches. After polishing, the Ag foils were sonicated for 5 minutes in 2M HCl and 5 minutes in MilliQ water to remove any impurities from the surface.

Cu foils were mechanically polished with 3 μ and 1 μ diamond suspension, following a procedure by Asperti et al.¹⁶, after which they were electropolished in H₃PO₄ for 3 minutes at 2.1V against a carbon rod as a counter and reference electrode. After rinsing with MilliQ water and drying in argon, the Cu foils were annealed in an oven at 230°C for 3 hours to oxidize the surface to enhance the roughness and improve its activity under reduction conditions¹⁷.

4.2.4 Electrode Characterization

Scanning Electron Microscopy (SEM, Jeol JSM 6500F) images of the silver and copper oxide electrodes were taken using a Jeol JSM 6500F SEM equipped with an ultradry energy dispersive X-ray spectrometry detector (ThermoFisher, USA). to visualize the surface morphology before the experiments. X-Ray diffractograms (XRD) were acquired with a Bruker D8 Advance diffractometer (Bruker, USA) with Bragg-Brentano geometry, employing a graphite monochromator and Vantec position-sensitive detector (Co K α radiation, divergence slit var12, scatter screen height 8 mm, 40 kV 40 mA). The results are presented in SI 4.5.5 and 4.5.6.

4.3 Results and Discussion

4.3.1 Custom Electrochemical Cell Design

The exploded view of the electrochemical cell is shown in **Figure 4.1**. The cell is comprised of a stainless-steel anode end plate (grade: 304/1.4301, Xometry Europe GmbH) on one side and a PEEK cathode end plate on the other side sandwiching the catholyte and anolyte flow plates that are separated by a Nafion 117 membrane. At the anode side the electrical connection is realised by the steel endplate, connected to the electrode. Since the anode (**Figure 4.1a - part 11**) is located inside the slot in the flow plate, a protrusion from the steel end plate pushes the electrode into the slot thereby ensuring a good electrical connection. At the cathode side a 3D printed (Elastic 50A resin, Formlabs) frame (**Figure 4.1c**) was designed (with similar dimensions as the electrode slot in the flow channel (**Figure 4.1e**) to secure both the working electrodes in place, while offering openings at the back to provide separate electrical contacts. The material of the holder is insulating and a protrusion between the electrodes ensures they are insulated from each other, a criterion crucial to operate them in a bipotentiostatic mode. This material was selected for the holder as it can bend, stretch, compress, and withstand repeated

use without tearing or quickly springing back to its original shape. This ensures that post assembly and during operation at high pressures, the holder can stretch and seal the chamber, making it leak tight.

At the back of the electrode holder, two holes are cut out, to electrically connect the electrodes (Figure 4.1d). Custom laser cut steel rods were used to provide connection between the external potentiostat and the electrodes. A bolt provided electrical contact between the back of the electrodes and the steel rods. To ensure there will be a connection between the bolt and the rod, a nut was added. This nut was used to secure the rod into the groove in the back of the plate,

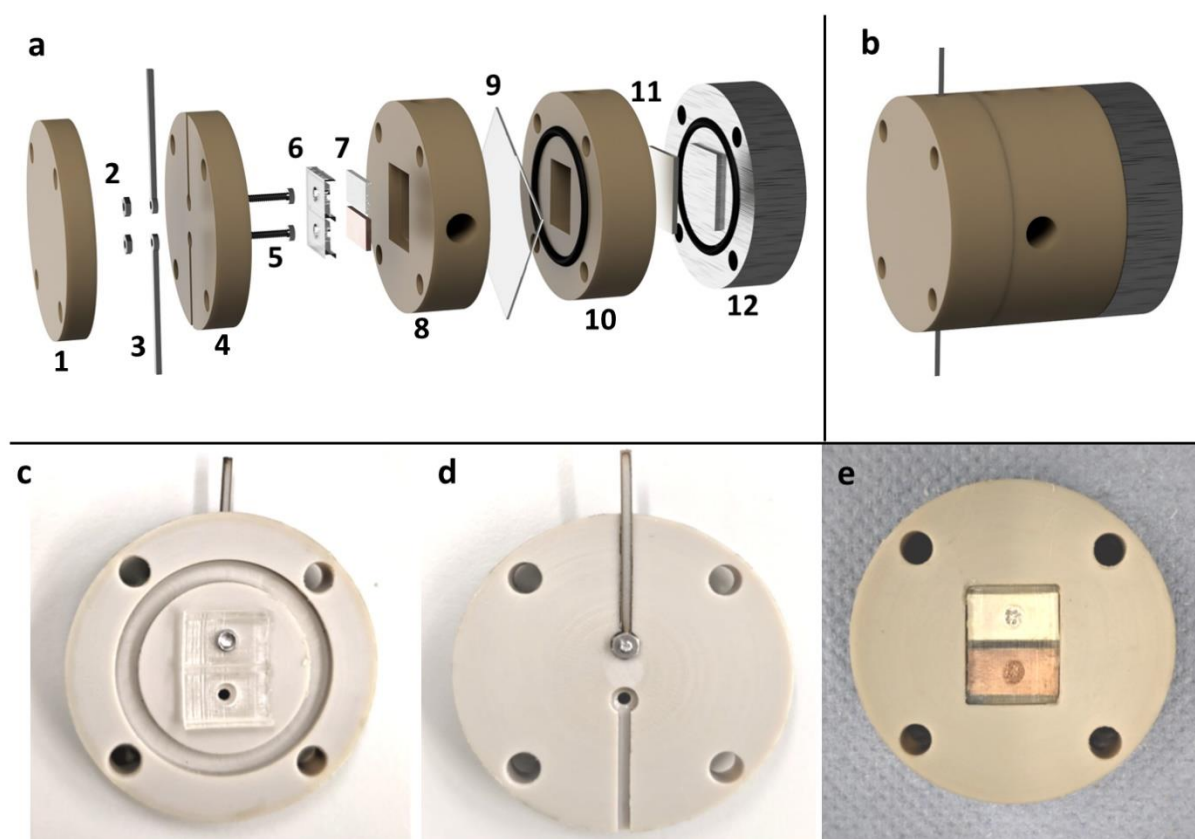


Figure 4.1: a) Exploded view of the electrochemical cell - (1) Endplate cathode back (2) Connection nuts (3) Connection rods (4) Endplate cathode front (5) Connection bolts (6) Electrode holder (made from Flexible 80A resin, Formlabs) (7) Cathodes (8) Catholyte chamber (9) Membrane (10) Anolyte chamber (11) Anode (12) Conductive endplate, b) Closed electrochemical cell, c) Front of the cathode endplate including the electrode holder connected at the top connection, d) Back of the cathode endplate fitted with the connection rod at the top side, e) Catholyte chamber fitted with the electrodes and electrode holder.

using the thread of the bolt (**Figure 4.1a – parts 2,3 and 5**). Grooves in the endplate conceal the nuts, allowing a seamless stacking of plates. A small piece of aluminium tape (pressed into a circular shape of diameter ~ 3 mm) was added to the head of the bolts before assembly to guarantee consistent contact with electrodes in the holder.

The 3D printed electrode holder was designed with adaptability in mind. Opting for a holder, as opposed to relying solely on pressing the electrodes into the flow plate, offers the notable advantage that, when modifying operational configurations and conditions, only this element necessitates replacement, sparing the need for a complete overhaul of the entire reaction chamber. This way it becomes possible to vary the distance between the electrodes, the electrode sizes, or their configuration with ease.

4.3.2 Electrochemical CO₂ Reduction at High Pressures

The electrochemical performance of the cascade system was studied using chronoamperometry (CA) to probe the impact of potential towards product selectivity. As a first step, a CO₂ pressure of 5 bar was applied and the potential on the Ag electrode was altered to determine the optimal conditions for the supply of CO to the Cu electrode, the second part of the cascade. For all the measurements discussed below, the electrolyte was circulated at 25 ml/min through the cell unless explicitly mentioned otherwise. The initial tests were conducted with 0.1 M CsHCO₃ to compare this study to the pioneering works of Lum et al.⁶ and Gurudayal et al.⁸ on this topic. Three different potentials (-0,8V, -1V and -1.2V vs RHE) were applied for the Ag electrode while keeping copper inactive. The major products produced were H₂, CO and formate (**Figure 4.2a**). The faradaic efficiency (FE) of H₂ decreased from 50% to 28% with an increase in potential while formate production displayed the opposite trend with a FE starting at 27% at -

0.8 V vs RHE and reaching 52% at -1.2 V vs RHE. For CO, the FE followed a volcano-like trend peaking at 14% at -1 V vs RHE. We therefore chose to apply -1 V vs RHE on silver for all further cascade experiments as this was the potential at which the highest amount of CO was obtained. Studies on the microenvironment near an Ag electrode have revealed that larger

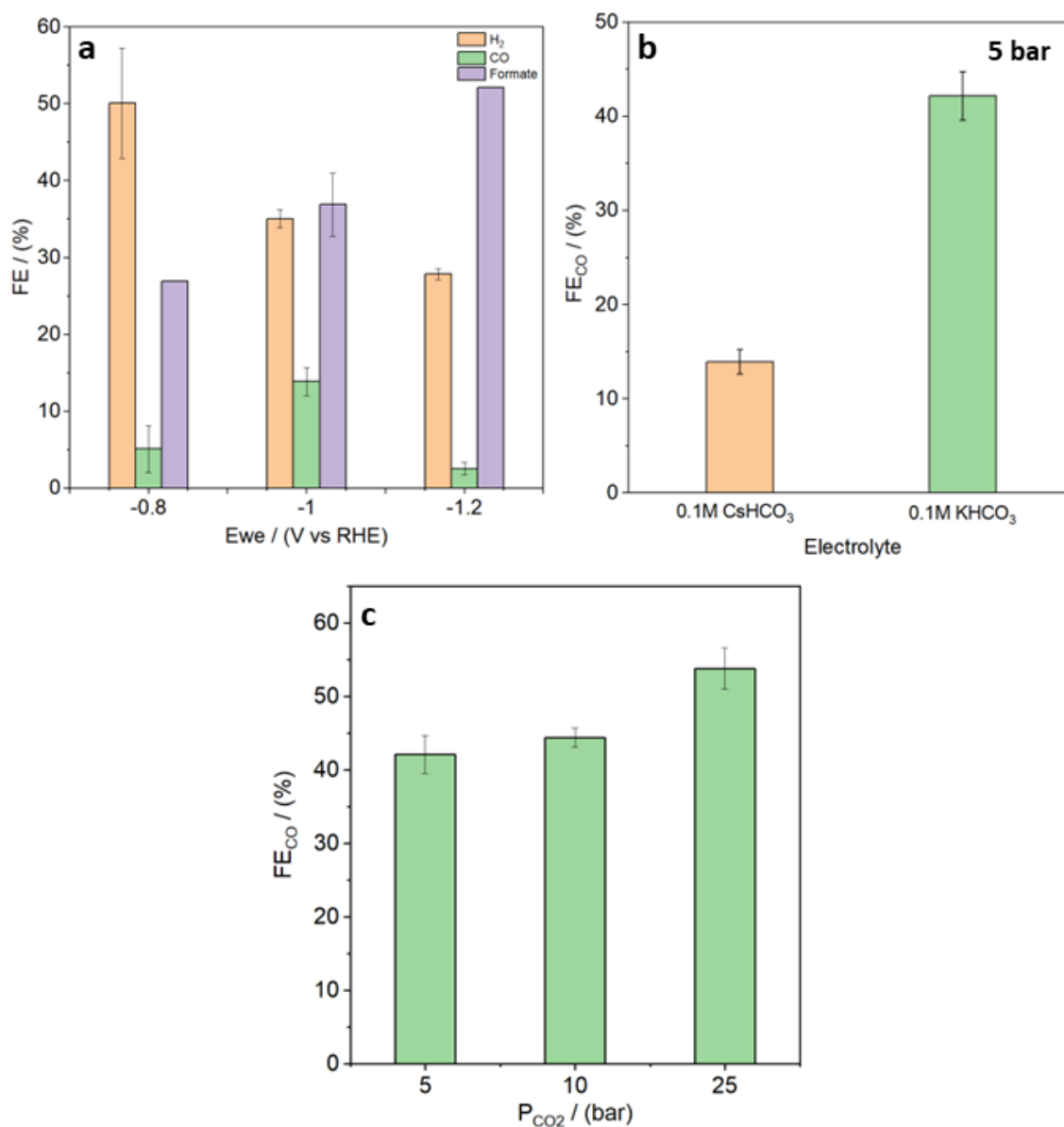


Figure 4.2: a) Faradaic efficiency as a function of potential applied to Ag cathode at 5 bar with 0.1M CsHCO₃ at a flow rate of 25 ml/min, b) FE_{CO} comparison for 0.1M CsHCO₃ and 0.1M KHCO₃ at 5bar and -1 V vs RHE, c) FE_{CO} versus applied pressure for 0.1M KHCO₃ at -1 V vs RHE (error bars represent the standard deviation from at least two independent repetitions).

cations with smaller hydration shell such as Cs^+ have a stronger electrostatic interaction with the electrode surface than K^+ . This results in a stronger stabilization of reaction intermediates like $^*\text{CO}$ and $^*\text{COOH}$ with strong dipole moments^{18,19}. This coupled with the stronger buffering strength²⁰ of Cs^+ compared to K^+ can result in a slightly lower pH leading to preferential formation of HCOOH over CO while using CsHCO_3 (alkaline pH favours CO formation on silver)¹⁸. Based on this understanding, CO_2RR experiments were also conducted at 5 bar by applying -1 V vs RHE on Ag using 0.1 M KHCO_3 (**Figure 4.2b**). We observed that the FE_{CO} increased to approximately 42 % for K^+ instead of 14% for Cs^+ . Since the goal is to maximize the supply/amount of CO delivered to the downstream Cu electrode for further reaction, 0.1 M KHCO_3 was used as the electrolyte for the rest of the experiments. **Figure 4.2c** shows the effect of a pressure increase on the FE_{CO} for 0.1 M KHCO_3 on Ag catalyst. At 10 and 25 bar the FE_{CO} increases further to 44% and 54%, respectively, indicating that the higher applied pressure²¹ (in this study, it is limited to 25 bar) is better suited to supply higher amounts of CO to the downstream Cu electrode.

Cascade experiments were successfully conducted at 25 bar by fixing the Ag electrode at -1 V vs RHE while varying the potential on the Cu electrode (-0.7V, -0.8V, and -0.9V vs RHE). The product distribution in cascade mode is shown in **Figure 4.3b**. The major products detected include H_2 , CO , formate, ethanol, ethyl acetate, acetaldehyde, and 2-propanol. The FE_{H_2} first decreases as the potential is changed from -0.7V to -0.8V before slightly increasing at -0.9V. The FE_{CO} shows a reverse trend to that of H_2 with a maximum at -0.8 V, while overall the FE_{CO} is lower when working in cascade mode compared to only Ag as active electrode, indicating the consumption of produced intermediate CO on Cu alongside CO_2 . The FE_{HCOOH} increases with

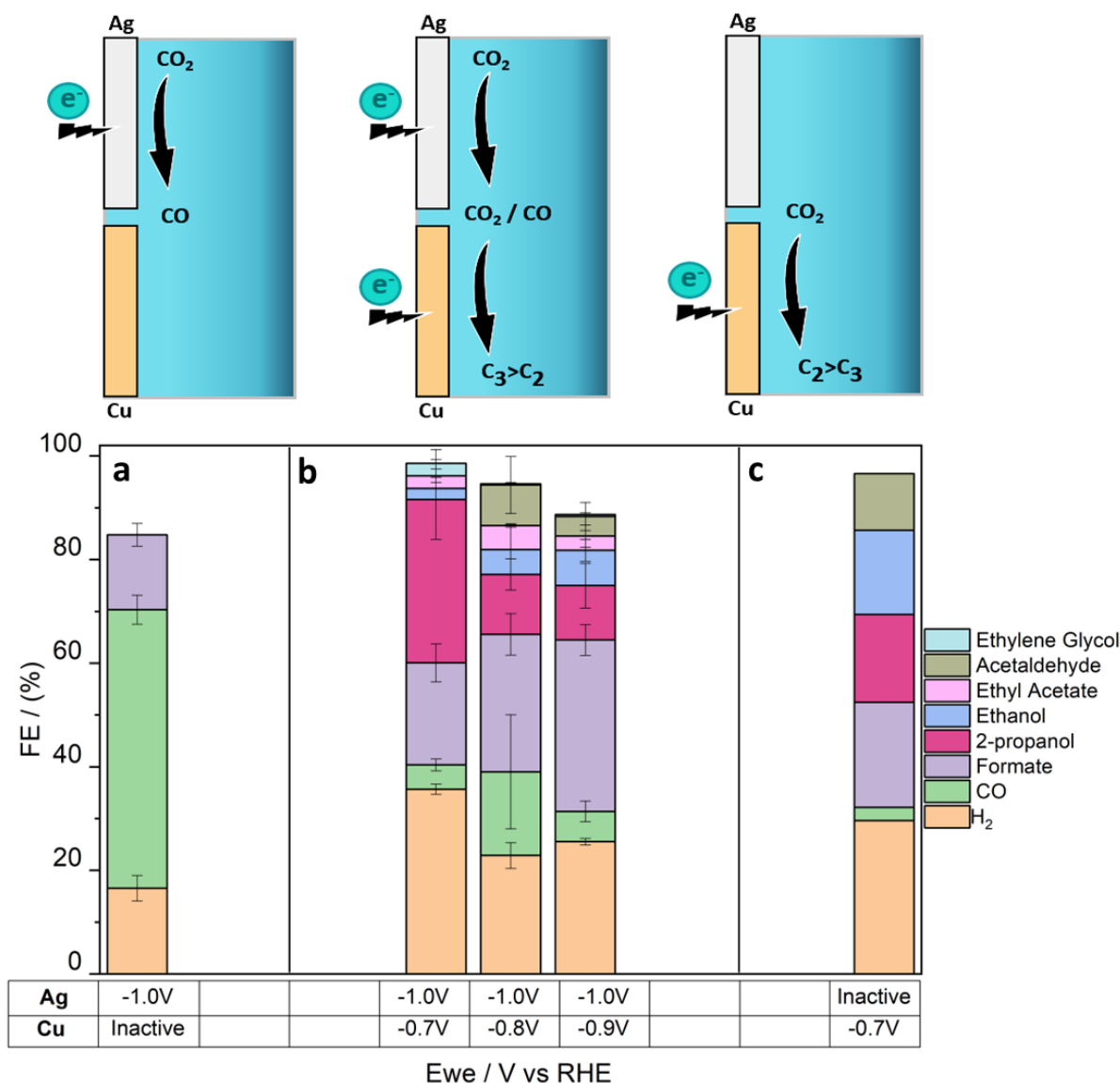


Figure 4.3: Faradaic efficiency as a function of potential applied to a) Ag cathode (held at -1.0V vs RHE and Cu inactive), b) Cascade Operation (Ag held at -1.0V and Cu at (left to right) -0.7V, -0.8V, and -0.9V vs RHE), c) Cu cathode (held at -0.7V vs RHE and Ag inactive). All experiments were performed in 0.1M KHCO₃ recirculated at 25 ml/min (error bars represent the standard deviation from at least two independent repetitions).

increased applied reduction potential on the Cu electrode in the cascade mode. This is attributed to the fact that the CORR does not produce any formate on a Cu electrode²². At lower potentials (-0.7V vs RHE in this case) CORR is more prominent on the oxide derived Cu electrode and can outcompete CO₂RR since CO reduction requires 2 fewer electrons than CO₂ reduction on a per carbon basis^{13,23}. The FE_{EtOH} is low at all applied potentials but it increases from 2.2% at -0.7V vs RHE to 6.8% at -0.9V vs RHE.

Notably, 2-propanol selectivity increases with decreasing applied potentials starting from 11% at -0.9V vs RHE and reaching 32% at -0.7V vs RHE. This trend matches the findings reported by Kun et al. using supersaturated CO₂ on an Ag-Cu alloy catalyst¹³. For the exact mechanism behind the formation of 2-propanol, we have some indications based on literature, but the details are not yet clear (section 3.3.1). In brief, the mechanism includes the dimerization of *CO species through C-C coupling, yielding a reduced dimer (*CO-COH) species. This can rearrange and further reduce to form a C₂ enol intermediate (*C₂H₃O), a precursor to ethanol. At low potentials and high pressures, an increased surface coverage of *CO can promote interactions between the enol and *CO species. Further proton-coupled electron transfers selectively lead to a C₃ enol species, culminating in 2-propanol, resembling the ethanol pathway. Limited ethanol presence, especially at higher pressures, therefore, stems from its conversion to 2-propanol at the Cu electrode. CO₂RR using the cascade mode on an Ag-Cu pair at ambient pressure has been shown to create a supersaturated reservoir of CO between the two electrodes⁸. It is likely that the combined effect of cascade mode with elevated pressure enables improved solubility and higher surface coverage, enhancing the production of 2-propanol. To verify this, a control experiment was conducted with the Ag electrode inactive and Cu active at -0.7V vs RHE (Figure 4.3c). We find that in this case the FE_{2propanol} is only 16.7% while the FE_{EtOH} reaches 16.3%, indicating an inferior selectivity towards 2-propanol due to lower amounts of surface CO species that are formed directly via CO₂RR on Cu. Also, the fact that ethyl acetate is observed (appreciable amounts) only in the cascade mode indicates higher concentrations of CO on the surface and therefore its enhanced coverage on copper due to a continuous supply by the upstream Ag electrode. Small amounts of ethylene glycol were also detected and the exact amounts are presented in SI 4.5.7.

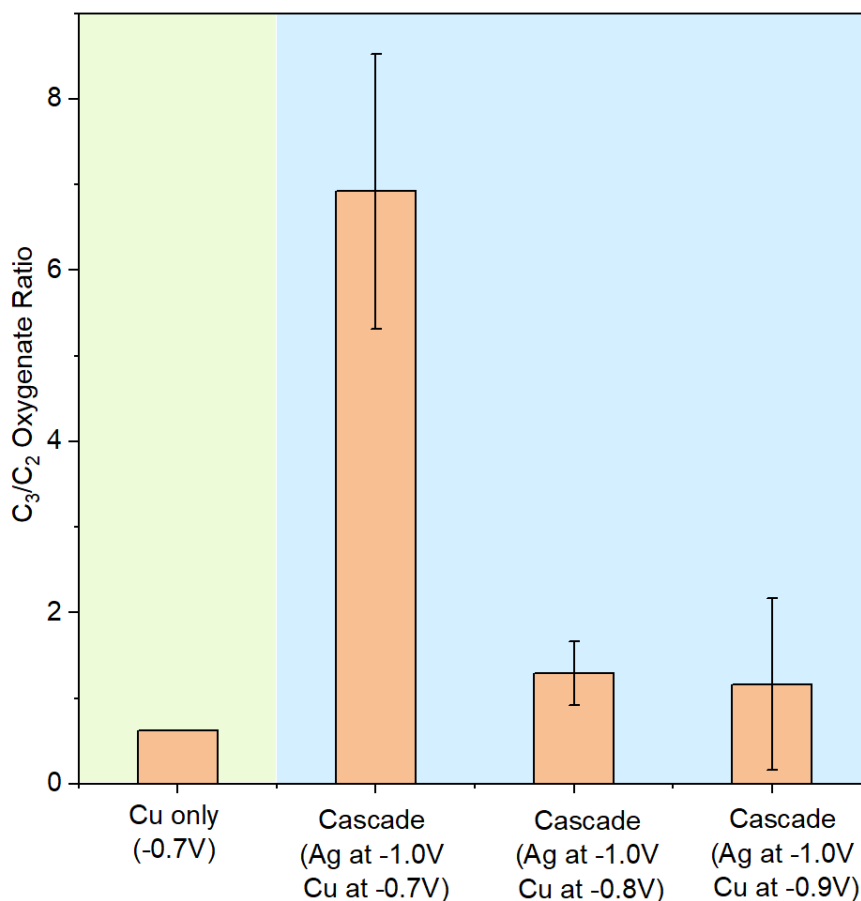


Figure 4.4: $C_3:C_2$ Oxygenate ratio for Cu only active mode (at -0.7V vs RHE), and cascade mode (Ag held at -1V and Cu at -0.7V, -0.8V, and -0.9V vs RHE) (error bars represent the standard deviation from at least two independent repetitions).

Strikingly, the $C_3:C_2$ oxygenate ratio is increased in the cascade case reaching a maximum of about 7 for Ag at -1V and Cu at -0.7V vs RHE while for CO_2RR on Cu only at the same applied potential this ratio is only 0.62.

Further, we probed the effect of flow rate of CO_2 saturated electrolyte on the 2-propanol synthesis as it can impact the surface concentration of the intermediates/reactants and their surface coverage^{24,25}. As shown in **Figure 4.5**, the $FE_{2propanol}$ increases from 31.7% to 39.9% while the FE_{H_2} decreases from 35.7% to 29.5% as the flow rate is reduced from 25 ml/min to 15 ml/min. FE_{CO} only decreases slightly to 4.7% from 4.9% with no appreciable changes to formate selectivity. At these moderately high pressures and low current densities, it is noteworthy to mention

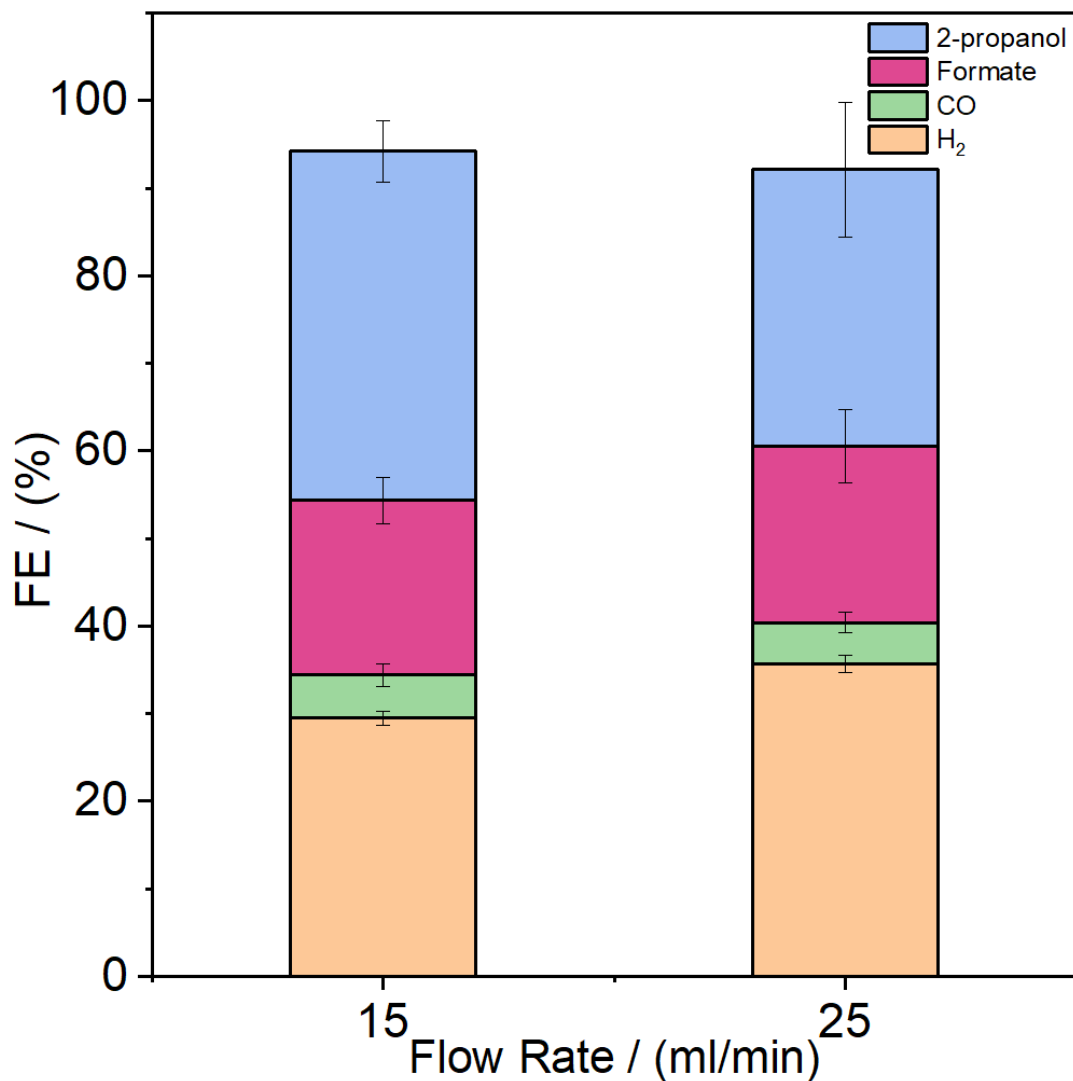


Figure 4.5: Effect of flow rate on 2-propanol selectivity for the cascade mode (Ag held at -1 V and Cu at -0.7V, -0.8V, and -0.9V vs RHE) (error bars represent the standard deviation from at least two independent repetitions).

that the CO₂RR is not likely affected by the transfer of CO₂ from the bulk region to the electrode surface²¹. However, the flow rate could influence the discharge of CO from the cathode to the bulk region. According to Lum et al., a non-equilibrium state is formed on copper (Cu), allowing for a significantly elevated local concentration of CO, surpassing its solubility limit, without diminishing the overall bulk CO₂ concentration⁶. Consequently, a lower flow rate can result in a higher concentration of CO at Cu, thereby increasing the residence time of its subsequent intermediates resulting in an enhanced 2-propanol selectivity.

Further flow rate optimizations, catalytic design strategies and carbon isotope labelled studies could be carried out to optimize this reaction and shed light on the exact mechanism.

4.4 Conclusions

We have demonstrated the attractiveness of combining elevated pressure with cascade electrocatalysis for converting CO₂ into C₃ products. The design of a novel elevated pressure cascade electrochemical cell for CO₂ electroreduction is presented, using two working electrodes/cathodes (Ag and Cu). Convective flow is used to transfer CO from Ag to Cu. In this study, at a pressure of 25 bar, tuning the potential and flow rate of the electrolyte led to an FE_{2propanol} of about 40% (at -0.7V vs RHE and 15 ml/min), marking the highest reported selectivity for this uncommon product from a copper electrode. Furthermore, the C₃:C₂ oxygenate ratio increased to about 7 in the cascade mode compared to a mere 0.62 in the non-cascade mode with only Cu as the active catalyst. We posit that the synergistic effect of high pressure and cascade operation creates a high concentration of the reaction intermediate CO resulting in its enhanced surface coverage on Cu, thereby promoting the formation of higher alcohols from CO₂. By using this strategy, we underscore the potential of integrating different engineering and operating parameters while using simple electrodes to positively influence the performance of the CO₂RR process. This is yet another example that highlights the importance of looking beyond developing new catalysts to target elusive higher reduction products from CO₂, thereby opening new avenues for this process.

4.5 Supplementary Information

4.5.1 Schematics of the High-Pressure Cascade Setup

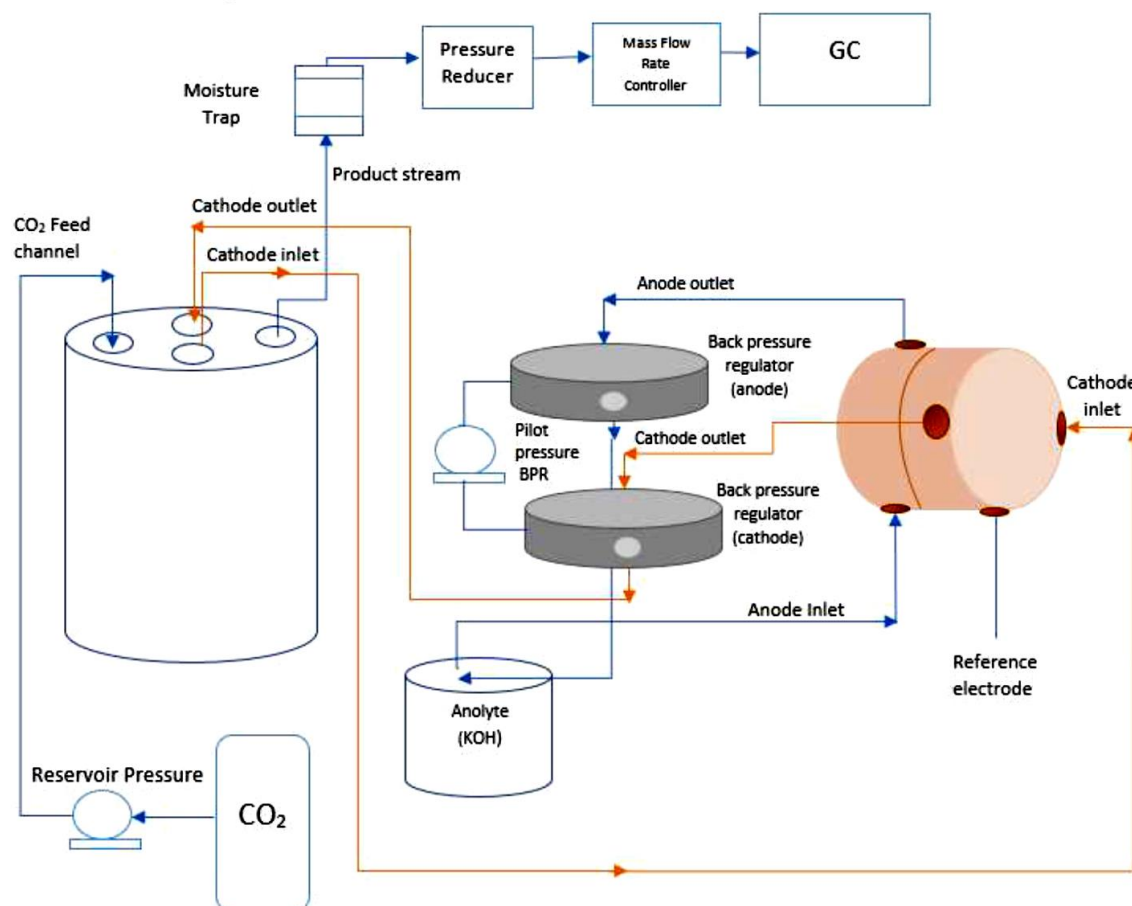


Figure S 4-1: A schematic representation of the high-pressure cascade setup.

4.5.2 Gas and Liquid Product Analysis

Gas Products - To monitor the gaseous byproducts produced during the reaction, an inline gas chromatograph (CompactGC 4.0, Global Analyzer Solutions, The Netherlands) was utilized. Gas cylinders (Linde Gas Benelux B.V., The Netherlands) containing tailored gas mixtures with CO₂ concentrations ranging from 50 to 8000 ppm were employed for GC calibration. Analysis of gas products was conducted at 2-minute intervals. The GC system features two TCD detectors, one for CO and one for H₂, alongside an FID detector for hydrocarbon analysis (C₁ - C₆). The FID channel is outfitted with an Rtx-1, 5.00 μm (15 m * 0.32 mm) analytical column. The first TCD channel comprises a Carboxen 1010 (3 m * 0.32 mm) pre-column and a Molsieve 5A (5 m * 0.32 mm) analytical column, while the second TCD channel includes a Carboxen 1010 (3 m * 0.32 mm) pre-column and a Molsieve 5A (7 m * 0.32 mm) analytical column, aiding in component separation before detection.

Liquid Products - The liquid products (major product: formate, intermediate products: 2-propanol/iso-propanol, minor products: acetate) obtained post-reaction were analyzed using an Agilent Technologies 1260 Infinity HPLC system from the USA. Standard solutions of desired chemicals (Sigma-Aldrich, USA, >98% formic acid) were prepared for system calibration, with concentrations ranging from 0.1 mM to 50 mM. Each analysis involved injecting 5 μL of the product sample onto two Aminex HPX-87H columns (Biorad) in series, heated to 60°C, with a 1 mM H₂SO₄ solution used as the eluent. Detection of products was carried out using a Refractive Index Detector (RID). For cross-checking and detecting intermediate and minor products present in the electrolyte samples such as ethanol, 1-propanol, 2-propanol, acetaldehyde, ethylene glycol, and propionaldehyde, ¹H NMR (400 MHz Agilent, USA), equipped with the built-in software OpenVnmrJ (University of Oregon, USA), was employed. NMR

samples were prepared by mixing 630 μL of the catholyte solution with 70 μL of D_2O (99.9 atom % D, Sigma Aldrich, USA), and 30 μL of a freshly prepared mixture containing 50 mM phenol (Sigma Aldrich, USA) and 10 mM DMSO (Sigma Aldrich, USA) as internal standards. The solution was then transferred to 5 mm NMR tubes (Norell Select, USA), which were thoroughly cleaned with acetone using an in-house setup and dried at 80°C before sample preparation. Water suppression techniques were employed to obtain clearer spectra.

4.5.3 Faradaic Efficiency Calculation

We employ a GC system that directly employs CO₂ as the carrier gas, and for calibration, we utilize gas mixtures containing ethylene, CO, CH₄, and H₂ at various concentrations, with CO₂ serving as the predominant component. Initially, the high-pressure gas stream from our reservoir passes through a pressure reducer, maintaining a constant pressure of approximately 3 bar, before reaching a mass flow controller (MFC, Bronkhorst). Through the MFC, we regulate the volumetric flow rate to the GC; specifically, we alternate between two values, 0.2 mln/min and 8 mln/min, to expedite the GC settling time (we call it the switching flow rate technique¹⁵). The GC columns have been adapted to accommodate CO₂ as the carrier gas, thereby integrating it into the baseline rather than treating it as a distinct entity.

We use the following set of equations for the non-cascade mode and cascade mode.

$$\text{FE gaseous products} = (n \cdot F \cdot X \cdot \text{molar flow rate}) / I$$

Where, n = number of electrons, F = Faraday's constant (96485 C/mol), X = mole fraction of gaseous product measured by the GC, I = total current applied.

For liquid product analysis,

$$\text{FE liquid products} = (n \cdot F \cdot C \cdot V) / Q_{\text{tot}}$$

Where, C = concentration derived from HPLC peak integration, V = volume of the catholyte from which the sample is collected for analysis, Q_{tot} = total charge passed during the experiment. For the cascade mode, the sum of the currents from the two channels is used for the calculation of the FE gases, while the currents from both channels are integrated to calculate the total charge passing through the reactor during the reaction for FE liquids⁸.

4.5.4 Reactor Assembly Drawing

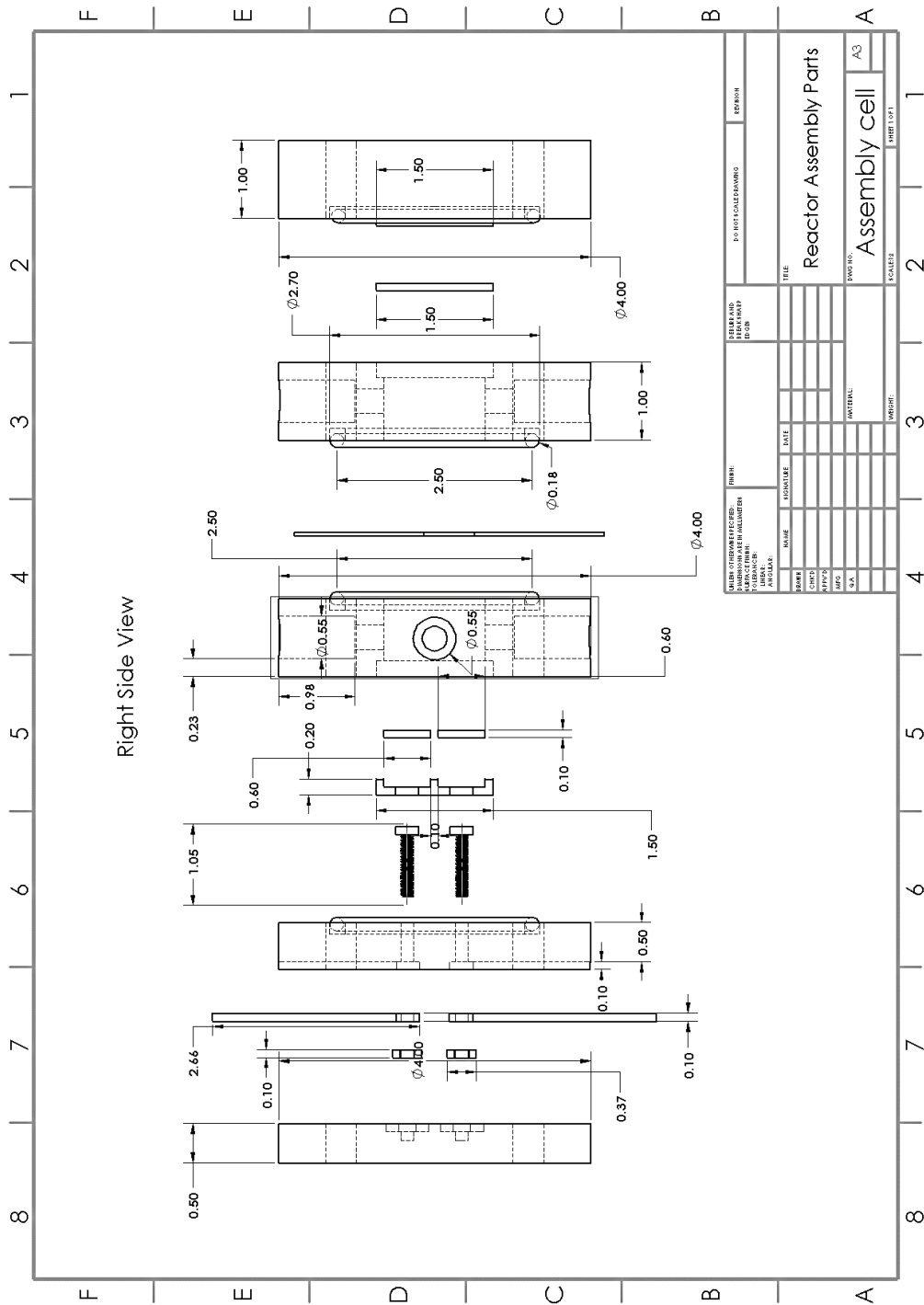


Figure S 4-2: A drawing with measurements for the reactor assembly parts.

4.5.5 SEM Images of Silver and Copper Oxide Foils

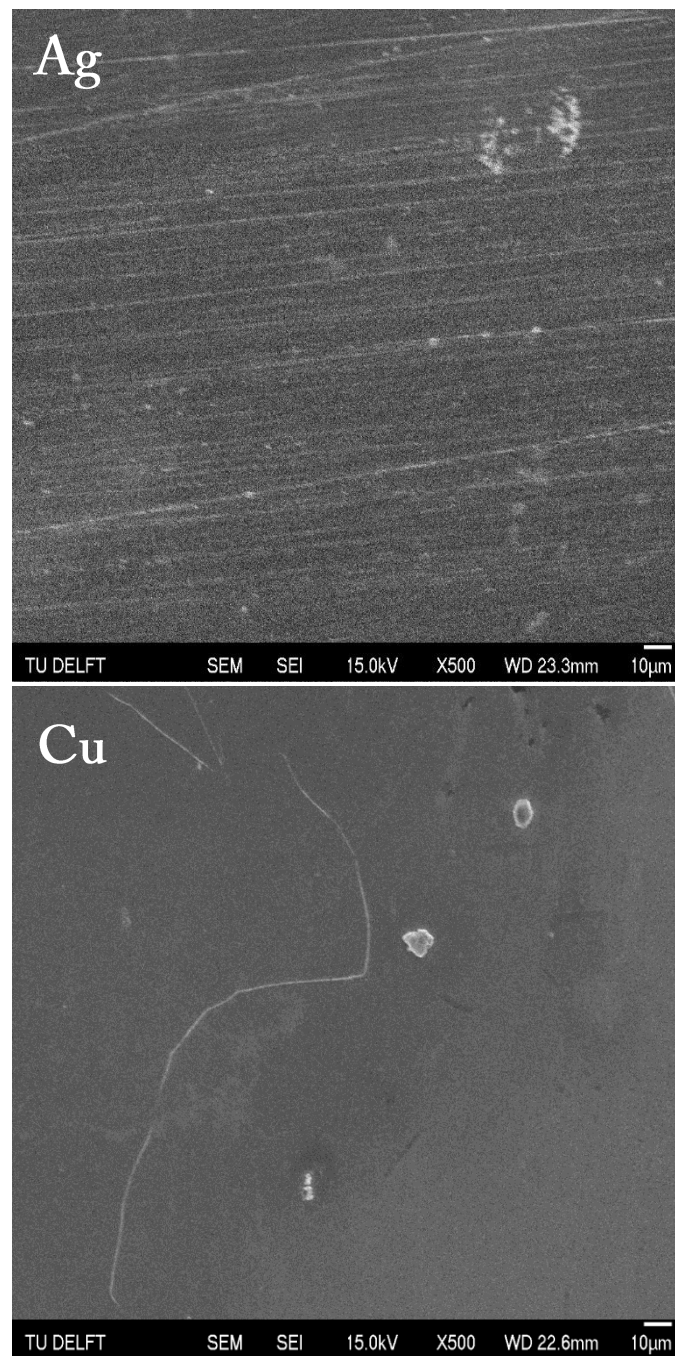


Figure S 4-3: Scanning Electron Microscopy (SEM) images of polished Ag foil and annealed (230°C) Cu foil.

4.5.6 XRD Spectra of Freshly Prepared Silver and Annealed Copper Oxide Foils

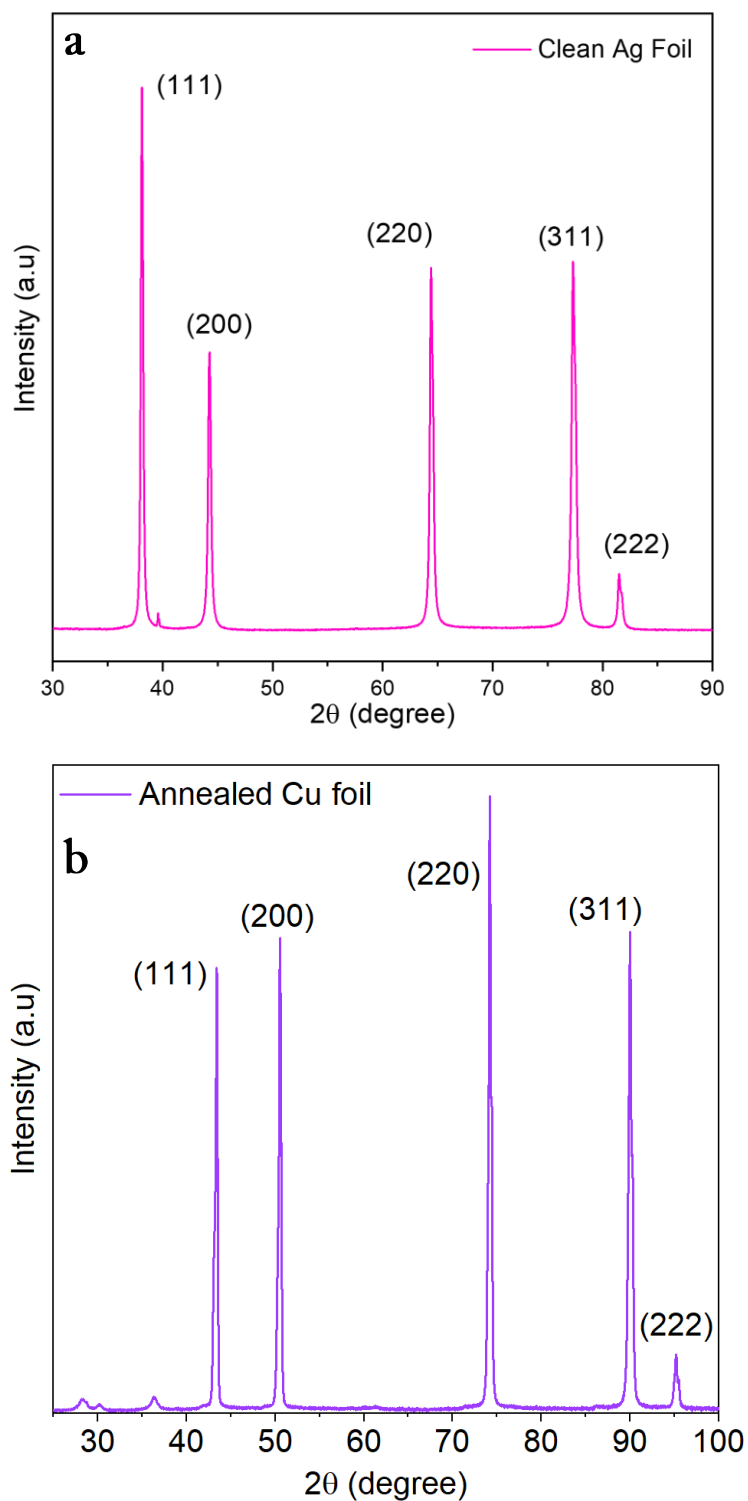


Figure S 4-4: The XRD spectra showing the different facets for a) Polished Ag foil, b) Annealed Cu foil.

4.5.7 Faradaic Efficiencies of Products

Table S 4-1: Faradaic Efficiencies of Products on bare Ag (-1V vs RHE) and Cu (-0.7V vs RHE) catalysts.

Electrode	H ₂	CO	Formate	Ethanol	Ethyl Acetate	2-Propanol	Ethylene Glycol	Acetaldehyde	Total FE (%)
Ag	16.6	53.8	14.5						84.9
Cu	29.6	2.6	20.3	16.3		16.9		10.9	96.6

Table S 4-2: Faradaic Efficiencies of Products in Cascade Mode with Ag fixed at -1V vs RHE.

E _{we} vs RHE (V) applied to Cu oxide foil	H ₂	CO	Formate	Ethanol	Ethyl Acetate	2-Propanol	Ethylene Glycol	Acetaldehyde	Total FE (%)
-0.7	35.7	4.7	19.7	2.15	2.45	31.5	2.4		98.6
-0.8	22.9	16.15	26.55	4.8	4.65	11.55	0.25	3.9	90.75
-0.9	25.55	5.85	33.1	6.8	2.75	10.5	0.35	1.9	86.80

Table S 4-3: Faradaic Efficiencies at Different Flow Rates for Cascade Mode (Ag (-1V vs RHE) and Cu oxide (-0.7V vs RHE)).

Flow Rate (mL/min)	H ₂	CO	Formate	Ethanol	Ethyl Acetate	2-Propanol	Ethylene Glycol	Acetaldehyde	Total FE (%)
15	29.49	4.89	19.94			39.91			94.24
25	35.7	4.7	19.7	2.15	2.45	31.5	2.4		98.6

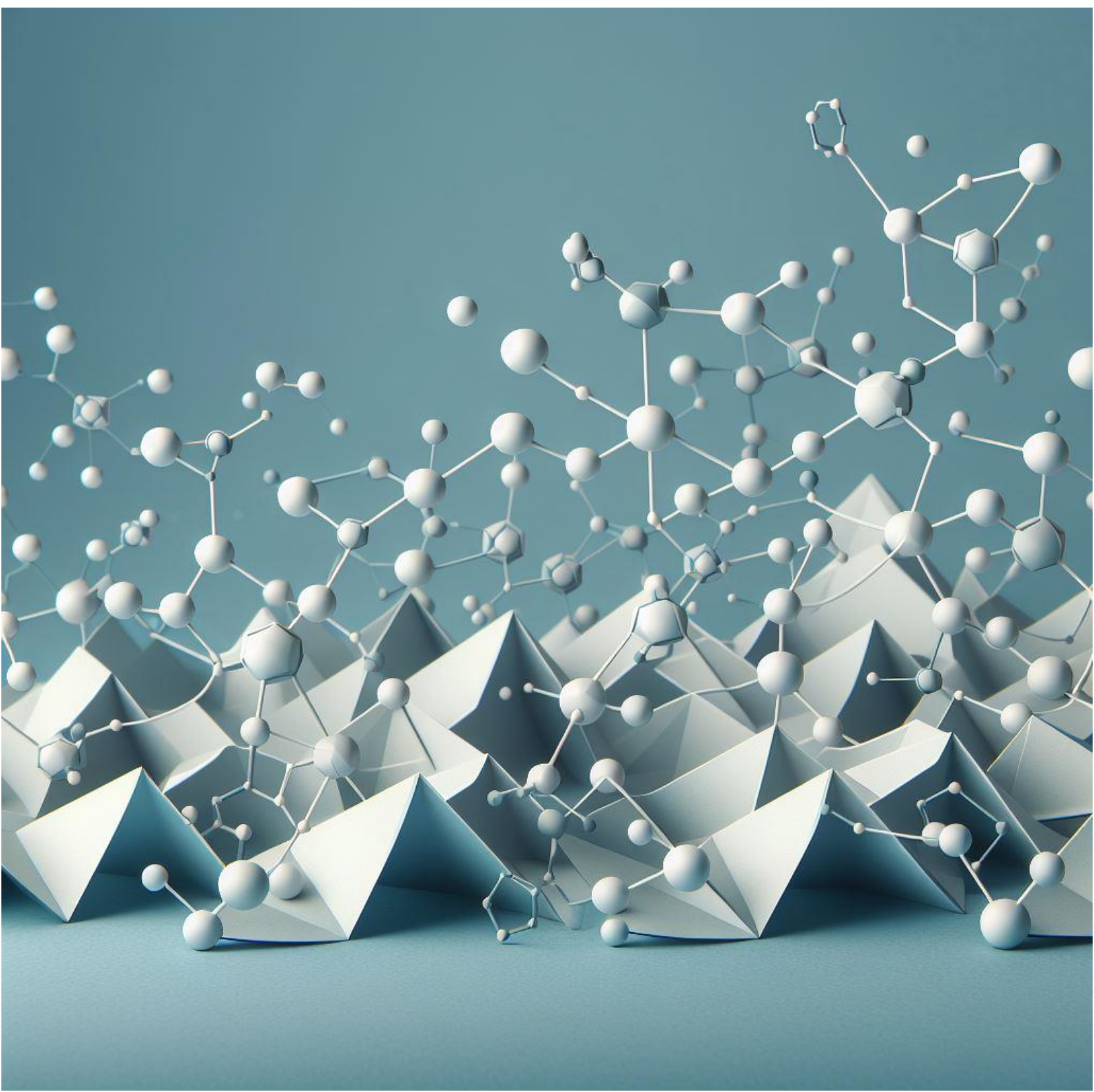
4.6 References

- 1 Shi, J. *et al.* Enzymatic conversion of carbon dioxide. *Chemical Society Reviews*, **44**, 5981-6000, (2015). <https://doi.org:10.1039/c5cs00182j>
- 2 Abild-Pedersen, F. *et al.* Scaling properties of adsorption energies for hydrogen-containing molecules on transition-metal surfaces. *Physical Review Letters*, **99**, 016105-016105, (2007). <https://doi.org:10.1103/PHYSREVLETT.99.016105/FIGURES/3/MEDIUM>
- 3 Wang, S. *et al.* Universal transition state scaling relations for (de)hydrogenation over transition metals. *Physical Chemistry Chemical Physics*, **13**, 20760-20765, (2011). <https://doi.org:10.1039/C1CP20547A>
- 4 Wang, C. *et al.* Silver modified copper foam electrodes for enhanced reduction of CO₂ to C₂+ products. *Materials Advances*, **3**, 4964-4972, (2022). <https://doi.org:10.1039/d2ma00188h>
- 5 Theaker, N. *et al.* Heterogeneously catalyzed two-step cascade electrochemical reduction of CO₂ to ethanol. *Electrochimica Acta*, **274**, 1-8, (2018). <https://doi.org:10.1016/j.electacta.2018.04.072>
- 6 Lum, Y. & Ager, J. W. Sequential catalysis controls selectivity in electrochemical CO₂ reduction on Cu. *Energy and Environmental Science*, **11**, 2935-2944, (2018). <https://doi.org:10.1039/c8ee01501e>
- 7 Hou, J., Chang, X., Li, J., Xu, B. & Lu, Q. Correlating CO Coverage and CO Electroreduction on Cu via High-Pressure in Situ Spectroscopic and Reactivity Investigations. *Journal of the American Chemical Society*, **144**, 22202-22211, (2022). <https://doi.org:10.1021/jacs.2c09956>
- 8 Gurudayal, G. *et al.* Sequential Cascade Electrocatalytic Conversion of Carbon Dioxide to C-C Coupled Products. *ACS Applied Energy Materials*, **2**, 4551-4559, (2019). <https://doi.org:10.1021/acsaem.9b00791>
- 9 Luo, W., Nie, X., Janik, M. J. & Asthagiri, A. Facet Dependence of CO₂ Reduction Paths on Cu Electrodes. *ACS Catalysis*, **6**, 219-229, (2016). https://doi.org:10.1021/ACSCATAL.5B01967/ASSET/IMAGES/LARGE/CS-2015-01967G_0006.JPG
- 10 Cheng, T., Xiao, H. & Goddard, W. A. Full atomistic reaction mechanism with kinetics for CO reduction on Cu(100) from ab initio molecular dynamics free-energy calculations at 298 K. *Proceedings of the National Academy of Sciences of the United States of America*, **114**, 1795-1800, (2017). https://doi.org:10.1073/PNAS.1612106114/SUPPL_FILE/PNAS.201612106SI.PDF
- 11 Akhade, S. A. *et al.* Poisoning effect of adsorbed CO during CO₂ electroreduction on late transition metals. *Physical Chemistry Chemical Physics*, **16**, 20429-20435, (2014). <https://doi.org:10.1039/C4CP03340J>

- 12 Sandberg, R. B., Montoya, J. H., Chan, K. & Nørskov, J. K. CO-CO coupling on Cu facets: Coverage, strain and field effects. *Surface Science*, **654**, 56-62, (2016). <https://doi.org:10.1016/J.SUSC.2016.08.006>
- 13 Li, C. W., Ciston, J. & Kanan, M. W. Electroreduction of carbon monoxide to liquid fuel on oxide-derived nanocrystalline copper. *Nature*, **508**, 504-507, (2014). <https://doi.org:10.1038/nature13249>
- 14 Qi, K. *et al.* Unlocking direct CO₂ electrolysis to C₃ products via electrolyte supersaturation. *Nature Catalysis*, (2023). <https://doi.org:10.1038/s41929-023-00938-z>
- 15 Morrison, A. R. T., Girichandran, N., Wols, Q. & Kortlever, R. Design of an elevated pressure electrochemical flow cell for CO₂ reduction. *Journal of Applied Electrochemistry*, **1**, 1-10, (2023). <https://doi.org:10.1007/S10800-023-01927-7/FIGURES/8>
- 16 Asperti, S., Hendriks, R., Gonzalez-Garcia, Y. & Kortlever, R. Benchmarking the Electrochemical CO₂ Reduction on Polycrystalline Copper Foils: The Importance of Microstructure Versus Applied Potential. *ChemCatChem*, **14**, e202200540-e202200540, (2022). <https://doi.org:10.1002/CCTC.202200540>
- 17 Diao, L. *et al.* Improving the activity of electrochemical reduction of CO₂ to C₁ products by oxidation derived copper catalyst. *Materials Reports: Energy*, **3**, 1-8, (2023). <https://doi.org:10.1016/j.matre.2023.100180>
- 18 Bui, J. C. *et al.* Engineering Catalyst-Electrolyte Microenvironments to Optimize the Activity and Selectivity for the Electrochemical Reduction of CO₂ on Cu and Ag. *Accounts of Chemical Research*, **55**, 484-494, (2022). <https://doi.org:10.1021/acs.accounts.1c00650>
- 19 Resasco, J. *et al.* Promoter Effects of Alkali Metal Cations on the Electrochemical Reduction of Carbon Dioxide. *Journal of the American Chemical Society*, **139**, 11277-11287, (2017). https://doi.org:10.1021/JACS.7B06765/SUPPL_FILE/JA7B06765_SI_001.PDF
- 20 Singh, M. R., Kwon, Y., Lum, Y., Ager, J. W. & Bell, A. T. Hydrolysis of Electrolyte Cations Enhances the Electrochemical Reduction of CO₂ over Ag and Cu. *Journal of the American Chemical Society*, **138**, 13006-13012, (2016). <https://doi.org:10.1021/jacs.6b07612>
- 21 Proietto, F., Berche, F., Galia, A. & Scialdone, O. Electrochemical conversion of pressurized CO₂ at simple silver-based cathodes in undivided cells: study of the effect of pressure and other operative parameters. *Journal of Applied Electrochemistry*, **51**, 267-282, (2021). <https://doi.org:10.1007/S10800-020-01505-1/FIGURES/6>
- 22 Hori, Y., Takahashi, R., Yoshinami, Y. & Murata, A. Electrochemical Reduction of CO at a Copper Electrode. *Journal of Physical Chemistry B*, **101**, 7075-7081, (1997). <https://doi.org:10.1021/JP970284I>
- 23 Wang, L. *et al.* Electrochemically converting carbon monoxide to liquid fuels by directing selectivity with electrode surface area. *Nature Catalysis*, **2**, 702-708, (2019). <https://doi.org:10.1038/s41929-019-0301-z>

- 24 Goyal, A., Marcandalli, G., Mints, V. A. & Koper, M. T. M. Competition between CO₂ Reduction and Hydrogen Evolution on a Gold Electrode under Well-Defined Mass Transport Conditions. *Journal of the American Chemical Society*, **142**, 4154-4161, (2020). https://doi.org:10.1021/JACS.9B10061/ASSET/IMAGES/LARGE/JA9B10061_0004.JPEG
- 25 Gupta, N., Gattrell, M. & MacDougall, B. Calculation for the cathode surface concentrations in the electrochemical reduction of CO₂ in KHCO₃ solutions. *Journal of Applied Electrochemistry*, **36**, 161-172, (2006). <https://doi.org:10.1007/S10800-005-9058-Y/METRICS>

Chapter 5 : Conclusions and Recommendations



5.1 Conclusions

The aim of the research presented in this dissertation was to optimize a two-catalyst system using pressure to maximize the two-step reduction to CO₂ to alcohols. To achieve this, we started from scratch by 1) designing and validating a high-pressure reactor system capable of conducting CO₂RR in a continuous manner while also being modular and flexible enough to incorporate different reactor configurations. 2) Using the system, we carried out benchmark studies on a Cu foam electrode by tuning of the pressure and electrolyte. 3) The knowledge obtained from the above study on a Cu electrode was used to optimize a novel high pressure sequential cascade catalytic (Ag Cu pair) system to boost the synthesis of higher alcohols from CO₂. The main conclusions are provided below.

In **Chapter 2**, we successfully designed and operated an elevated pressure divided CO₂RR flow cell for standard experiments in the field. The key to this design involved minimizing pressure differentials across the dividing membrane using double back pressure regulators piloted by the same pressure. Careful consideration of design parameters, such as reservoir and pump sizing, was crucial. The cell assembly/disassembly time was faster than some standard atmospheric designs due to the quick-release clamp design, completing the process within half an hour. Electrochemically, the cell performed well and the leakless reference electrode provided a stable reference potential across a range of both reactor and reservoir pressures (stable within 10 mV between 1 and 30 bar). Standard electrochemical experiments, such as linear sweep voltammetry, were successfully performed. Product characterization by in-line GC was possible by utilizing a switching flow rate system, which greatly decreased the settling time, allowing faster measurements (stable readings reached within 60 min for lower pressures and within 100

min at the highest pressure). The FE for CO₂RR products substantially increases from close to 26% at 2 bar to about 60% at 30 bar while H₂ is suppressed, and more importantly 85–90% of the charge balance was closed at lower pressure, dropping only to 82% at 30 bar which is still equivalent to several studies in the literature. The system explained here in detail is successful in its aims and configurable enough to be useful in studying a range of CO₂RR research questions relating to elevated pressure reactors like high current density or CO₂ conversion rate.

In **Chapter 3**, we report a systematic investigation of the effects of pressure, current density, cation size, and electrolyte concentration on the electrochemical CO₂ reduction using a copper foam electrode. At 25 bar, the electrode shows a remarkable selectivity of 70% for formate in 0.5 M CsHCO₃ with j_{HCOOH} of -12.7 mA/cm². Furthermore, we report the formation of the uncommon product iso/2-propanol, with a FE of 11% in 0.5 M KHCO₃ at 25 bar, which is the highest reported selectivity for this product under moderate pressures on a polished copper foam. The conducted experiments shed light on the idea that electrolyte choice coupled with the right operating conditions can be a viable option to enhance the selectivity towards profitable products such as formate on a simple copper electrode. Moreover, a pressurized CO₂ feed can potentially unlock new C-C coupling pathways on copper and pave the way towards the production of elusive higher CO₂ reduction products. This also brings up the question whether newly developed catalysts should be tested under elevated pressure conditions.

Finally, in **Chapter 4**, we present the design of a novel elevated pressure sequential cascade reactor using two working electrodes (Ag and Cu). Convective flow is used to transfer CO from Ag to Cu. In this pioneering study, under a pressurized condition of 25 bar, tuning the

potential and flow rate of the electrolyte led to an $FE_{2\text{propanol}}$ of about 40% (at -0.7V vs RHE and 15ml/min), marking the highest reported selectivity for this uncommon product. Furthermore, the $C_3:C_2$ oxygenate ratio increased to about 7 in the cascade mode compared to a mere 0.62 in the non-cascade mode with only Cu as the active catalyst. We posit that the synergistic effect of high pressure and cascade operation creates a high concentration of the reaction intermediate CO resulting in its enhanced surface coverage on Cu, thereby promoting the formation of higher alcohols from CO_2 . Further flow rate optimizations, catalytic design strategies and carbon isotope labelled studies could be carried out to optimize this reaction and shed light on the mechanism.

5.2 Recommendations

In this section, a few recommendations are provided based on the projects mentioned in this thesis.

- The effect of high pressure on the electrochemical CO_2 reduction should be tested at higher current densities to bring it closer to industrial requirements. This can be achieved by working with other reactor configurations such as zero-gap or membrane electrolyzers that have already been well studied and optimized at ambient pressure condition to reach high current densities. The clamp system developed in this study is flexible enough to incorporate different reactor designs and stacks. This can further be extended to other unconventional reactors such as tubular reactor employing segmented Taylor flow of CO_2 to improve mass transport and conversion, potentially reaping the benefits of pressurized CO_2 feed.

Furthermore, this investigation can be expanded to include unconventional reactor designs like tubular reactors employing segmented Taylor flow of CO₂, aimed at enhancing mass transport and conversion rates, and potentially leveraging the advantages of pressurized CO₂ feed. Scale up studies could help bridge the gap between lab-scale studies as conducted in this thesis and industry. The modular clamp system enables easy and efficient stacking of multiple reactor layers. This could facilitate conducting the CO₂RR at elevated pressures in both series and parallel configuration.

- Extending the cascade system to add more electrodes like Ni-N-C, known for being highly selective towards CO (almost 100%) across a wide range of pressures, is a promising idea. Further, different electrode configurations could be explored, and potentially integrated with other chemical synthesis methods such as biochemical conversions as a viable concept.
- Operando experiments using techniques such as SEIRAS and RAMAN coupled with electrochemical measurements at high pressure on the cascade catalytic system could shed light on the mechanism behind the synthesis of higher alcohols and give a more accurate relationship between the applied pressure, surface coverage and product distribution.

Acknowledgements

My journey through my PhD, although it often demanded solitary reflection on my work, would have been incomplete without a solid support system. Over the years, I've been lucky to meet and be surrounded by some truly amazing people.

All this work would not have been possible without **Ruud Kortlever** entrusting me with this opportunity, especially with my limited experience in this field. Since day one, you have been very kind and approachable. Our conversations have always been very productive and fun, and I enjoyed them. We bounced ideas off each other, and it's rewarding to see that some of them panned out as exciting projects. I am grateful for this experience as it has made it clear to me what I wish to pursue. For that, and many more reasons, I thank you.

Ruud van Ommen and **Wiebren de Jong**, thank you so much. I have always enjoyed our quick meetings, every now and then. It really helped me align my thoughts. You are some of the kindest people I have come across, especially with the wealth of experience you bring to the table.

Andrew, you have been a great mentor throughout this journey and really helped me establish a research direction that I enjoyed exploring.

Asvin, my friend, all the time we spent in the lab will be cherished but even more so outside the lab and on the field. You are a very kind and helpful soul; be it work related or not, and I hope you stay the same. Your patience and systematic work ethic is commendable. All the discussions outside of the scientific ones helped me stay sane during the difficult days in the lab. I am happy to have found a good friend in you and I thank you for all your help. I wish you the very best in all your endeavors.

Iris, thank you so much for being you. It surprises me how friendships start but, in this case, it was because it was so easy to approach and talk to you. I admire your multitasking, and the effort you take to sort out any issues that come your way. All those times spent breaking our heads trying to solve problems in the lab was fun. You still owe me a soccer game. I wish you only the best in life.

Boaz, buddy, I am so happy we ended up working in the same group after our masters. Your work ethic is truly impressive, and it's motivated me on numerous occasions. I enjoyed all our scientific discussions during the last few years, and thanks to you I have found myself enjoying board games a lot more. **Isabell**, I will cherish all the time spent discussing and collaborating on interesting projects. I wish you all the very best.

To **Daniel, Simone, Henga, Katie, Shilong, Marilia, Ahmed, Sohan, Shahid, Aviral, Andrea, Christos**, and all the others that have been part of this incredible experience. I thank you for making this journey a memorable one and wish you all the very best. **Michel**, you are the best. I don't think I would have been able to complete my PhD if not for your timely guidance and assistance in the lab.

To my close friends that have been part of this journey - **Pranav, Vikram, Ashwin, Akash, Arvind, Praveen, Harshitha, Narayani, Srushti, Manoj, Advith**, thank you for the numerous outings, potlucks, fun games, and life discussions. These really kept me positively distracted during the tough times. I cherish each one of our relationships and hope our bonds continue to grow stronger.

To **amma, appa, Radha, thatha, and paati**. I wouldn't be here without your guidance, support, patience, and blessings. You all have sacrificed so much for me, and I am forever indebted to you. **Viji amma and Murali appa**, thank you for all the love, and blessings. You both are very understanding, and an integral part of my PhD journey.

Finally, to the love of my life, **Vaishu**. Your unwavering support has been an immense source of strength for me, and I'm deeply grateful for your invaluable contributions and sacrifices. Without your presence and efforts, none of this journey would have been complete. Thank you for being my partner in crime, for your constant encouragement and love, and for simply being yourself, even amidst my endless ramblings at times. These words hardly capture the depth of my gratitude, but, from the bottom of my heart, thank you. Here's to a life filled with fun, good health, and boundless happiness.

Curriculum Vitae

Nandalal Girichandran

16-04-1993 Born in Chennai, Tamil Nadu, India.

Education

2012–2016 B.tech in Chemical Engineering
National Institute of Technology, Tiruchirappalli, India

2017–2019 M.Sc in Chemical (Process) Engineering
Faculty of Applied Sciences, TU Delft, Netherlands

2019–2023 Ph.D. in Electrochemical CO₂ Conversion
Faculty of Mechanical Engineering, TU Delft, Netherlands

Thesis:

Supervisor: Dr. R. Kortlever

Promotors: Prof.dr.ir. W. de Jong, and Prof.dr.ir. J.R.van Ommen

Publications

Included in this thesis:

- ✉ *Morrison, A.R.T., ***Girichandran, N.** et al. *Design of an Elevated Pressure Electrochemical Flow Cell for CO₂ Reduction*. *J Appl Electrochem* 53, 2321–2330 (2023). <https://doi.org/10.1007/s10800-023-01927-7>. (* Co-first authors)
 - ✉ **Girichandran, N.**, Saedy, S., Kortlever, R.. *Electrochemical CO₂ Reduction on a Copper Foam Electrode at Elevated Pressures*. *Chem Eng*, 150478, ISSN 1385-8947 (2024). <https://doi.org/10.1016/j.cej.2024.150478>.
 - ✉ **Girichandran, N.**, Mohan, L. et al. *Elevated Pressure Cascade Electrocatalytic Conversion of CO₂ to C₃ Products*. (In preparation)
-

Not Included in this thesis:

- ✉ Lawrence, K.R., Kumar, A.S., Asperti, S., van den Berg, D., **Girichandran, N.**, Kortlever, R.. *Advances in Electrochemical Carbon Dioxide Reduction Toward Multi-Carbon Products*. *Chemical Valorisation of Carbon Dioxide*, ed. G. Stefanidis and A. Stankiewicz, The Royal Society of Chemistry, chapter: 17, 388-412 (2022). <https://doi.org/10.1039/9781839167645-00388>.
 - ✉ Bagemihl, I., **Girichandran, N.** et al. *Enhancing the Electrochemical Reduction of CO₂: Exploring Taylor Flow in a Polymer Electrolyte Membrane Electrolyser*. (In preparation)
 - ✉ Izelaar, B., Karanth, P., **Girichandran, N.** et al. *The Effect of Potential on the Li-Mediated NRR Performance*. (In preparation)
-

Others:

- ✉ Murugesan, P., **Girichandran, N.**, et al. *Structural, Optical and Photocatalytic Properties of Visible Light Driven Zinc Oxide Hybridized Two-Dimensional π -Conjugated Polymeric g-C₃N₄ Composite*. *Optical Materials*, Volume 75, 2018, 431-441. (2018) <https://doi.org/10.1016/j.optmat.2017.10.051>.